Materials Today Chemistry 10 (2018) 221–258

Contents lists available at ScienceDirect

Materials Today Chemistry

journal homepage: www.journals.elsevier.com/materials-today-chemistry/

Graphene quantum dots from chemistry to applications

P. Tian [a], L. Tang [a, **], K.S. Teng [b], S.P. Lau [c, *]

[a] Kunming Institute of Physics, Kunming, 650223, People's Republic of China
[b] College of Engineering, Swansea University, Bay Campus, Fabian Way, Swansea, SA1 8EN, United Kingdom
[c] Department of Applied Physics, The Hong Kong Polytechnic University, Hung Hom, Kowloon, Hong Kong

ARTICLE INFO

Article history:
Received 7 August 2018
Received in revised form
20 September 2018
Accepted 21 September 2018

Keywords:
Nanostructured graphene
Graphene quantum dots
Optical properties
Electrical properties
Optoelectronics

ABSTRACT

Graphene quantum dots (GQDs) have been widely studied in recent years due to its unique structure-related properties, such as optical, electrical and optoelectrical properties. GQDs are considered new kind of quantum dots (QDs), as they are chemically and physically stable because of its intrinsic inert carbon property. Furthermore, GQDs are environmentally friendly due to its non-toxic and biologically inert properties, which have attracted worldwide interests from academic and industry. In this review, a number of GQDs preparation methods, such as hydrothermal method, microwave-assisted hydrothermal method, soft-template method, liquid exfoliation method, metal-catalyzed method and electron beam lithography method etc., are summarized. Their structural, morphological, chemical composition, optical, electrical and optoelectrical properties have been characterized and studied. A variety of elemental dopant, such as nitrogen, sulphur, chlorine, fluorine and potassium etc., have been doped into GQDs to diversify the functions of the material. The control of its size and shape has been realized by means of preparation parameters, such as synthesis temperature, growth time, source concentration and catalyst etc. As far as energy level engineering is concerned, the elemental doping has shown an introduction of energy level in GQDs which may tune the optical, electrical and optoelectrical properties of the GQDs. The applications of GQDs in biological imaging, optoelectrical detectors, solar cells, light emitting diodes, fluorescent agent, photocatalysis, and lithium ion battery are described. GQD composites, having optimized contents and properties, are also discussed to extend the applications of GQDs. Basic physical and chemical parameters of GQDs are summarized by tables in this review, which will provide readers useful information.

1. Introduction

1.1. History of graphene quantum dots development

Carbon, which is one of the most abundant elements, has been widely researched since 19th century and has experienced a continuous surge in its studies. The entire development of carbon material to date is shown in Fig. 1. In the year 1859, Brodie [1] synthesized the graphite oxide to ascertain the molecular weight of graphite via some hazardous experiments, and coined its name 'Graphon'. At that time, the properties of graphite oxide were not described until 1918 by Kohlschütter and Haenni [2]. Further study on the structural property of graphite oxide was carried out by Bernal using single-crystal diffraction measurements [3] in 1924. As the characterization technology enhances, the electronic properties of graphite were first investigated by Wallace [4] and he introduced the idea of graphene in 1947. One year later, Ruess and Vogt [5] successfully detected a few layers graphite via transmission electron microscopy (TEM). In 1957, Hummers and Offeman [6] developed a new method, which is safer and more efficient than Brodie's method, in the preparation of graphite oxide. The idea of a single layer graphite sheet, which was initially described by Boehm [7] in 1962 and by some theoretical physicists [8], having a massless Dirac equation in 1984 was considered implausible in that era. During the development of carbon materials, a football-shaped fullerene was discovered by Smally [9] in 1985, which represented eureka moment in the scientific world, leading to the award of the Nobel Prize in 1996. This is the first carbon allotropy which inspires scientists around the world in exploiting carbon materials. In 1987, Mouras [10] introduced the word 'graphene' to represent single sheets of graphite although stable single-layer graphite sheet

* Corresponding author.
** Corresponding author.
E-mail addresses: scitang@163.com (L. Tang), apsplau@polyu.edu.hk (S.P. Lau).

https://doi.org/10.1016/j.mtchem.2018.09.007

Fig. 1. The history of carbon materials development.

still remained non-existent by theoretical calculations. Another carbon allotropy so-called carbon nanotubes (CNTs) was later discovered by Iijima [11] in 1991. More than a decade later, an astonishing experiment on graphene was carried out by Geim and Novoslov [12] in Manchester University, where a monolayer graphene was developed using a Scotch tape technique in 2004. Their work has led to many exciting scientific researches into the two dimensional material, which could offer many novel applications. In 2010, a Nobel Prize was awarded to Geim and Novoslov for their experimental work on graphene. It was again awarded to researchers working on carbon materials. To date, the different graphitic forms, such as 0D fullerene, 1D carbon nanotubes, 2D graphene and 3D graphite, had successfully been discovered.

Since the discovery of graphene, the properties and applications of graphene have been extensively studied and exploited. However, researchers have realized many limitations of graphene, such as zero bandgap and low absorptivity etc. Structural modification of graphene was subsequently investigated to overcome the shortcomings. Graphene quantum dots (GQDs) were fabricated by Ponomarenko and Geim [13] in 2008 based on the previous work on carbon dots (CDs) by Xu [14] et al., in 2004. The GQDs are different from CDs because they possess graphene lattice inside the dots, which are smaller than 100 nm in size and less than 10 layers thick [15]. CDs are usually quasi-spherical carbon nanoparticles having a size of less than 10 nm [15]. The GQDs have many novel properties, such as its unique fluorescent properties discovered by Pan [16] et al., in 2010, due to its quantum confinement effect. The ability to modulate the properties of GQDs is important if the material is to be used in diverse applications. Modification of GQDs properties by means of doping was first investigated by Zhao [17] and collaborators in 2012 involving the use of nitrogen as dopant in GQDs. Besides, GQDs exhibit better solubility than CNTs. This is due to the large edge effect of GQDs, which can be modified by functional groups, unlike the CNTs that are limited by its one dimensional characteristics.

Graphene exhibits an infinite exciton Bohr radius [18]. However, GQD is a zero-dimensional material by converting two-dimensional graphene. This resulted in quantum confinement and edge effects, which the crystal boundary significantly modifies electron distribution due to the reduced dimension of the crystal to nanometer scale. Additionally, GQDs have non-zero bandgap, which is different from graphene. Previous theoretical calculations as well as optical and electrical experiments have demonstrated the existence of bandgap in GQDs. The semi-metal graphene can turn into either semiconductor or insulator GQDs. The broadening of the optical absorption of graphene has led to higher energy spectral due to the opening of the bandgap in GQDs. GQDs also exhibit different chemical and physical properties when compared with other carbon-based materials, such as CD, CNTs, fullerene and graphene etc., due to its special edge and quantum confinement effects. In the field of nanomaterials, many of the physical and chemical properties of nanomaterials are usually determined by the fabrication methods. Based on the GQDs preparation methods developed in recent years, these methods can be classified into two categories, namely top-down and bottom-up, according to the precursor material. As shown in the central part of Fig. 2, top-down method refers to direct cutting of graphene-related materials (such as graphene [16], graphene oxide [19], carbon nanotubes [20], carbon fibers [21], carbon black [22], graphite powder [23] and coal [24] etc.) into quantum size via various processes. In bottom-up approach, graphene-like smaller polycyclic aromatic hydrocarbons (PAHs) molecular precursors (such as benzene [25], hexaperi-hexabenzocoronene [26], glucose [27] and fullerene [28] etc.) are converted to GQDs by stepwise chemical reaction. In addition to quantum confinement and edge effects, GQDs exhibited many important characteristics, such as stable PL, non-toxicity,

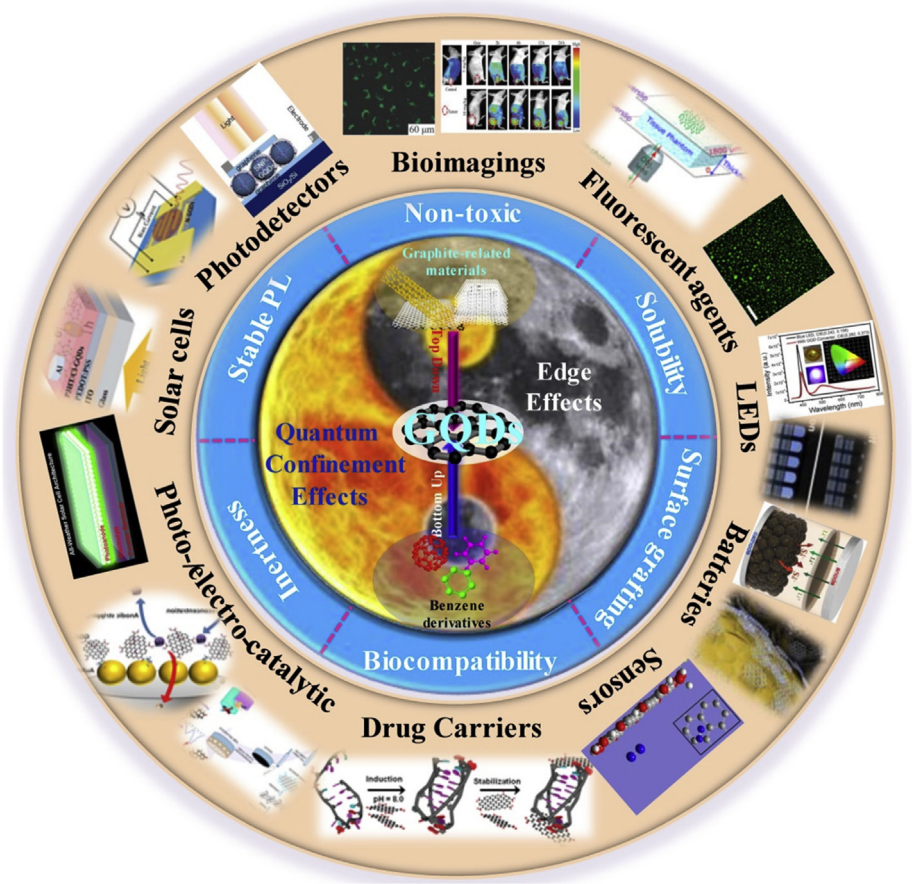

Fig. 2. The graphene quantum dots (GQDs) related inherent effects, preparation methods, properties and applications.

good solubility, surface grafting, biocompatibility and inertness [29], as shown in middle rings in Fig. 2. Some of these characteristics are overwhelmingly superior to traditional semiconductor quantum dots, hence prompted many potential applications of GQDs in solar cells [30–34], photodetectors [35–40], bioimagings [41–44], fluorescent agents [45–48], light-emitting diodes [49] (LEDs), batteries [50], sensors [51,52], drug carriers [53–58] and photo-/electro-catalytic [59] and so forth, as shown in marginal ring of Fig. 2.

The two effects, namely edge and quantum confinement effects, belong to the basic characteristics of GQDs. The unique chemical and physical properties of GQDs, such as non-toxicity, solubility, surface grafting, biocompatibility, inertness and stable PL, are results of its basic characteristics. Based on these properties, a series of applications are developed.

1.2. The outlooks of graphene quantum dots

The research on GQDs is still at an early stage, and many challenges of GQDs have yet to be addressed, as shown in Fig. 3. Although there are many important advantages and potential applications of GQDs, further research to enhance the properties of the material is required in order to meet the application requirements. Therefore, the studies of GQDs have been on-going to address the five urgent issues as stated in Fig. 3.

To meet the industry requirements, it is necessary to mass produce GQDs at relatively low cost. However, the product yield of GQDs using current preparation methods [60] is considerably low (<10% mostly), therefore new methods, such as photo-Fenton

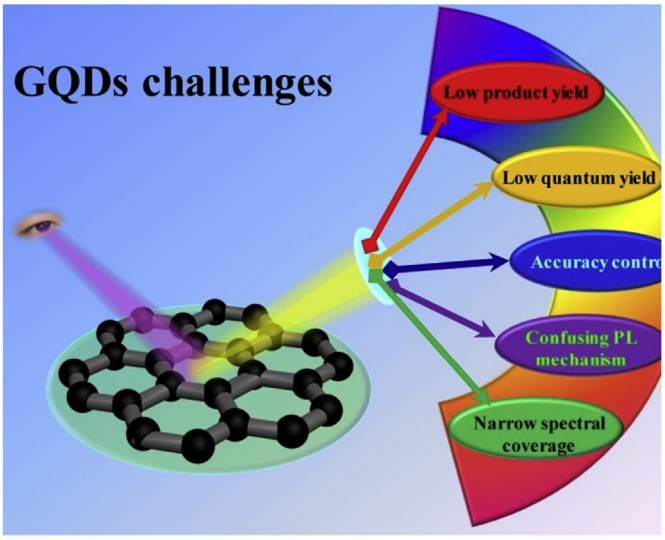

Fig. 3. The challenges of GQDs according to the recent researches.

reaction method (highest yield of 45% [60]) and facile fabrication technique using coals [24], that can improve the product yield need to be exploited. Besides, the reported quantum yields (QYs) of GQDs are mostly at a range between 2% and 22.9% [60], which is much lower than the traditional semiconductor QDs. Thus the low QYs presented a challenge. Recent researches showed that the QYs of GQDs can be enhanced by surface modifications, such as the

formation of carbon-metal nano-composites [61]. In addition, the electronic and optical properties of GQDs, such as band gap [62] and fluorescence [63,64] etc., are dependent on their sizes and shapes. Therefore, the modulation of the intrinsic properties of GQDs is dependent on the accuracy in controlling its sizes and shapes etc. Conditions of fabrication methods are keys to solving this issue. GQDs have displayed various unique phenomena, such as up-conversion PL [65–67]. However, the current mechanisms were mainly acquired according to the optical behaviors leading to confusing results due to the different preparation conditions, hence there is a lack of understanding on the exact PL mechanism. Consequently, some forms of standard measurements coupled with theoretical studies should be carried out to better understand the PL phenomenon. To date, most of the reported PL colors of GQDs were ranged from blue to yellow [60]. The narrow spectral coverage of GQDs is limiting its applications in optoelectronic devices. The expanding of the spectral coverage of GQDs to all visible wavelengths and even near-infrared (NIR) is an important area of research in the future. Some groups [27,68,69] have obtained the NIR PL spectrum by doping nitrogen into GQDs.

The future of GQDs is more promising once the above challenges have been solved. In this review, we discuss the current preparation methods of GQDs in Section 2, and the functionalization of GQDs, such as heteroatoms doping, sizes and shapes controlling and forming its composite with other functional materials, in Section 3. In Section 4, some applications related to GQDs will be reviewed. Finally, a conclusion will be presented.

2. Preparation methods for graphene quantum dots

According to the current fabrication methods of GQDs as reported in literatures, the syntheses of GQDs can be classified into two main categories, namely top-down and bottom-up preparation approaches. As shown in Fig. 4, top-down approach involves direct cleaving of bulk carbon materials into nanoscale GQDs via liquid exfoliation and electron beam lithography techniques etc. Such approach has the advantages of abundant raw materials and would usually produce oxygen-containing functional groups at the edge, thus facilitating their solubility and functionalization. However, this approach has also suffered from some disadvantages, such as low yield, large density of defects, and non-controllable of size and shape and so on. While as the bottom-up approach is based on the growth of appropriate molecular precursors, such as small molecules and polymers, into nano-sized GQDs by hydrothermal, microwave-assisted hydrothermal, soft-template and metal-catalyzed methods etc. Such bottom-up approach possesses advantages, such as fewer defects and controllable of size and morphology; contrary to the top-down approach. However, the bottom-up approach has suffered from poor solubility, small dot size and aggregration issue *etc*. In the next context, detailed preparation methods are presented. Bottom-up methods will be presented first and then followed by top-down.

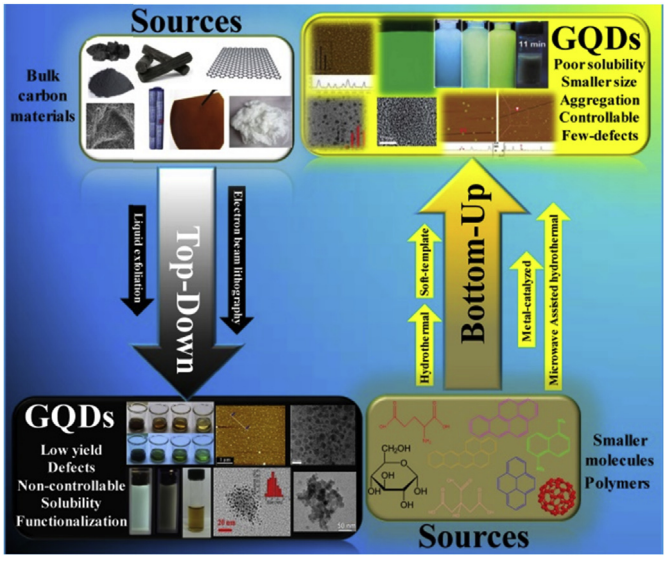

Fig. 4. The categorized illustrations on the various preparation methods of GQDs.

2.1. Bottom-up methods

As previously mentioned, bottom-up methods are based on growth of the sources including graphene-like smaller polycyclic aromatic hydrocarbons (PAHs) and appropriate molecules into GQDs. However, this method can be subdivided into four main routes, which cover hydrothermal method, microwave-assisted hydrothermal method, soft-template method and metal-catalyzed method, according to the way external energy is provided and the characteristics of fabrication.

2.1.1. Hydrothermal method

Hydrothermal method involves various techniques of crystallizing substances from high-temperature aqueous solutions to high vapor pressures. The fabrication of single-crystalline GQDs through the hydrothermal method has been demonstrated by many research groups. In early 2012, Dong et al. [69] successfully fabricated GQDs, having a size of ~15 nm, using citric acid (CA) as source in the hydrothermal method that produced a photoluminescence (PL) quantum yield (PLQY) of 9.0%. The mechanism of synthesizing GQDs using CA via hydrothermal method is depicted in Fig. 5a. The atomic force microscopy (AFM) image of GQDs prepared by Dong and co-workers is displayed in Fig. 5b, which indicated that the GQDs were mostly nano-sheets of ~15 nm in size with height in the range of 0.5–2.0 nm. Using CA and ethylenediamine (EDA) as carbon source materials, Yang's group [70] successfully produced nitrogen doped GQDs (N-GQDs) with a size of 5–10 nm, which exhibited relatively high PLQY of 75.2%. They suggested that the high PLQY was possibly due to two factors: the higher production yield (60%–70%), and the large number of surface defects, groups and edges from N-doping using EDA. Below is an equation related to the PLQY, which is expressed as [75,76]:

$$\Phi_{\chi} = \Phi_{st}\left(K_{\chi}/K_{st}\right)\left(\eta_{\chi}/\eta_{st}\right) \quad (1)$$

where Φ is QY, K is the slope determined by the curves, η is the refractive index of the solvent, st refers to a standard with known quantum yield and χ indicates unknown samples. For the aqueous solution, η_{χ}/η_{st} was 1. Besides, Dong [71] et al. also prepared the N-GQDs using CA as precursor, and the resultant size was between 2 and 8 nm as indicated by the TEM image of the N-GQDs shown in Fig. 5d. The fringes of the carbon lattice can be clearly seen in the inset of Fig. 5d. Additionally, Chen and co-workers [77] fabricated amine-functionalized N-GQDs using CA and tris(hydroxymethyl) aminomethane (Tris-HMA), and its PLQY was 59.2%. CA as precursor has been widely adopted in the growth of GQDs using hydrothermal method [78,79].

Apart from CA, some graphene-like smaller polycyclic aromatic hydrocarbons (PAHs) can also be used as precursors in the preparation of GQDs. The GQDs emitting bright green fluorescence with high yield of 63% were synthesized with pyrene via hydrothermal method by Wang et al. [72]. Fig. 5e depicts the

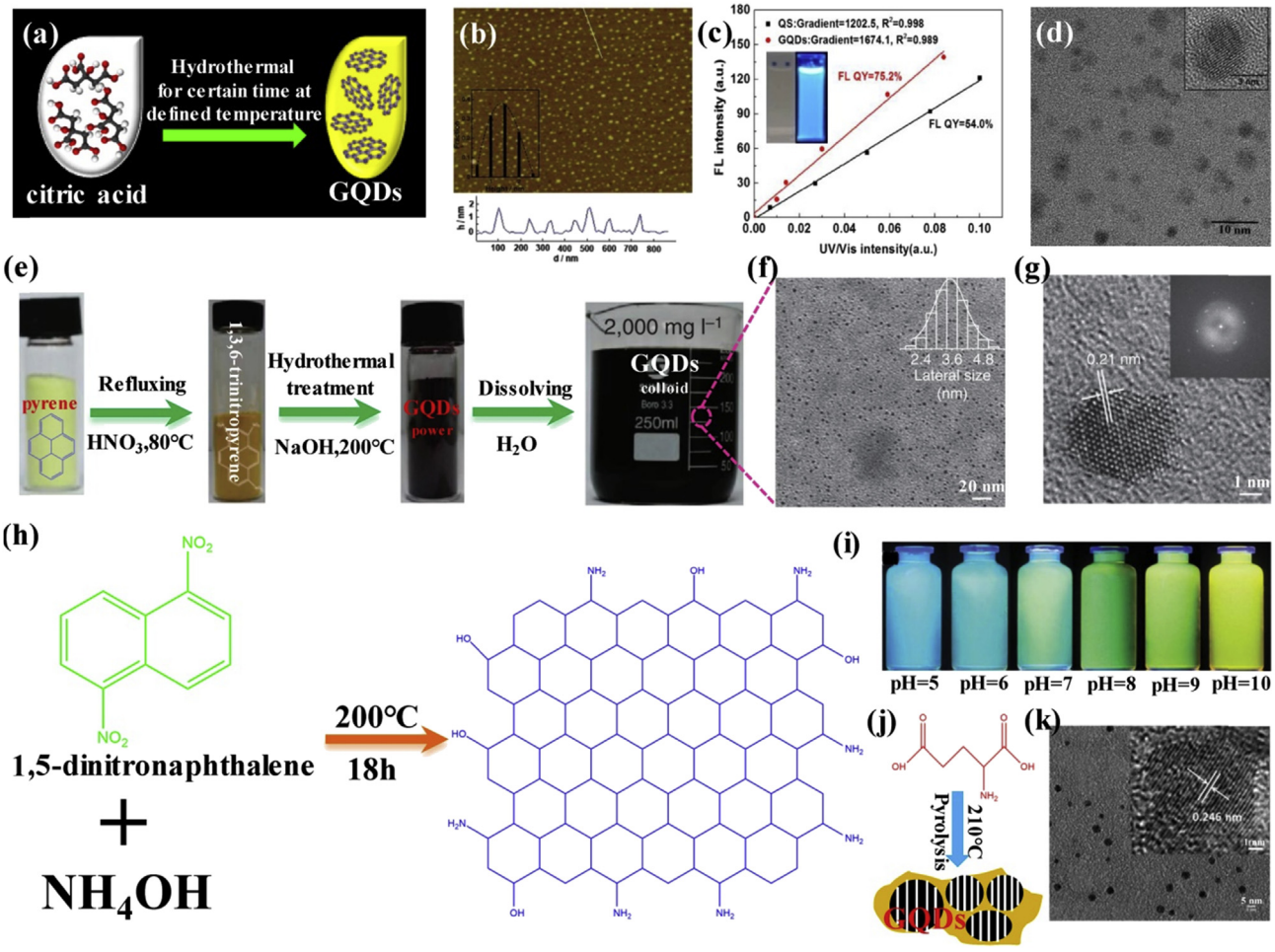

Fig. 5. The hydrothermal method based multifarious precursors. (a) The schematic diagram of the preparation of GQDs via hydrothermal method with certain time and temperature based on the source of citric acid (CA); (b) The AFM of the GQDs synthesized by using the CA [69]; (c) Fluorescence (FL) intensity and UV–vis intensity of the N-GQDs fabricated by using CA (excited at 365 nm), the inset shows photography of the N-GQDs in aqueous solution under visible light (left) and 365 nm UV light (right) [70]; (d) TEM image of N-GQDs prepared by using CA, inset is high-resolution transmission electron microscopy (HRTEM) [71]; (e) Synthetic procedure of OH-functionalized GQDs (OH-GQDs) based on the source of pyrene via hydrothermal treatment [72]; (f) and (g) show the TEM and HRTEM image of GQDs prepared by using pyrene, respectively. The insets of (f) and (g) are lateral size distribution and fast Fourier transform (FFT) pattern, respectively [72]; (h) Schematic illustration of the hydrothermal synthesis of GQDs with bifunctional groups based on the source of 1,5-dinitronaphthalene [73]; (i) Digital photography of the GQDs solutions synthetized by using 1,5-dinitronaphthalene at different pH conditions under 365 nm UV irradiation [73]; (j) and (k) present the schematic diagram and the TEM image of GQDs which was synthetized through the pyrolysis of L-glutamic acid, respectively. The inset of (k) is the typical single GQDs with a lattice parameter of 0.246 nm [74].

entire procedures. The dispersion showed highly uniform lateral size as indicated in TEM of GQDs in Fig. 5f. Fig. 5g showed the defect-free GQDs with spacing of 0.21 nm corresponding to that of graphene (100) planes. Furthermore, distinguishable benzene rings, which were well arranged in a hexagonal honeycomb carbon network, can be seen in the inset of Fig. 5g. Guo's group [73] prepared GQDs with tunable PL emission by hydrothermal approach using 1,5-dinitronaphthalene as raw material as shown in Fig. 5h. Interestingly, the amine-functionalized GQDs exhibited a distinct tunable PL emission from bluish green to yellow by changing the pH level from 5 to 10, as shown in Fig. 5i. This phenomenon can be attributed to the protonation and deprotonation of the amine-groups in acid or alkaline solutions. Broadening of the PL emission has been a challenge for previous materials. However, Zhao et al. [74] addressed the challenge by the formation of GQDs through pyrolysis of L-glutamic acid and the fabrication process is shown in Fig. 5j. The PL emission of GQDs fabricated by the raw material was tunable to NIR in the range from 800 to 850 nm. The morphology of the GQDs is shown in Fig. 5k, and high crystallinity of the GQDs is shown in inset of Fig. 5k. The lattice spacing was 0.246 nm similar to the characteristic spacing of graphene.

2.1.2. Microwave-assisted hydrothermal method

Hydrothermal growth of GQDs usually takes long time. Thus, a fast and effective method was exploited by assisting with microwave, so-called microwave-assisted hydrothermal (MAH) method. The previously mentioned hydrothermal usually takes several hours, thus the method is not ideal for industrial mass production of GQDs. It is possible to shorten the growth duration of GQDs to a few minutes or even seconds by assisting with microwave.

Yang [80] co-author reported the fabrication of fluorine-doped GQDs by using MAH method and the growth of F-GQDs is depicted in Fig. 6a. The high crystallinity of the F-GQDs with an in-plane lattice spacing of 0.214 nm is shown in the HRTEM image (Fig. 6c). According to the size distribution, the size of F-GQDs was 2.38 ± 0.04 nm by Gaussian fitted calculation. The PL of F-GQDs was shifted to green (seen in Fig. 6b) as compared to simple GQDs, though the size of the prepared F-GQDs was much smaller than that of most GQDs. According to their analysis, the red-shifted PL might be ascribed to the

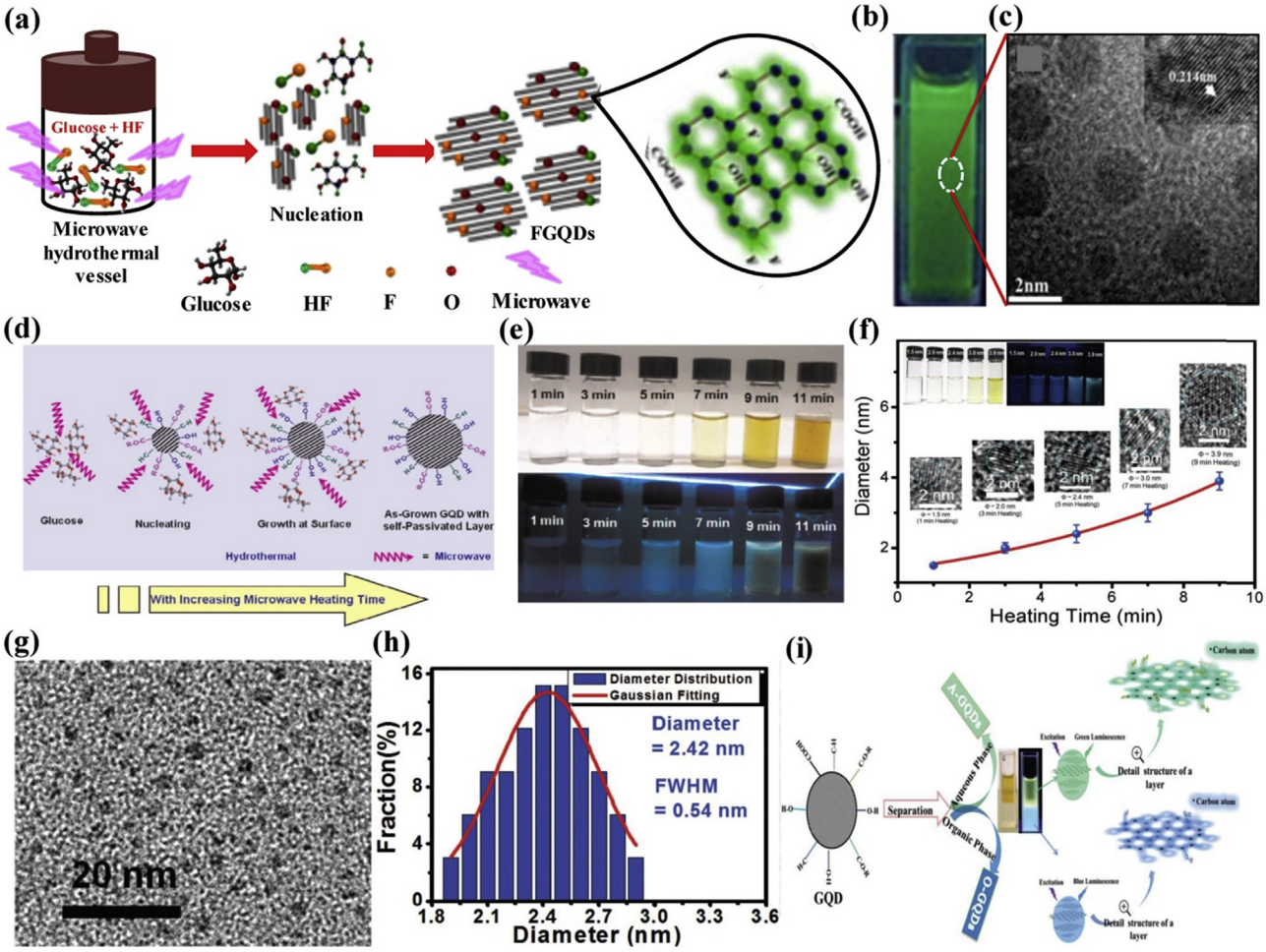

Fig. 6. Preparation and related analysis of GQDs prepared by microwave-assisted hydrothermal. (a) Microwave-assisted hydrothermal growth process of GQDs [80]; (b) Digital photography of the aqueous F-GQDs under the 360 nm UV illumination [81]; (c) HRTEM image with observed lattice fringe of GQDs prepared by MAH route [80]; (d) and (e) show the growth mechanism of GQDs with the heating time and the GQDs solutions irradiated by ambient light (top) and 365 nm UV lamp (bottom), respectively [81]; (f) The diameter of the GQDs as a function of microwave heating time, the top inset shows the photographs of the GQD solutions prepared at various heating times irradiated by ambient light (top left) and 365 nm UV lamp (top right). The bottom inset shows the corresponding TEM images of the GQDs prepared at various heating times [63]; (g) and (h) present the TEM and the diameter distribution of GQDs, respectively [81]; (i) Schematic and the corresponding photographs of the interface separation process and detailed structures of the obtained A- and O-GQDs [82].

doping of fluorine. The relationship between size of GQDs prepared by MAH method and the heating time was studied by Tang [63,81] et al. As shown in Fig. 6d, the glucose molecules dehydrated to form nucleation crystal of GQDs in the first step, and then the glucose and chemically active functional groups attached at the edges or the surface of growing GQDs. Finally, as-grown GQDs with certain size were prepared at different duration of microwave heating. Fig. 6e shows a series of GQD solutions, which were prepared by various heating times, irradiated by the ambient (top) and UV lamp (bottom). The emission color of the solutions are obviously changed. To understand this phenomenon, the diameter of the GQDs as a function of heating time was characterized using TEM and the curve plotted in Fig. 6f. The diameter of the GQDs increased monotonically from 1.5 to 3.9 nm when the heating time increased from 1 to 9 min, therefore increasing the heating times would lead to further growth of the GQDs. Moreover, the MAH method provided GQDs with uniform size distribution as shown in Fig. 6g and h. Feng et al. [82] also synthesized the GQDs and separated the A- (aqueous phase) and O- (organic phase) GQDs) by inducing the solvent. The whole separation of GQD solution and related structure of A- and O-GQDs is represented in Fig. 6i. Zhao and co-workers [83] obtained the oxygen-rich GQDs by MAH method and the level of doping with nitrogen was at 5.7%.

Hence, the MAH method combined the advantages of both hydrothermal and microwave techniques. The microwave heating provides simultaneous, homogeneous and fast heating, which has led to uniform size distribution of quantum dots and non-surface passivation.

2.1.3. Soft-template method

A novel method, known as soft-template, was developed for facile, low-cost and environmental friendly fabrication of GQDs. It provides nanoscale reaction cavity without complicated separation and purifying processes. Therefore, this route is in favor for mass production.

Yang and co-author [84] prepared GQDs by the soft-template approach. The TATB which is a planar and highly symmetric molecule with six strong intramolecular hydrogen bonds between $-NH_2$ and $-NO_2$ functional groups, and possesses a graphitic-like layered structure was used as the carbon source and template. Firstly, the TATB was annealed in the thermal process, which resulted in breaking down of various chemical bonds, along with the generation of expanding gases (e.g., NO, NO_2, and H_2O). Subsequently, the graphitic-like TATB multilayer developed into single layers as a result of the expanding gas. Finally, oxidative exfoliation

was employed to obtain dispersed N-GQDs. The preparation process of GQDs using TATB is displayed in Fig. 7a. Morphology and size of GQDs via the soft-template route using TATB is as shown in Fig. 7b. The AFM image shows well-dispersed and few-layer GQDs. One of the main advantages of soft-template method is controllable uniform size of GQDs. Müllen's [26] research group achieved monodispersed disk-like GQDs of ~60 nm using HBC as precursor via the soft-template method. Detailed steps on the preparation are shown in Fig. 7c. The HBC molecules were condensedly stacked followed by the formation of a graphitic framework with fewer defects during the pyrolysis step. Subsequently, the artificial graphite was oxidized and exfoliated with a modified Hummers method, and then reduced with hydrazine. Finally, the GQDs prepared by using HBC as template was obtained. Homogeneous nanodisks of ~60 nm in diameter and 2–3 nm in thickness were observed from the AFM image (seen in Fig. 7d and e). These GQDs demonstrated strong blue PL emission under excitation at 365 nm as shown in Fig. 7f. Apart from using the polymer as template, some small molecules were also used. For instance, Gao and co-workers [85] utilized small molecular carbon disulphide as template to fabricate GQDs doped with sulphur. As shown in Fig. 7g, the mixture liquid was burnt to form the carbon powder, which was then exfoliated to GQDs. The uniformity and dispersity of the GQDs were characterized by TEM (seen in Fig. 7h) showing an average diameter of 2.46 nm according to statistic calculation from Fig. 7i. Besides, Do et al. [86] used CA as the template to synthesize GQDs, which demonstrated high-quantum yield of 83%. It is worth mentioning that the PL intensity in a long-wavelength range (>500 nm) was observed to increase with increasing nitrogen content.

In brief, the soft-template can be a candidate for solving at least one of the challenges of GQDs, such as low-product yield.

2.1.4. Metal-catalyzed method

Metal-catalyzed method is a scarce route for preparation of GQDs. Loh et al. [28] utilized ruthenium as metal catalyst and used C_{60} as a precursor to synthesize GQDs (seen in Fig. 8a). Interestingly, this method can modify the shape of GQDs by the annealing temperature, as shown in Fig. 8b–c. The scanning tunnelling microscopy (STM) measurement was carried out on the GQDs grown on the surface of Ru (0001) at different annealing temperature for certain duration. The triangular and hexagonal shaped GQDs were obtained by annealing at 725 K and 825 K for 2 min respectively, as shown in Fig. 8d–g. However, special structure of raw material and metal-catalyst were necessary for the fabrication of GQDs using this method, thus this route is uncommon.

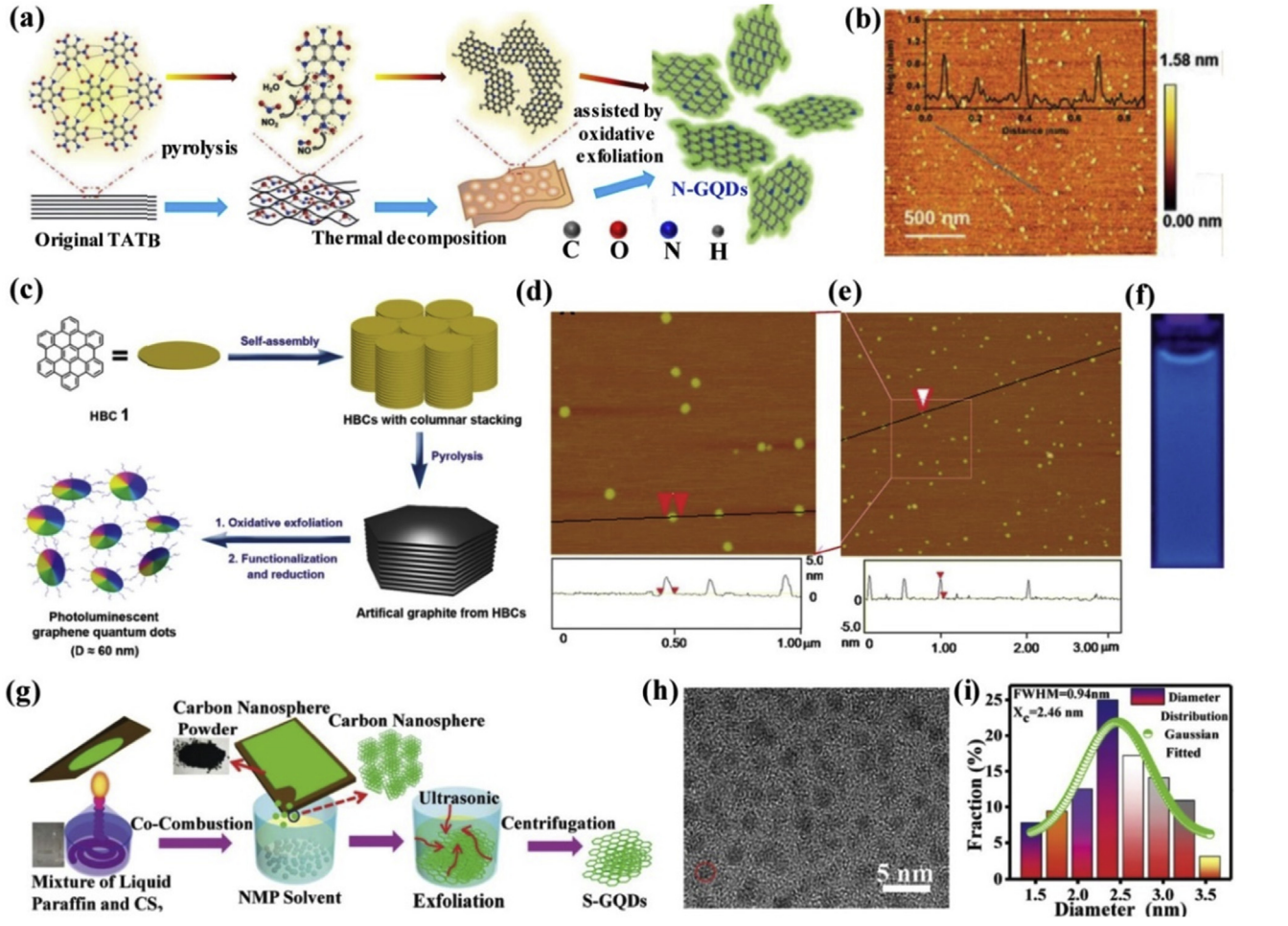

Fig. 7. Schematic diagrams and related characterized results of GQDs by using soft-template approach. (a) Illustration of the formation process of GQDs from single-layer 1,3,5-Triamino-2,4,6-trinitrobenzene (TATB) intermolecular condensation by soft-template route [84]; (b) AFM image of GQDs which was synthesized by using TATB deposited on a freshly cleaved mica surface. Inset: height profile along the dark line in the AFM image [84]. (c) Processing diagram for fabrication of GQDs via soft-template method based on the carbon source of Hexa-peri-hexabenzocoronene (HBC) [26]; (d–e) and (f) AFM topography images of GQD prepared by using HBC and height profiles along the line in the images, and optical photograph obtained under excitation at 365 nm UV lamp, respectively [87]; (g) Schematic representation of the GQDs prepared by soft-template route [85]; (h) and (i) show the TEM and diameter distribution of GQDs fabricated by former method, respectively [85].

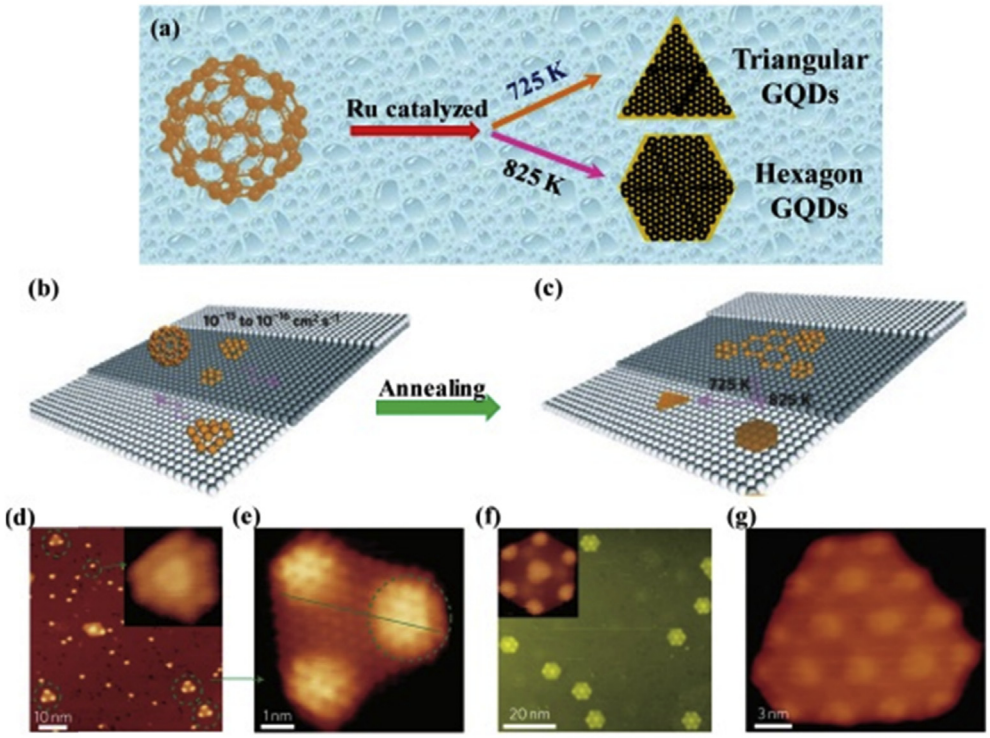

Fig. 8. Illustration and STM image of transformation of GQDs through C_{60} by metal-catalyzed method. (a) Schematic diagram of Ru metal catalyzed cage-opening for C_{60} under different temperatures; (b–c) The majority of C_{60} molecules adsorbed on the terrace and temperature-dependent growth of GQDs with different equilibrium shapes from the aggregation of the surface diffused carbon clusters; (d) STM image of C60/Ru sample after annealing at 725 K, inset shows magnified view of mushroom-shaped dots. (e) Magnified views of triangular from (d); (f–g) Hexagon-shaped GQDs obtained after further annealing the sample at 825 K [28].

2.2. Top-down methods

An opposite route of the bottom-up method is top-down method, according to the relationship between precursors and products. Top-down approach usually fabricates the GQDs by breaking down the bulk material by physical or chemical means. The first GQDs was developed using this approach, thus top-down routes is very effective in the discovery of new materials and research of its structure and properties. Among top-down routes, liquid exfoliation method, by means of hydrothermal, electrochemical, oxidation and ultrasonic etc., and electron beam lithography method are commonly used routes. There are other less common routes, such as magnetron sputtering technique, which will also be described in this section.

2.2.1. Liquid exfoliation method

Nowadays liquid-phase exfoliation is often used for the preparation of graphene, where intercalation of graphite was performed using strong oxidizing agents, followed by expansion of graphite layers via thermal or chemical techniques. Such synthesis approach has increasingly been used in the preparation of GQDs by many groups [87–91]. The preparation of GQDs usually required the use of acid in cutting graphene, as shown in Fig. 9a. Wu and co-workers [16] produced GQDs that demonstrated blue luminescent via the liquid exfoliation route. The GQDs exhibited uniform size distribution with new PL results. Bulk carbon materials have been used in the synthesis of GQDs. For instance, carbon fibers (CF) was used as the precursor in the preparation of GQDs by Peng's [21] liquid exfoliation approach, as shown in Fig. 9b. AFM measurement indicated that the GQDs were consisting of 1–3 graphene layers (seen in Fig. 9c). Their results also showed that the PL emission color was influenced by the synthesis temperature. Besides, Tour et al. [24] managed to increase the product yield of GQDs through the use of coal via the same method as shown in Fig. 9d.

Similarly, Li [92] used coal for the preparation of GQDs. Fig. 9e shows the morphology and single crystalline of the GQDs. However, there was nonuniformity in the size distribution of the GQDs as observed from the TEM image, which could be caused by the fabrication conditions. On the other hand, graphite [97,98] has been considered the best source in the preparation of GQDs. Wang and co-authors [93] fabricated GQDs by sonication of graphite in liquid. Fig. 9f shows the complete preparation process of the GQDs based on the use of graphite as source. The TEM image of the GQDs showed an average lateral size of 2.5 nm (Fig. 9g), and the HRTEM indicated good crystallinity of the GQDs with lattice spacing of 0.335 nm corresponding to the c-axis orientation, as shown in Fig. 9h. Similar experiment was also carried out by Pei et al. [96] A more facile route was recently developed by Zuo and co-workers [94]. As shown in Fig. 9i, cotton was first annealed and then followed by liquid exfoliation. GQDs doped with fluorine were subsequently obtained. Similar shape of PGNFs to the CF can also be used as the source for GQDs in liquid exfoliation method, as demonstrated by Li's [95] group. The SEM image in Fig. 9j shows high-purity platelet graphite nanofibers (PGNFs) with diameters of ~10–40 nm and zigzag-like surfaces. The TEM images of the prepared GQDs are shown in Fig. 9k and l. The C–C bond length in the GQDs was 0.146 nm which is close to the ideal C–C bond length for graphite (0.142 nm). The GQDs also exhibited good crystallinity as indicated in the inset of Fig. 9l. Similar to Zuo' work, Zhao and co-authors [99] also used the cotton as the carbon source in the preparation of GQDs. The difference was the use of chlorine as dressing agent, thus the GQDs were doped with chlorine (Cl-GQDs) showing many distinctive properties from pure GQDs, such as the

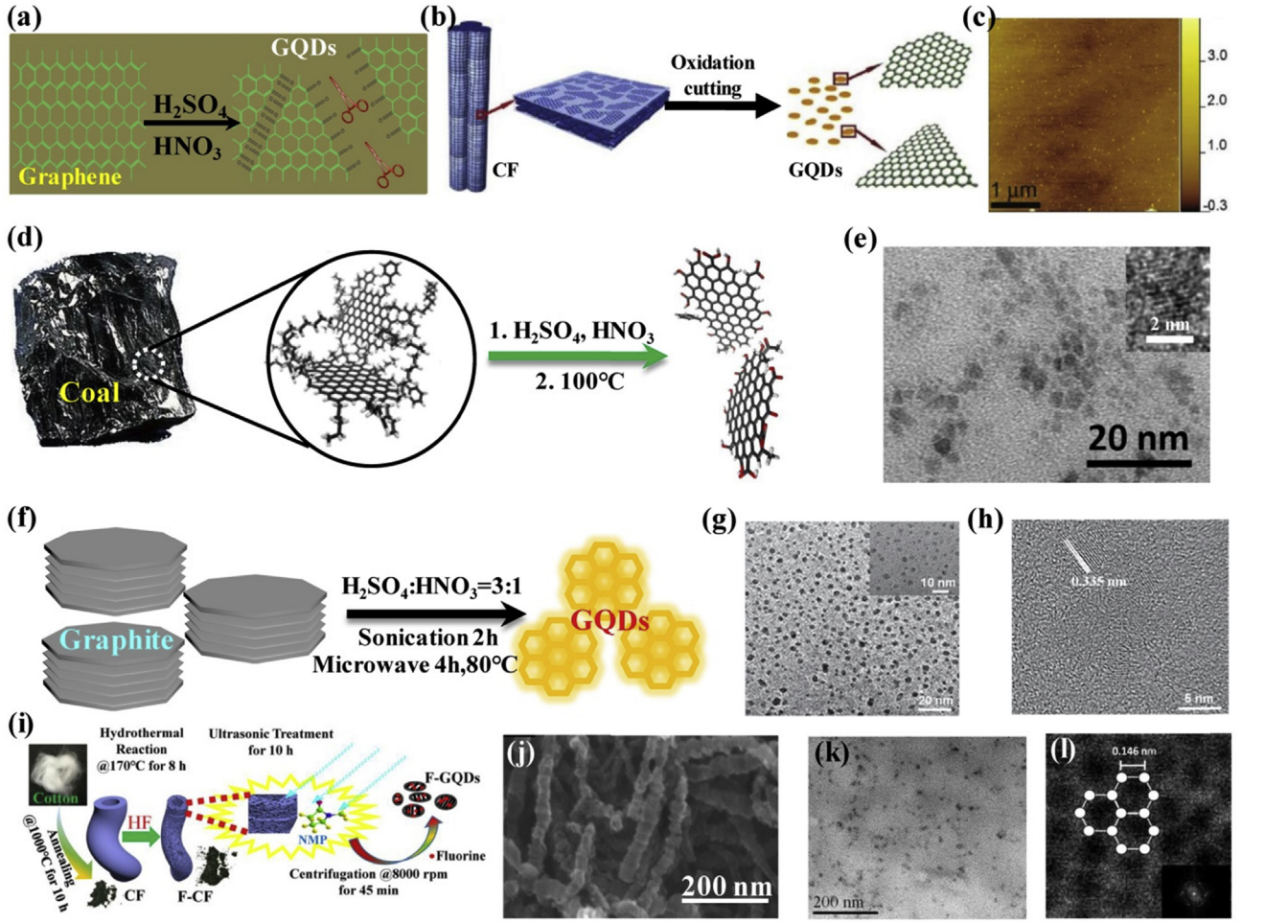

Fig. 9. Diagram and corresponding measured image of the GQDs by using different sources via liquid exfoliation approach. (a) Illustration on the formation of GQDs by cutting graphene in the acid environment, commonly used the mixture of H_2SO_4 and HNO_3; (b) Representation scheme of the transformation of GQDs through oxidation cutting of carbon fibers (CF) [21]; (c) AFM image of GQDs by cutting CF [21]; (d) Schematic illustration of the synthesis of GQDs by using coal [24]; (e) TEM image of the GQDs by using coal via liquid exfoliation method, the inset is the HRTEM image of the GQDs [92]; (f) Schematic presentation of the preparation of GQDs by sonication-assisted liquid exfoliating graphitic carbon precursor [93]; (g) and (h) show TEM and HRTEM images of GQDs prepared by sonication-assisted exfoliation route, respectively (the inset in panel (g) is the magnified TEM image of GQDs) [93]; (i) Illumination of entire fabricated process of GQDs through the cotton [94]; (j) SEM image of platelet graphite nanofibers (PGNFs) [95]; (k) and (l) display the TEM of GQDs by using PGNFs, the inset of (l) represents a FFT pattern [95].

intensity and peak of UV–vis absorption. The overall fabrication process of GQDs is shown in Fig. 10a. Apart from 3D graphite, 2D graphene and 0D fullerene, the 1D carbon nanotube can also be cut into GQDs. In the reported work of Dong et al. [20], SWCTs with an average diameter less than 2 nm and a length of 5–15 μm were cut by means of chemical oxidation using a three-step sediment to form the GQDs1 and GQDs2 respectively, as shown in Fig. 10b. Interestingly, the aqueous solutions of GQDs1 and GQDs2 were yellow under white light, but their UV–vis absorption spectra are dissimilar (seen in Fig. 10h). Among the optical properties of GQDs1 and GQDs2, their PL characteristics were obviously different.

However, the former liquid exfoliation assisted both the hydrothermal and chemical oxidation. A new technique, known as electrochemical exfoliation, was recently introduced to the liquid exfoliation method. Huang and co-workers [100] used the electrochemical workstation to prepare GQDs with higher product yield by using graphene paper as anode and platinum (Pt) sheet as counter electron. During the electrochemical oxidation and cutting process, the colorless electrolyte solution quickly turned black with product yield of 28% (after 120 min) in an ammonia solution because of the rapid generation of GQDs, as shown in Fig. 10c. A possible mechanism was proposed suggesting the graphene sheets or graphite flakes rapidly broke apart due to the harsh electrochemical exfoliation conditions in the strong electrolyte system, hence leading to the low yield of GQDs. However, in a weak electrolyte environment, the relatively prolonged oxidation interaction and suppressed intercalation induced exfoliation resulted in the continuous and efficient formation of GQDs, as displayed in Fig. 10d. Fig. 10e shows the TEM image of GQDs using electrochemical route, which produced homogeneous and good crystallinity GQDs. Kun and collaborators [101] also synthesized GQDs doped with boron (B-GQDs) by using CF as anode and Pt as cathode in the electrochemical workstation, as shown in the left of Fig. 10f. Their preparation process of GQDs and a detailed diagram showing the formation mechanism is represented on the right of Fig. 10f. The UV–visible absorption spectra of the above GQDs synthesized with different ratios of H_2O/IL (e.g. 0-a, 15%-b and 30%-c) is shown in Fig. 10g. A clear red shift from 265 to 348 nm was observed when the ratio of H_2O/IL increased from 0% to 30%, this was attributed to a new hydrogen-bonded network formed that resulted in a change to the internal organization and the liquid structure of the ILs. The inset of Fig. 10g shows the fluorescence of GQDs solutions at different concentrations under the 365 nm lamp illumination. It showed that the PL properties were influenced by the ratio of H_2O/IL. Graphene oxide

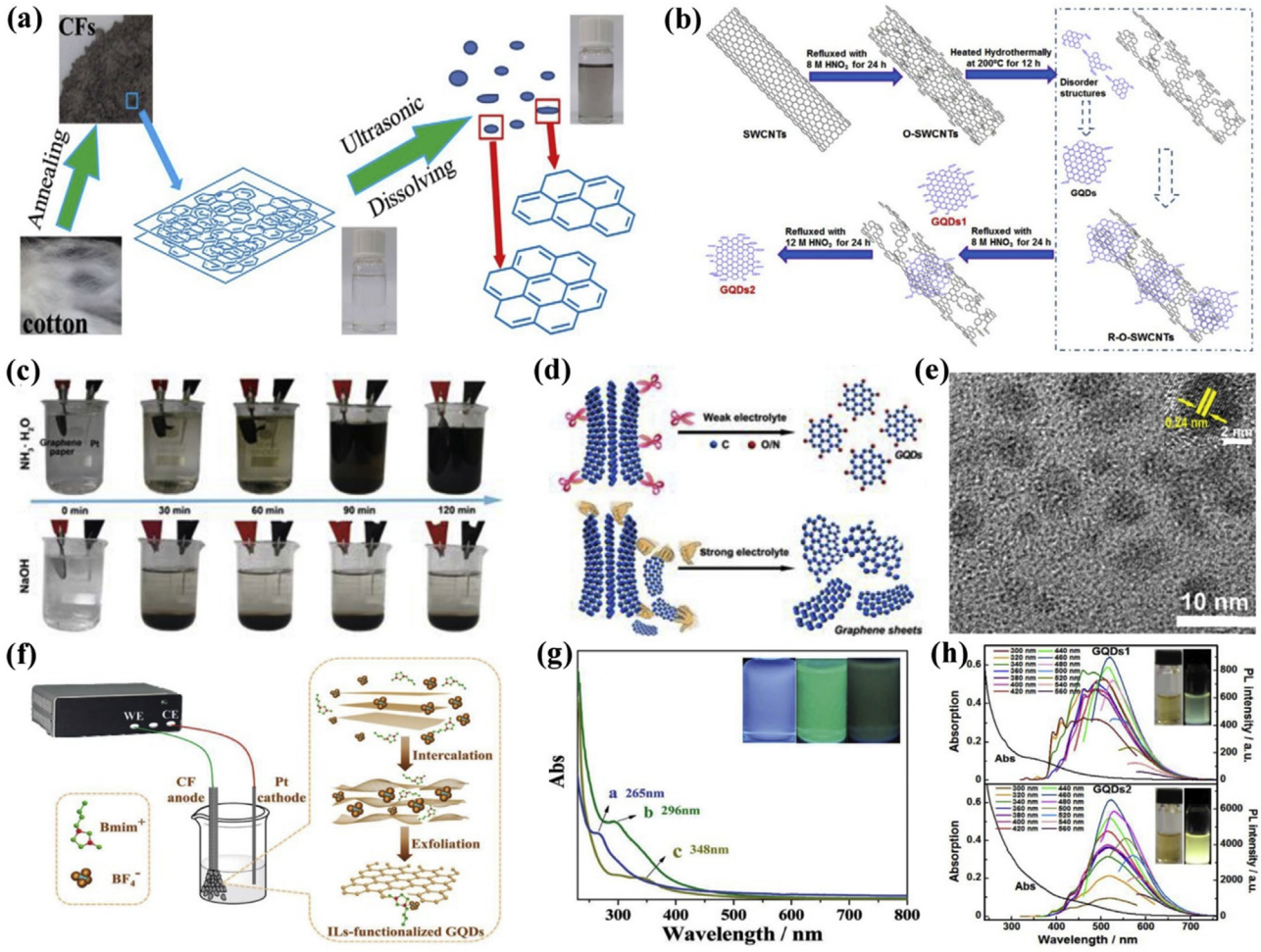

Fig. 10. Schematic illustration and corresponding measurements of the GQDs by different liquid exfoliation method. (a) Diagram illustration on the preparation process of GQDs derived from cotton [99]; (b) Schematic representation of preparation of GQDs from single-walled carbon nanotubes (SWCNTs) [20]; (c) Digital photography of the electrolytic process of graphene paper in ammonia (top) and NaOH (bottom) solutions under different reaction times [100]; (d) Mechanism illustration of the preparation of GQDs in strong and weak electrolyte solutions [100]; (e) TEM display of the GQDs derived from graphene paper via electrochemical cutting approach, the inset is the HRTEM image of the GQDs [100]; (f) Schematic diagram of the preparation of B-GQDs by using CF as precursor via the electrochemical exfoliation [101]; (g) UV–vis spectrum of the B-GQDs solution with different ratio of H_2O/1L:a-0%, b-15%,c-30%, the inset shows the photography of corresponding GQDs under UV Light with 365 nm irradiation [101]; (h) UV–vis absorption and PL emission spectra (recorded for progressively longer excitation wavelengths in 20 nm increments) of GQDs1 (top) and GQDs2 (down) in water solution. Inset: Optical photographs of GQD solutions under visible light (left) and a UV beam of 365 nm (right) [20].

has also been used as carbon source in the preparation of GQDs as shown by the work of Teng et al. [102]. The TEM image, as shown in Fig. 11a–c, indicates homogenous GQDs with good crystallinity were prepared by the liquid exfoliation method.

Generally, the liquid exfoliation route occurs in the liquid and the properties of products are often determined by the process environment and conditions. Therefore, the chemical and physical properties of the GQDs can be precisely controlled by modifying the fabrication parameters.

A novel technique, different from liquid exfoliation, was exploited in the fabrication of GQDs by Liu's [103] research group via the use of magnetron sputtering. As shown in Fig. 11d, a composite film comprising of GQDs and ZnO is formed at the substrate after magnetron sputtering on the target of graphite and ZnO composite. Subsequently, the composite film is treated with acid and then dialyzed to separate the GQDs from ZnO. Fig. 11e shows the TEM image of the highly crystalline and uniform GQDs.

2.2.2. Electron beam lithography method

Electron beam lithography method was first used in the preparation of GQDs [13]. However, it was not widely used due to the requirement of expensive equipment. Besides, the size of GQDs was limited by the processable scale of lithography technology and the diameter of GQDs was arbitrary modified. Nevertheless, this method opened up an important field of 0D carbon materials, which have so far generated great excitement within the scientific world.

Table 1 provides a summary on the related properties of GQDs produced by current state-of-the-art bottom-up and top-down methods. It is worth noting that the product yield of GQDs via bottom-up approach is generally higher than the top-down approach. Furthermore, the physical and chemical properties of GQDs can be easily modified when prepared using bottom-up approach as compared to the top-down. Also, the choice of source for bottom-up route is wider than the opposite route. In any case, the selected method would very much depend on your applications.

3. Functionalization of graphene quantum dots

Pure GQDs have many limitations which restrict its application. In order to expand its application in a variety of fields, GQDs can be functionalized by various methods to customize its properties for specific applications. Functionalization of GQDs could modify its

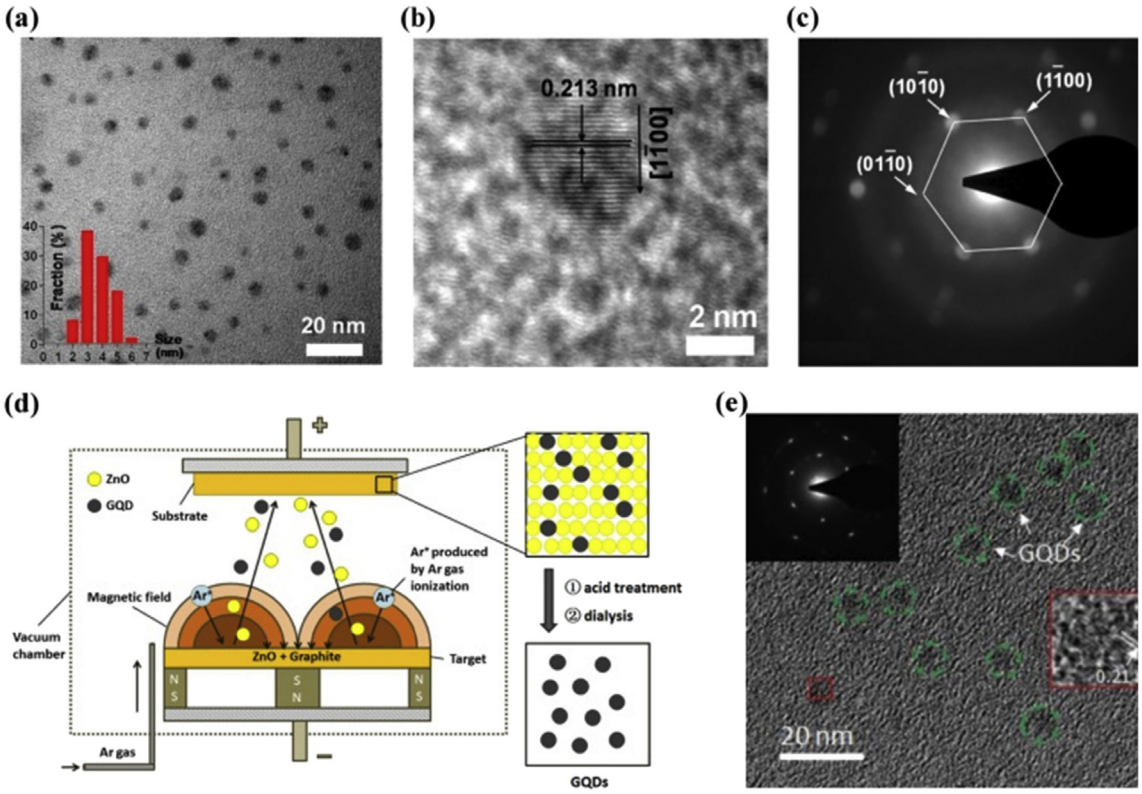

Fig. 11. Novel preparation routes of GQDs. (a–b) TEM of GQDs prepared by using graphene oxide (GO) as carbon source [102]; (c) Selected area electron nanobeam diffraction pattern of GQDs in plane (b) [102]; (d) Schematic of fabrication process of GQDs via magnetron sputtering technique [103]; (e) TEM and HRTEM images of GQDs fabricated by magnetron sputtering route, the left top inset shows the selected area electron diffraction (SAED) pattern in the red cycle of (e) [103].

Table 1
Related properties of GQDs by using the bottom-up and top-down method in state-of-the-art.

Main-methods	Sub-method	Source	Diameter (nm)	PLQY	Color of PL	Product yield	Advantages	Disadvantages	Ref.
Bottom-up	Hydrothermal	CA	~15	9.0%	blue	—	high yield, easy to dope	small size,	[69]
	Hydrothermal	CA+EDA	5–10	75.2%	blue	60%–70%		long period	[70]
	Hydrothermal	CA	2–8	34%	blue	—			[71]
	Hydrothermal	Pyrene	3.5 ± 0.6	23%	green	63%			[72]
	Hydrothermal	1,5-dinitronaphthalene	1.5	—	Green- yellow	—			[73]
	Hydrothermal	L-glutamic acid	4.66 ± 1.24	54.5%	NIR	—			[74]
	Hydrothermal	CA+Tris-HMA	0.5–4	59.2%	blue	—			[77]
	MAH	glucose	2.38 ± 0.04	—	green	—	short period, uniform size,	small size	[80]
	MAH	glycerol	1–5	—	green/blue	9.8%			[82]
	MAH	glucose	~3	5.2%	green	—			[83]
	Soft-template	TATB	2–5	—	green	—	low-cost, environmentally	aggregration	[84]
	Soft-template	HBC	59.6	~3.8%	blue	—	friendly		[26]
	Soft-template	CA	2.0	83%	blue	—			[86]
Top-down	Liquid exfoliation	graphite	6.0	3.6%	blue	—	precisely controlled	environmental	[88]
	Liquid exfoliation	GO	3.3 ± 0.7	0.9%	green	—		disruption, non-	[89]
	Liquid exfoliation	graphite	3–4	22.3%	blue	—		uniform size	[90]
	Liquid exfoliation	graphite	5.6	13.6%	blue	—			[91]
	Liquid exfoliation	coal	2.30 ± 0.78	51%	blue	20%			[24]
	Liquid exfoliation	coal	4.7	47.0%	blue	25.6%			[92]
	Liquid exfoliation	graphite	2–6	2.4%	blue	3.8 mg/ml			[96]
	Liquid exfoliation	GO	2–6	12.8%	—	—			[102]
	Electrochemical exfoliation	graphene paper	3–8	46%	cyan	28%	short period, homogenous and good crystallinity	low yield	[100]

optical, chemical and electronic properties, which allow the materials to be used in wide-ranging applications. As shown in Fig. 12, doping with heteroatoms, forming composites with inorganic materials or polymers, and the controlling of size and shape of GQDs can be considered as functionalization. The basic properties of GQDs are changed via those means, which could potentially address some of the challenges faced by GQDs. Research into the functionalization of GQDs remains a hot-topic in the study of carbon nanomaterials. In this section, we will introduce the various functionalization methods in the following sequence: doping with a variety of heteroatoms in Section 3.1, the controlling of size and shape to tune the properties of GQDs in Section 3.2, and lastly the improved performances of GQDs via forming composites will be described in Section 3.3.

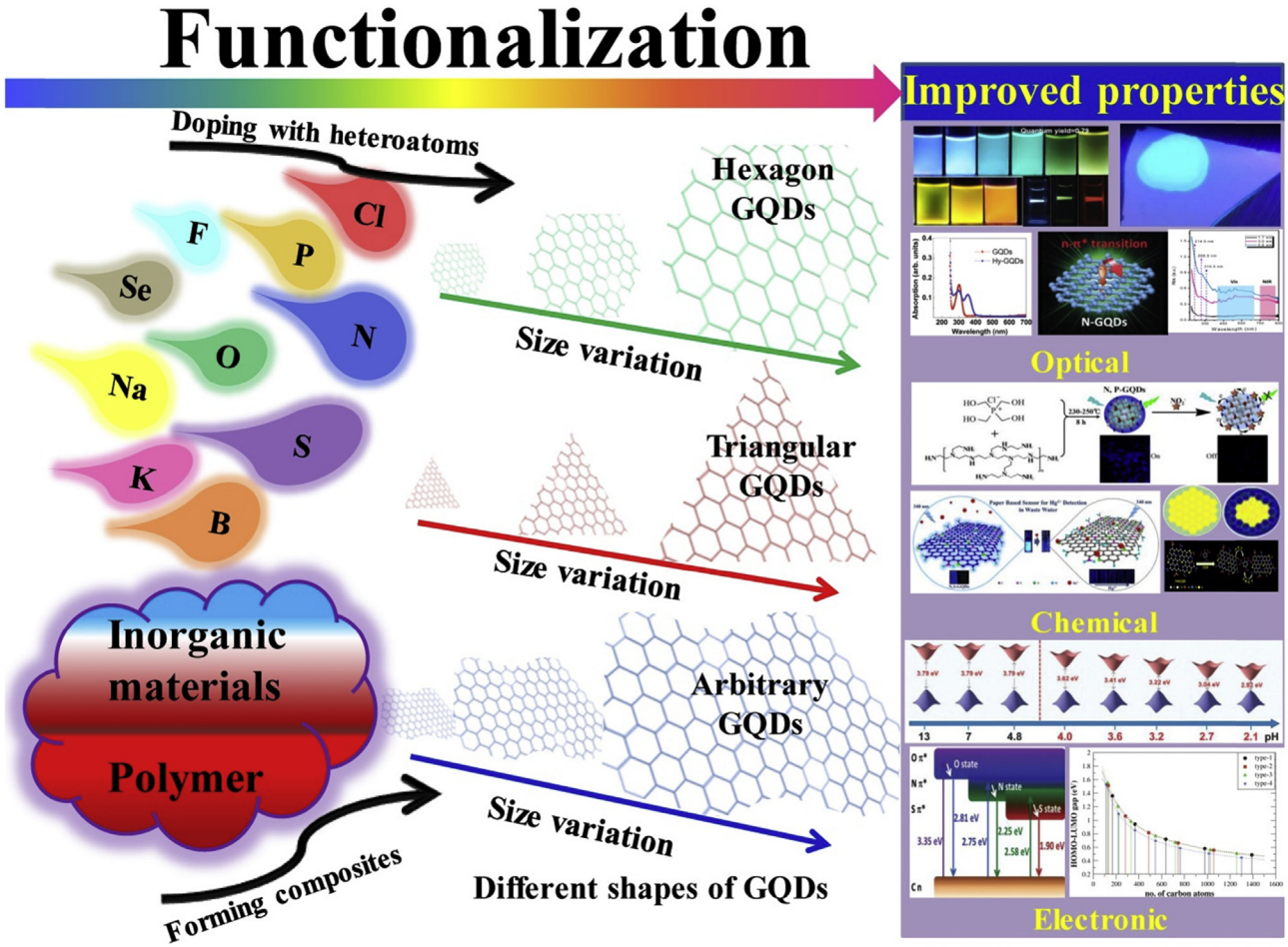

Fig. 12. Schematic diagram on the functionalization of GQDs via various methods and the improvement of GQDs properties.

3.1. Doping of graphene quantum dots via a variety of heteroatoms

Doping of semiconducting materials is an essential process in the semiconductor industry as it can modulate the basic physical, chemical and electronic properties of the materials, hence making them useful in device applications. Similarly, functionalization of GQDs by means of doping can modify its optical, electronic and chemical properties for novel applications. In general, we can categorize the doping method into three groups depending on the number of doping atoms, as shown in Fig. 13a. An effective doping can tune the optical, chemical, electrochemical and electronic etc. properties of GQDs. It is possible to characterize the effect of doping, for example, through determining the change in the color of PL, the conductivity and water solubility of the doped GQDs. The various heteroatoms doping and doping methods will be introduced in this section. The effect of doping GQDs resulting in the change of its basic properties will be described as well. To date, the heteroatoms used in the doping of GQDs include potassium (K), sodium (Na), boron (B), nitrogen (N), phosphorus (P), oxygen (N), sulphur (S), selenium (Se), fluorine (F) and chlorine (Cl), as shown in top-left diagram of Fig. 12. Besides, these atoms can be co-doped into the GQDs, which can enhance certain properties of GQDs. The change in properties could cause by the electronegativity and other basic properties of the dopant atoms. The doping of GQDs with single, double and multiple heteroatoms will be presented as follows.

3.1.1. GQDs doped with single heteroatom

Single heteroatom doping of GQDs has shown to alter the properties of the GQDs. This section will describe the changes in the properties of GQDs by doping with single atom and less emphasis is given to the doping methods.

Boron atom is near by the carbon in the periodic table, hence it can be easily introduced into the GQDs. Wang and co-workers [104] demonstrated the doping of B into GQDs via MAH method, as shown in Fig. 13b. TEM images reveal non-uniform dispersion of B-GQDs and high-quality crystalline structure as shown in Fig. 13c and d respectively. Interestingly, obvious absorption peaks ocurred at 230 nm, 260 nm and 320 nm, which was different from un-doped GQDs, are shown in Fig. 13e. The prominent peaks at 230 nm was ascribed to the transition of the π-π* aromatic sp^2 domains, while the other two weaker peaks were attributed to C=O n-π* transition. The B-doped GQDs have shown to enhance its PL intensity as demonstrated by Yang et al. [105]. They obtained high quantum yield of 95% from their B-GQDs, which were fabricated by evaporating B-GQDs borax aqueous solution. Highly intensive fluorescence of their B-GQDs under 405 nm excitation is shown in Fig. 13f–h. The B-GQDs were also synthesized by means of bottom-up approach as demonstrated by Tam and co-authors [106], as shown in Fig. 13i. The electrocatalytic activity has been enhanced by B doping into GQDs. Apart from doping GQDs with B element, Qian et al. [107] doped GQDs with K atom and the resultant absorption spectrum is shown in Fig. 13j. Two peaks were apparent at 222 nm

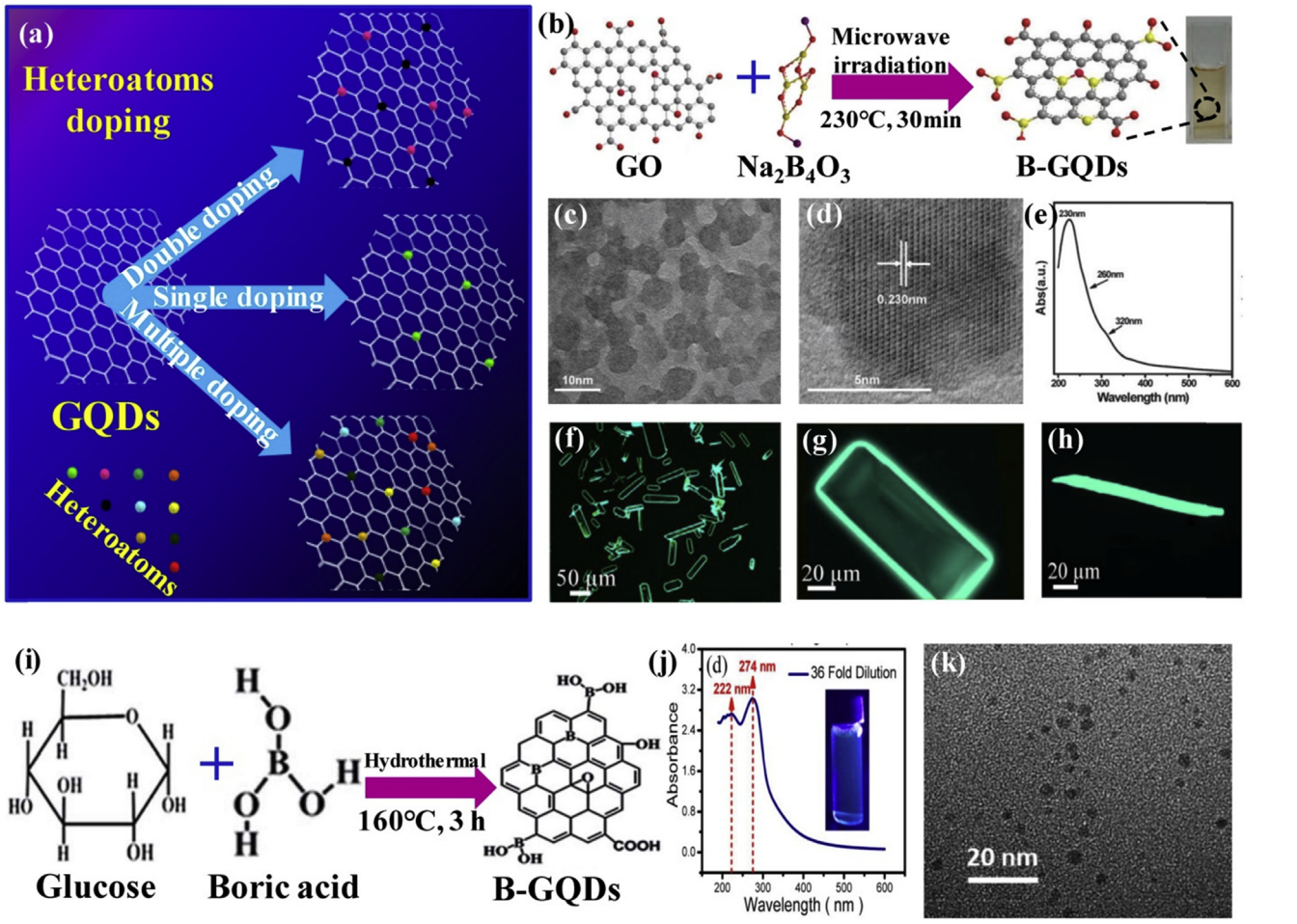

Fig. 13. Schematic diagrams of the different doping methods and results, and related proposed mechanism of single atoms doping. (a) Illustration of three kinds of doping techniques. (b) Preparation process of B doped into GQDs (B-GQDs) through GO and borax as carbon and boron source, respectively. The right picture is optical digital image [104]; (c), (d) and (e) show TEM image of B-GQDs, individual B-GQDs and UV–vis absorption spectra of B-GQDs, respectively [104]; (f–h) Fluorescence microscopy image of B-GQDs crystals obtained by evaporating aqueous B-GQDs at room temperature with different rotation directions and solutions under lighting at laser of 405 nm [105]; (i) Diagram of preparation of B-GQDs through hydrothermal route [106]; (j) and (k) show UV–vis absorption and TEM image of K doped into GQDs (K-GQDs), respectively. The inset of (j) is optical image of aqueous K-GQDs solution under UV 365 nm excitation [107].

and 274 nm, which indicated blue-shift due to K doping. The PL of K-GQDs is shown in the inset of Fig. 13j under 365 nm radiation. Similar results were also obtained by doping GQDs with Na atom as studied by Yazdi and co-workers [108]. They reported blue-shift of the absorption peaks from their Na-doped GQDs. Hence, the doping of B, K and Na into GQDs can tune the optical absorption to short wavelength and enhance its PL intensity.

Apart from the above-mentioned elements, other elements were also widely researched. Among all the elements, N atom doping of GQDs is considered the earliest [17] and widest [70,77,85,109–134] studies performed on doped GQDs. The N-GQDs were fabricated by solid-to-solid process through using melamine as carbon and nitrogen sources which were carried out by Zhu et al. [135]. The preparation process is shown in Fig. 14a. Interestingly, this method of preparation has produced high quality N-GQDs, as shown in Fig. 14b–c. Fig. 14c shows a lattice spacing of 0.24 nm from the TEM image. In addition, UV–vis absorption spectra of N-GQDs were studied, as represented in Fig. 14d. The observed three absorption peaks were due to the aromatic sp^2 domains around 210 nm, n-π^* transition absorption peak around 240 nm and band-gap transition absorption peak around 270 nm, while the long tail extending to the visible range spectrum. It is important to note that the band gap can be tuned through controlling the preparation conditions, such as doping concentration, preparation temperature and pH level. The band gap structure of N-GQDs prepared by the solid-to-solid method is displayed in Fig. 14e. The double plotted graphs showing the dependent of band gap on doping concentration and synthesis temperature is shown in Fig. 14f. From the graphs, we can deduce that the doping concentration decreased with the synthesis temperature, while the band gap was significantly influenced by the doping concentration due to the high electronegativity. Furthermore, when the N-GQDs were in an acidic environment, the graphitic N was gradually protonated and then showed a weaker negative induction effect than that of un-protonated graphitic N. This resulted in a high π electron cloud density, which led to a narrowed band gap. This phenomenon is represented in Fig. 14g, which shows the decreasing band gap of N-GQDs by reducing the pH level in the N-GQDs at a doping concentration of 5.5 at%. In addition, Sun and co-workers [136] fabricated high-crystalline N-GQDs via cutting graphene oxide (GO) precursor (refer to Fig. 14h), and the quantum yield was significantly improved to 74% through controlling the size and nitrogen doping. Microwave-assisted hydrothermal technique was used by Tang and co-workers [27] in the preparation of N-GQDs (refer to Fig. 14i), the resultant absorption peak was modified and exhibited at near-infrared region instead of situating at yellow

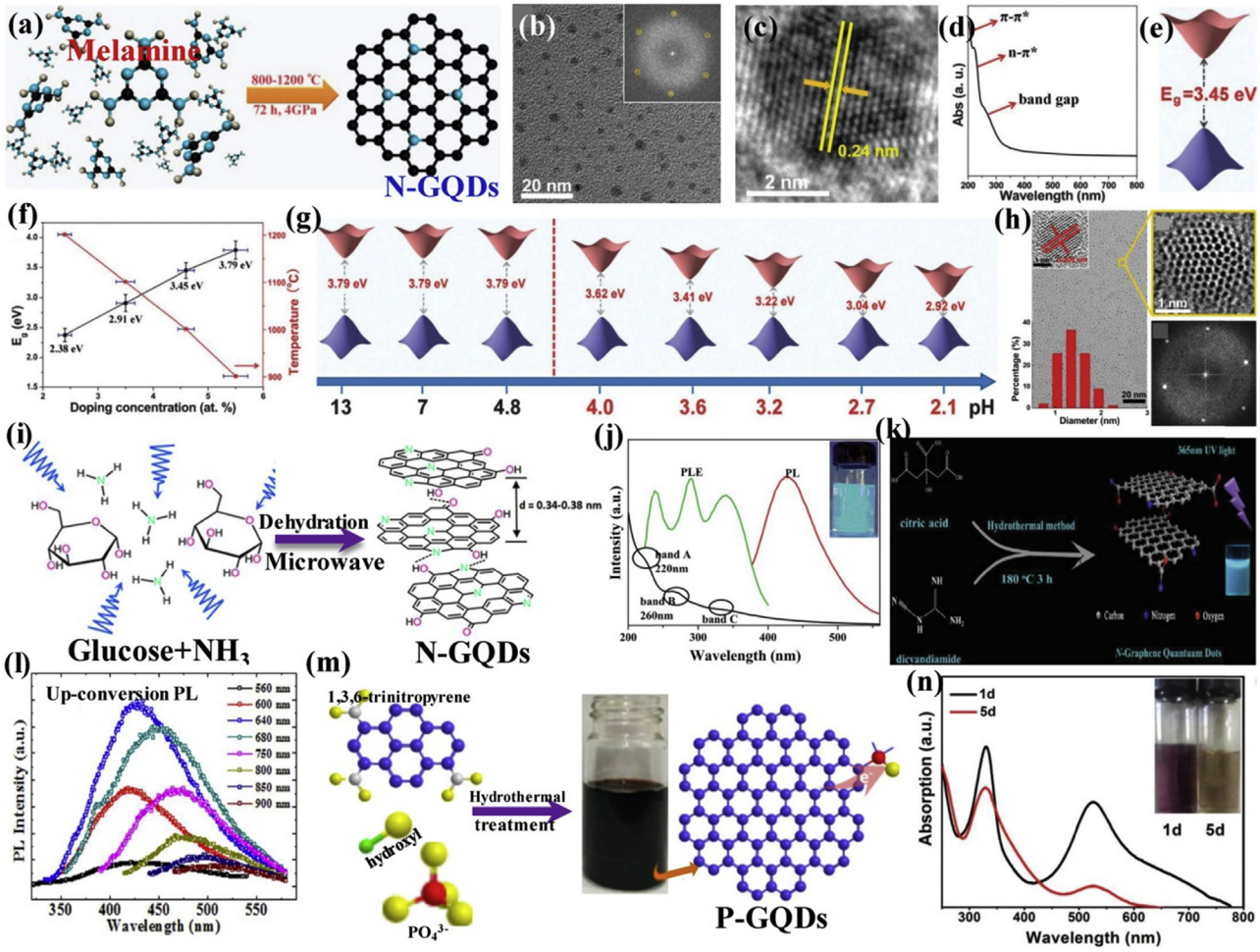

Fig. 14. Diagram of fabricated and measured results of N and P doped into GQDs. (a) and (b–c) show the preparation process schematic and TEM images of N doped GQDs (N-GQDs) [135]; (d) and (f–g) represent the UV–vis spectra and the energy band gap tuneable of N-GQDs [142]; (h) TEM display of N-GQDs via cutting graphene oxide (GO) precursor [136]; (i) Diagram illustration of N-GQDs by using microwave-assisted hydrothermal routine [27]; (j) Optical characters of N-rich GQDs, UV–vis absorption (black line), PLE spectrum (green line) and PL spectrum (red line), inset shows photograph of N-rich GQDs under UV 365 nm lighting [137]; (k) The illustration on the formation of N-GQDs by utilizing hydrothermal treatment [138]; (l) Up-conversion PL spectrum of N-GQDs at different excitation wavelength [139]; (m) Synthetic process and structural illustration for P doped GQDs (P-GQDs) [140]; (n) UV–vis absorption of the 2,2-diphenyl-1-picrylhydrazyl (DPPH) with water P-GQDs which is fabricated by electrochemical routine before (1d) and after (5d) the scavenging period, inset is the color of the DPPH before and after the scavenging period [141].

[142,143] or blue [144,145] regions. A novel metal catalytic strategy was also used to prepare N-rich GQDs by Lv's research group [137]. Fig. 14j displays the optical properties of their N-rich GQDs, which revealed excellent luminescence behavior. Huang [138] demonstrated the formation of N-GQDs via hydrothermal method using CA and dicyandiamide as carbon and nitrogen sources. Their technique demonstrated a high quantum yield of 36.5%. The strategy is illustrated in Fig. 14k. Up-conversion of PL was observed in N-GQDs prepared using hydrothermal method. This means that the emission wavelength of the N-GQDs was shorter than the excitation wavelength as studied by Li et al. [139]. The resultant PL curves for the N-GQDs are shown in Fig. 14l. An excellent quantum yield of 94% for N-GQDs was achieved by Sun and co-workers [146].

Apart from the N doping, P-doped GQDs was also studied [93]. Liu [140] fabricated P-doped GQDs (P-GQDs) having good stability and dispersion, and exhibited wide visible-light absorption region. Fig. 14m shows the synthesis process of P-GQDs. It is possible to tailor the electronic properties of P-GQDs via the process. P-GQDs can also be prepared using an electrochemical route as performed by Ma and co-workers [141] to investigate the free radical scavenging ability of P-GQDs. UV–vis absorption of the DPPH in water with P-GQDs before and after the scavenging period was measured and is shown in Fig. 14n. The inset represents the change in color of the DPPH solution from purple to yellowish which indicated the excellent scavenging ability of P-GQDs.

Group VI and VII elements were also studied for doping of the GQDs. Li et al. [147] doped the GQDs with S atom using hydrothermal method and the preparation process is shown in Fig. 15a. TEM image, shown in Fig. 15b, indicates S-GQDs with uniform size were prepared. The electron diffraction pattern of the S-GQD indicates both in-plane (d_2 = 0.213 nm) and basal plane (d_1 = 0.344 nm) diffractions, as shown in Fig. 15c. Jin et al. [148] analyzed the optical variation of S-GQDs. Fig. 15d shows the fluorescence of S-GQDs at different preparation temperatures. Strong luminescence was observed for S-GQDs prepared at a temperature of 170 °C. Their finding suggested that the excessively high temperature introduced a large number of S atoms, which subsequently covered the surface of S-GQDs resulting in the decrease of the fluorescence intensity. Moreover, the UV–Vis absorption spectra of S-GQDs were compared with undoped GQDs, as shown in Fig. 15e. For S-GQDs, there existed a new absorption peak at 350 nm, which was absent from the undoped GQDs. In addition, the intensity of the overall absorption wavelength of S-GQDs was larger than the undoped GQDs. Interestingly, Wang and co-workers [149] prepared S-GQDs using durian

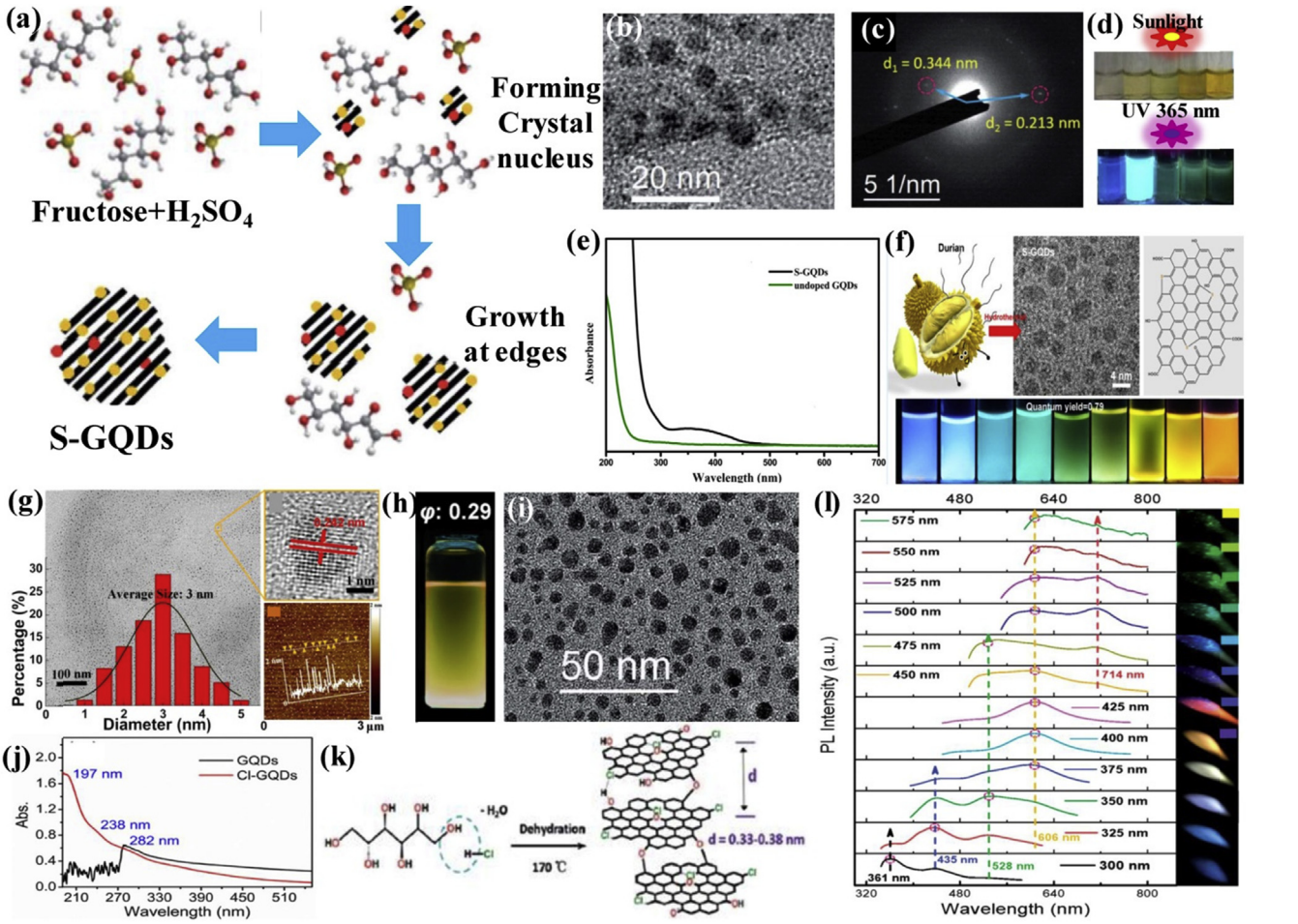

Fig. 15. Representations and resultant image of VI and VII elements doped into GQDs. (a), (b) and (c) show preparation process schematic diagram, typical TEM and electron diffraction pattern of GQDs doped with S (S-GQDs) via hydrothermal approach, respectively [147]; (d) and (e) represent the optical image of S-GQDs aqueous solution under sunlight (top) and UV 365 nm (bottom) radiation and the UV–vis absorption spectra of S-GQDs (black line) and undoped GQDs (green line), respectively [148]; (f) Diagram and some corresponding results of S-GQDs prepared by using durian as carbon and sulphur source via bottom-up method [149]; (g) and (h) are the TEM or AFM images and digital picture of PL under 365 nm excitation of Se doped GQDs (Se-GQDs) [150]; (i), (k) and (l) display the TEM image, proposed preparation process and emission spectra under different excitation wavelengths of 300–750 nm of Cl doped GQDs (Cl-GQDs) [151]; (j) UV–vis absorption spectra of Cl-GQDs and undoped GQDs solutions [99].

flesh as precursor in a bottom-up approach. TEM image of the S-GQDs and its preparation process are shown in top part of Fig. 15f. Importantly, the PL characteristics of the S-GQDs were strongly determined by the doping concentration, as shown in bottom part of Fig. 15f. The color of PL from the S-GQDs can be tuned from blue to yellow, which is distinctively different from other elemental doping. Besides, the quantum yield was high and can reach up to 79% for S-GQDs exhibiting yellow PL. Group VI elemental doping of GQDs, such as O and Se doped GQDs, were also prepared to form GOQDs and Se-GQDs. Yang and co-workers [150] prepared Se-GQDs by using GOQDs as precursors. Fig. 15g shows the uniform size and high-quality crystalline of their Se-GQDs, which displayed yellow luminescence with a quantum yield of 29% (shown in Fig. 15h). Group VII elements, such as Cl and F, were also investigated for doping GQDs. Li and co-workers [151] prepared Cl doped GQDs (Cl-GQDs) using the process shown in Fig. 15k. TEM image of the Cl-GQDs is shown in Fig. 15i. Multicolor light emission was demonstrated from the Cl-GQDs as shown in Fig. 15l. Besides, Zhao et al. [99] reported the optical absorption peaks of Cl-GQDs occurred in deep-UV unlike the undoped GQDs. Zuo and co-workers [94] prepared F-doped GQDs, however its properties were rarely studied.

In brief, single elemental doping route has been studied extensively and in great depth, but most studies have been focussed on the N-GQDs. It would be of interest to explore other doping elements.

3.1.2. GQDs doped with double heteroatom

The doping of double atoms was initiated to utilize the advantages of various doped elements and has been performed by researchers around world [160–172]. UV–vis absorption spectra of S and N co-doped GQDs (S, N-GQDs), which were prepared by Qu et al. [152], is shown in Fig. 16a. Three absorption bands were found at 338 nm, 467 nm and 557 nm, which were different from previous report. The extending absorption bands were attributed by the introduction of S and N atoms. The PL quantum yields for S, N-GQDs were 61%, 45% and 8% at wavelength of 340 nm, 440 nm and 540 nm, which represented blue, green and red emission, respectively. They explained the PL process of S, N-GQDs using the proposed mechanism shown in Fig. 16b. There were O, N, S states, which could relate to the π^* orbital of the C=O (excitation energy was above 3.10 eV), C=N (excitation energy was above 2.75 eV) and C=S (excitation energy was above 1.90 eV) bonds in the S, N-GQDs. The observed cyan light under excitation wavelength of 440 nm could due to the overlapping of the N and O states in some degree. Moreover, the S π^* orbital and S state, which were formed by introducing S doping, contributed to a weaker electronegativity. As a result, S, N-GQDs can absorb lower energy and emit light with longer wavelength. A high quantum yield of 87.8% for S, N-GQDs had been realized by using one-step bottom-up molecular fusion in a hydrothermal process [153] as shown in the diagram of Fig. 16c. The S, N-GQDs prepared by

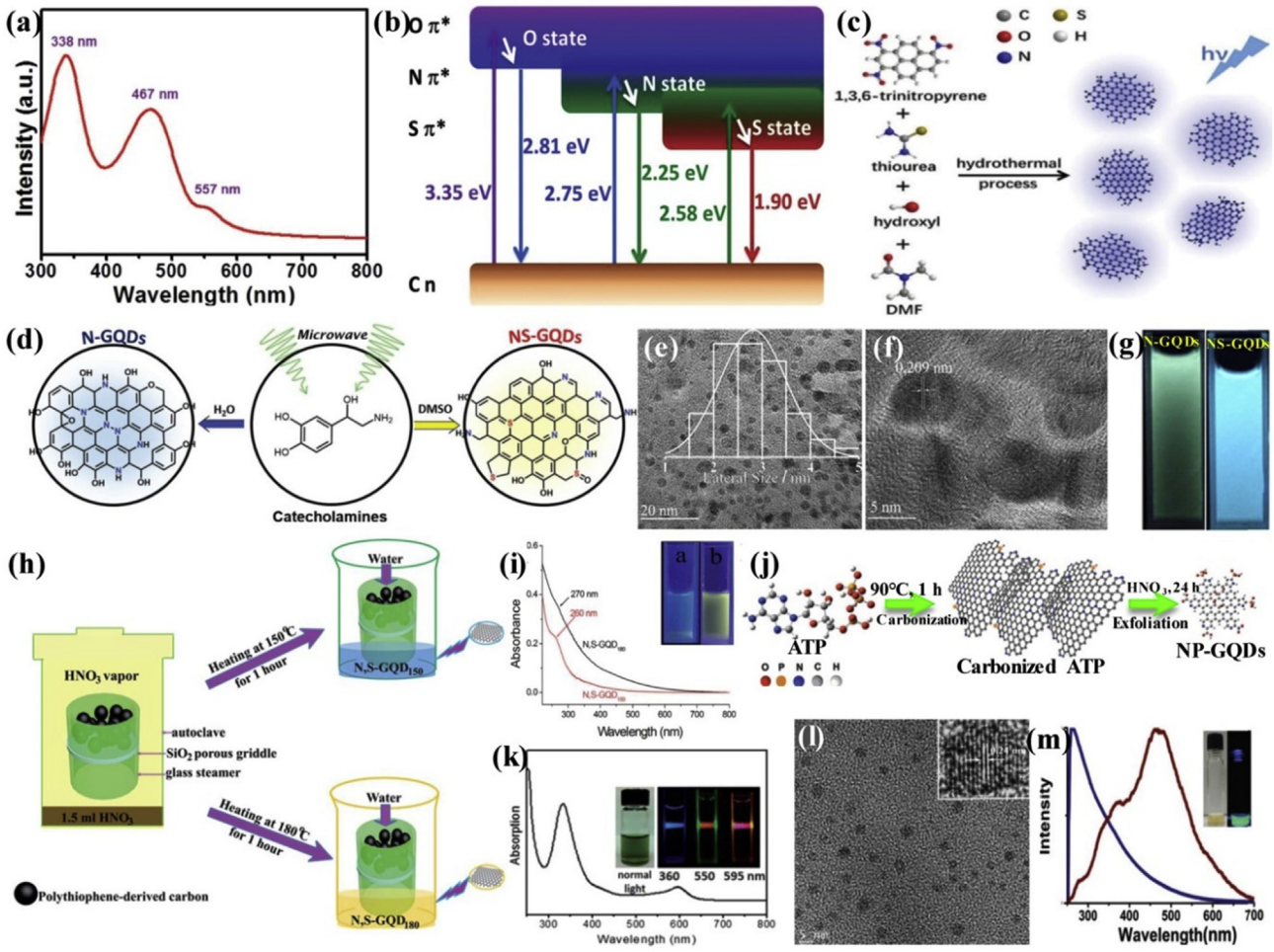

Fig. 16. Diagram, proposed mechanism and characterized results of double elements doped GQDs. (a) and (b) show UV–vis absorption and proposed energy-level diagram of S and N co-doped GQDs (S,N-GQDs) through solvothermal synthetic approach [152]; (c) Schematic illustration of the prepared S,N-GQDs by hydrothermal routine [153]; (d) Diagram of N-GQDs and S,N-GQDs by using microwave-assisted hydrothermal method [154]; (e–f) and (g) represent the TEM image of S,N-GQDs and the comparison of N-GQDs (left) with S,N-GQDs (right) under the irradiation with 385 nm wavelength, respectively [155]; (h) and (i) display the schematic diagram and UV–vis absorption spectra of S,N-GQDs with tuneable fluorescence, respectively. The inset of (i) shows the photographs of S,N-GQDs prepared with different temperatures under UV lamp lighting with 365 nm [156]; (j), (l) and (m) are illustration of the synthesis procedure, TEM image and absorption spectrum of P and N co-doped GQDs (P,N-GQDs), respectively. The inset of (m) displays the optical image of an aqueous solution of P,N-GQDs under visible (left) and UV lamp (right) lighting [157]; (k) UV–vis spectra of S,N-GQDs, the insets are digital picture of concentrated S,N-GQDs water solution and diluted solution excited at different wavelengths of light [158].

this method displayed bright blue fluorescence with quantum yield of 23.2%. They have successfully demonstrated the co-doping of S and N atoms into the lattice of GQDs. Kim's group [154] fabricated various doped GQDs by dissolving organic materials in different solvents. As shown in Fig. 16d, catecholamine was first dissolved in water and N, N-dimethyl sulfoxide (DMSO). N-GQDs and S, N-GQDs were then synthesized using microwave-assisted hydrothermal method. Besides, Li et al. [155] fabricated N, S-GQQDs via a facile, cheaper, and environmental friendly hydrothermal method using ammonia, S powder as dopant and GQDs mixed precursor. A relatively high QY of 41% was obtained from the S, N-GQDs and the TEM image on the materials showed uniform size as well as high-crystalline structure (refer to Fig. 16e–f). In addition, the PL properties of N-GQDs and S, N-GQDs were investigated. PL emission of the NS-GQDs exhibited a clear blue shift of 54 nm as compared to a red shift observed from the N-GQDs (refer to Fig. 16g). However, such findings have been debated. Interestingly, Xu and co-workers [156] used a porous polythiophene-derived carbon as the sulphur source, while HNO_3 vapor was presented as the scissor and the nitrogen source, to prepare the S, N-GQDs using the novel method, as shown in Fig. 16h. The color of PL can be modified from blue to yellowish-green by varying the synthesis temperature between 150 °C and 180 °C as shown in Fig. 16i. Qu et al. [158] demonstrated that the introduction of S atom could alter the surface states of GQDs resulting in the extension of the absorption band to visible region (refer to Fig. 16k). S, N co-doped GQDs showed different emission colors under excitation of 420–520 nm as shown in the insets of Fig. 16k. To date, the main researches have been focussed on the S, N co-doped GQDs, but P, N co-doped has been less studied. Chen's [157] research group synthesized N and P co-doped GQDs from a single biomolecule precursor via a simple strategy, as illustrated in Fig. 16j. Such P, N-GQDs exhibited high quality structure and excellent optical characteristics (refer to Fig. 16l and m respectively). As shown in Fig. 16m, the absorption band was extended and the prominent PL peak occurred at 460 nm while a shoulder peak was found at 360 nm. Such optical characteristic was attributed to the introduction of S atoms. Limited work was reported on N, B co-doped into GQDs. However, Favaro [159] and co-authors prepared N, B co-doped GQDs to enhance the electrochemical activity and they noted a clear decrease in the overpotential as a function of dopant concentration according to the sequence: N> B > B,N.

In summary, the co-doped technique was indeed able to control the properties of GQDs. However, the choice of the doping elements usually depends on the application of GQDs.

3.1.3. GQDs doped with multiple atoms

In addition to the double heteroatom doped GQDs, multiple atom doping also paly important role in some field such as batteries, solar cells and so forth. Pillai and co-workers [173] fabricated F, S, N-doped GQDs, the QY could reach up to 70%. The fabrication procedure and TEM images are presented in Fig. 17 (a–c). Another group [174] also prepared F, S, N-doped GQDs (see Fig. 17 (d–f)) and utilized them to optimize the performance of dye-sensitized solar cells with power conversion efficiency (PCE) of 11.7% ± 0.22 and a fill factor (FF) of 71 %, and a QY of 70%. The tested properties of the solar cells can be seen in Fig. 17 (g). In a word, the multiple atom doped GQDs is an interesting approach, it should be extensively studied in the future. Fig. 18 is a plot to present the absorption peaks of various doped GQDs in the literature and the electronegativity of the dopant. It is noted that the absorption peaks are mostly concentrate on the blue region. The absorption peak can be extended from deep UV to red t by using S, N or N doping.

3.2. Tunable properties of graphene quantum dots by controlling size and shape

Another strategy to tune the optical, physical and chemical properties of GQDs is via controlling the size and shape of the GQDs. Several methods have been applied to modify the size and morphology of GQDs.

3.2.1. Theoretical study of GQDs bandgap

Fig. 19a shows a decrease of the energy band gap with increasing size of the GQDs, hence demonstrating a relationship between energy band gap and size of the materials. Besides, Chen and co-workers [175] studied the relationship between the band gap and size using density-functional theory (DFT) and time-dependent DFT calculations as shown in Fig. 19b. It was suggested that the PL of a large GQD, consisting of heterogeneously hybridized carbon network, was essentially determined by the embedded small sp^2 clusters isolated by sp^3 carbons. There was a slight difference between theoretical prediction and experimental work in the degree of tuning the band gap by changing the size of GQDs, however the trend was in good agreement as studied by Ye and co-workers [176]. The band gap of GQDs, which influences its photoluminescent, can be tuned by tailored GQDs size via chemical methods.

3.2.2. Modification of GQDs bandgap via controlling size and shape

Based on the above-mentioned theoretical studies, numerous experimental studies have been performed to investigate the modification of GQDs bandgap. As shown in Fig. 19c, GQDs were capable of emitting light ranging from blue-green (2.9 eV) to orange-red (2.05 eV), depending on its size, functionalities and defects. Kim's [19] research group studied the relationship between PL and size of GQDs. Anomalous size dependences on the visible PL was also found in their experiment, which could due to shape and edge-state variations in the GQDs, as shown in Fig. 19d–e. Both the size and morphology of GQDs were investigated to study their effect on tunable bandgaps. For example, studies were performed on GQDs with different shapes (e.g. circular to polygonal) and the corresponding edge-state variations as the size of GQD increases suggested that the PL behaviors were attributed to the novel feature of GQDs. Furthermore, morphology of GQDs can solely influence its band gap. Sarkar and co-workers [177] performed theoretical studies on the relationship between the shape of GQD and its band gap, as shown in Fig. 19f. Besides, they also explored the possibility of

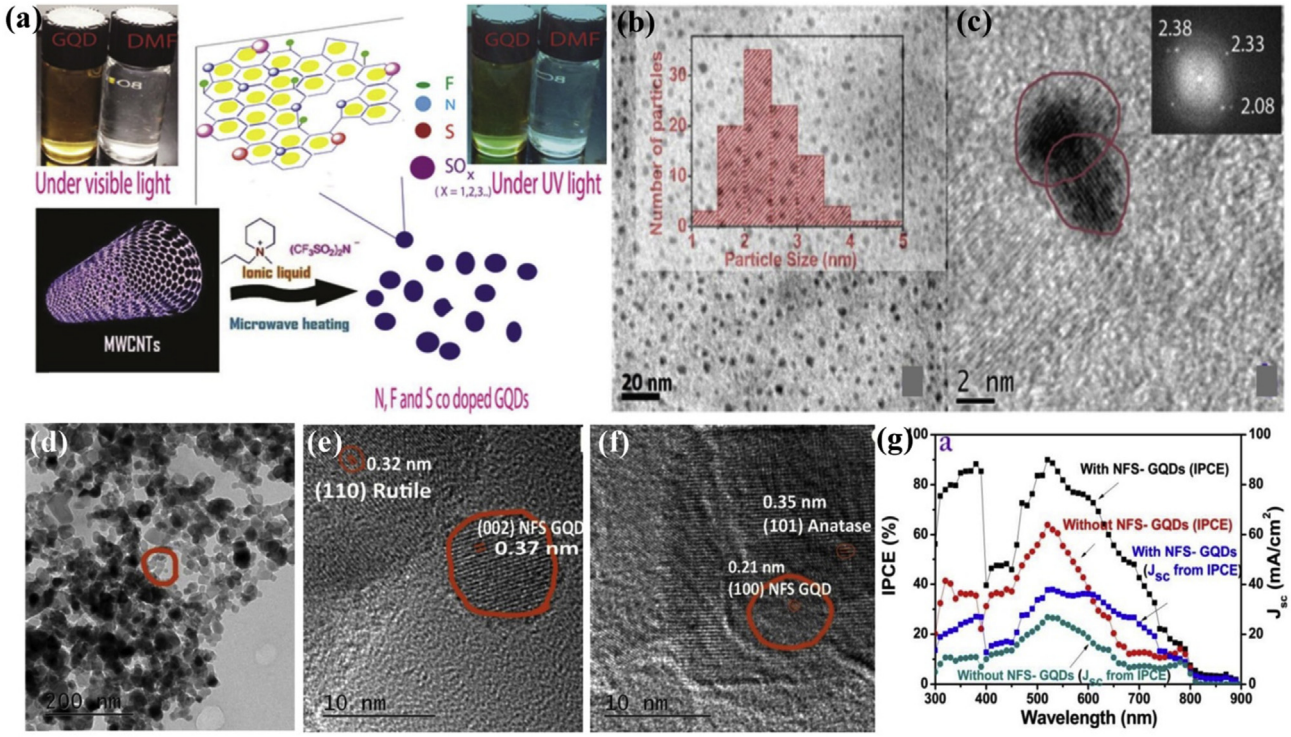

Fig. 17. Diagram and characterized images of multiple atoms doped GQDs. (a) schematic diagram indicating the formation of co-doped GQDs; inset shows a comparison of the same concentration of co-doped GQDs in DMF under visible light and UV light respectively (left: co-doped GQDs in DMF and right: DMF) [173]; (b–c) TEM image of N, F and S co-doped into GQDs (N, F, S-GQDs), inset of (b) and (c) are the particle size distribution and fast Fourier transform (FFT) pattern, respectively [173]; (d–f) TEM image of N,F,S-GQDs and (g) shows the properties of dye-sensitized solar cells with or without N, F, S-GQDs [174].

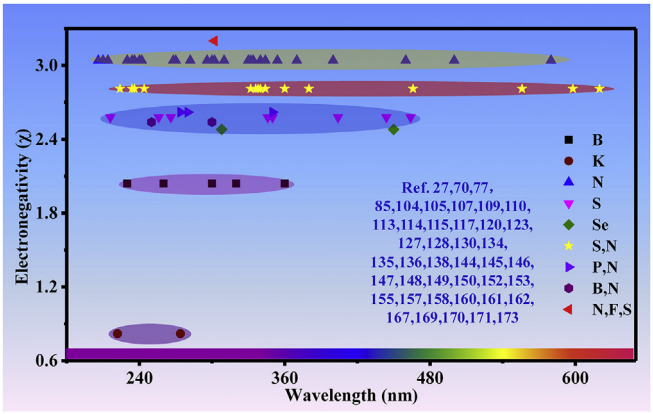

Fig. 18. Statistical plot of absorption peak and electronegativity of the doped element.

tuning the band gap by functionalizing the GQDs with different organic groups, and the fact that the covalent functionalization shifted both the HOMO and LUMO energies without significantly changing the HOMO–LUMO gap were explained by the analysis of the density of states of different functionalized GQDs. The theoretical analysis is in agreement with recently reported experimental work.

The properties of GQDs modified by its size and shape have been investigated using different methodologies, such as Raman scattering [178], density of states [179], magnetic properties [180,181], faraday optical rotation (FOR) [182] and optical characterizers [130,183,184]. This topic on band gap engineering of GQDs via tailoring its size and shape has attracted great interests from both theoretical [185,186] and experimental [18,187] researchers. This is a promising technique in extending the application of GQDs in the near future.

3.3. Graphene quantum dot composites to optimize performances

There are several drawbacks of GQDs, such as difficult to assemble into film and poor conductivity etc. The formation of GQD composites could overcome some of the challenges and enhance the performances of the material, thus leading to many novel applications. As shown in Fig. 20a, polymer materials [191,192] and nano-materials [193–198] can be used to form composite with GQDs. Follow the sequence of organic and inorganic materials

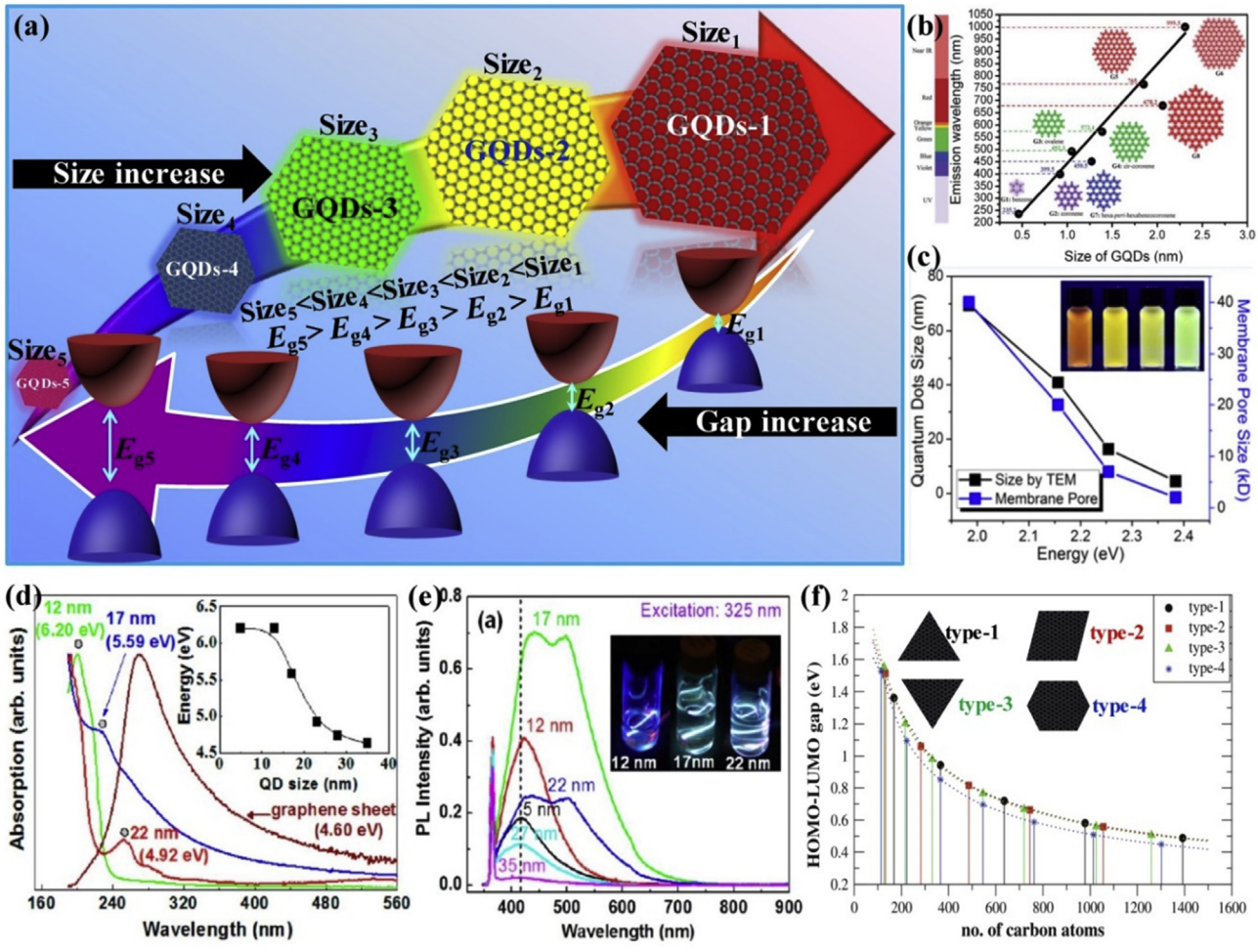

Fig. 19. Schematic illustration, corresponding measured results and analysis of GQDs depended on size and morphology. (a) Modulation of band gap for GQDs via size variation; (b) Calculated emission wavelength (nm) using TDDFT method in vacuum as a function of the diameter of GQDs. The solid line is the linear fitting of zigzag-edged GQDs with various sizes [175]; (c) The curves of band gap with the increase with the size of GQDs, inset shows the color of PL tuneable with the size of GQDs [176]; (d) and (e) represent the UV–vis spectra and PL of GQDs with various sizes, inset is digital picture of different luminescence of GQDs with different sizes [19]; (f) The energy gap as a function of total number of conjugated carbon atoms (N) and various morphologies for type-1 GQD (dash line with black circle), type-2 GQD (dash line with red square), type-3 GQD (dash line with green triangle) and type-4 (dash line with blue star), insets represent GQDs with different morphologies [177].

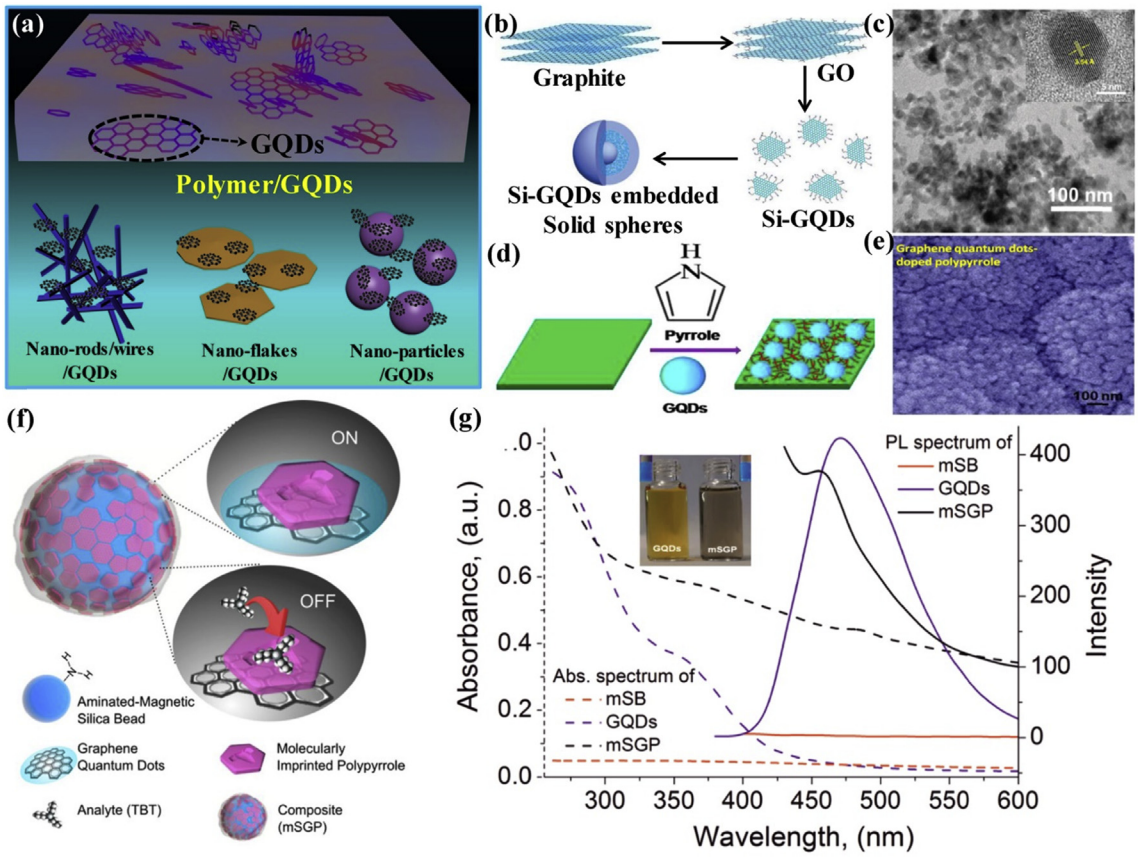

Fig. 20. Diagrams and related measured images of GQDs composites with organic and inorganic materials. (a) Illustration on the formation of GQDs composites with polymer or inorganic (nano-rods/wires, nano-flakes and nanoparticles) materials; (b) and (c) represent fabrication process and TEM image of the composite of GQDs with hollow mesoporous silica spheres, inset of (c) shows the HRTEM image of individual Si-GQDs [188]; (d) and (e) are scheme of the preparation process of GQDs-polypyrrole (PPy) film and the SEM image of composites with PPy and GQDs (10%) [189]; (f) and (g) display the schematic representation of the magnetic silica beads/graphene quantum dots/molecularly imprinted polypyrrole (mSGP) composites and spectroscopic characterization of the mSGP composites, inset of (g) is the optical picture of water solutions of GQDs (left) and mSGP (right) [190].

composites, the forming of composites with GQDs and other materials will be described.

Organic materials have a lot of merits, such as easy to form film, high carrier mobility and so on. These virtues could complement the performances of GQDs. Wen and co-workers [188] fabricated fluorescent organosilane-functionalized GQDs (Si-GQDs) and subsequently embedding them into mesoporous hollow silica spheres as bio-label for the first time. The entire preparation process is shown in Fig. 20b. TEM image, shown in Fig. 20c, displays the high crystalline quality of Si-GQDs and the characteristic of GQDs. Chen and co-workers [189] developed composite of GQDs and polypyrrole (PPy) as counter electrode of dye-sensitized solar cells (DSSCs) to optimize the performances of the solar cells. The fabrication procedure is presented in Fig. 20d. The composite formed a compact and uniform electrode as shown in Fig. 20e. As the composite film of GQD and PPy consisted of porous structures, there were more active sites resulting in higher charge transfer rate. The performance of DSSCs was greatly enhanced by the composite film and achieved the highest PCE of 5.27%, which was ~20% higher than that of plain PPy (4.46%) based DSSCs. There is no doubt that the composites of GQDs and organic materials have enormous potential in future. Interestingly, Zor et al. [190] prepared a novel multifunctional composite consisting of magnetic silica beads, GQD and molecularly imprinted polypyrrole. The formation of the fabricated composite material is shown in Fig. 20f. The composite exhibited enhanced optical and magnetic properties. For example, the absorption spectrum of the composite was extended to greater wavelength, as displayed in Fig. 20g. Whereas, the inset of Fig. 20g indicates the obvious difference in the color of aqueous solution of GQDs and mSGP. The enhanced properties of GQD composite would benefit many applications. There has been a growing interest in developing new GQD composites in recent years. Malik's [199] group prepared nanofiber composite, which consisted of GQDs and polyaniline, as supercapacitor electrode materials. The composite material led to an enhanced current density of 1 Ag^{-1} as well as cyclic stability. The preparation process of the composite is shown in Fig. 21a. Qu et al. [200] fabricated composite of 0D GQDs and 3D graphene (3DG) by assembling them via a novel benign electrochemical method, as shown in Fig. 21b. The GQDs-3DG composite material was then used to develop supercapacitor with enhanced performances, which relied on the high surface area and increased active sites of the GQDs.

Apart from the composites of GQDs and organic materials, many inorganic materials have been used to form GQD composites to improve the performances of devices. Dhar and co-workers [201] demonstrated the composite of ZnO and GQDs can enhance the performance of UV photodetector with superior external quantum efficiency (EQE) of ~57681% (at -1 V bias) at wavelength of ~340 nm. The device structure is shown in Fig. 21c. The composite of ZnO nanorods/poly(3,4-ethylenedioxythiophene) polystyrene sulfonate (PEDOT:PSS) and GQDs exhibited far better performances than GQD modified ZnO NRs and pure ZnO NRs. Other shape of ZnO, such as leaf-shaped ZnO (L-ZnO) [202], was also used in forming composite with GQDs. TEM image of the L-ZnO and GQDs composite is as

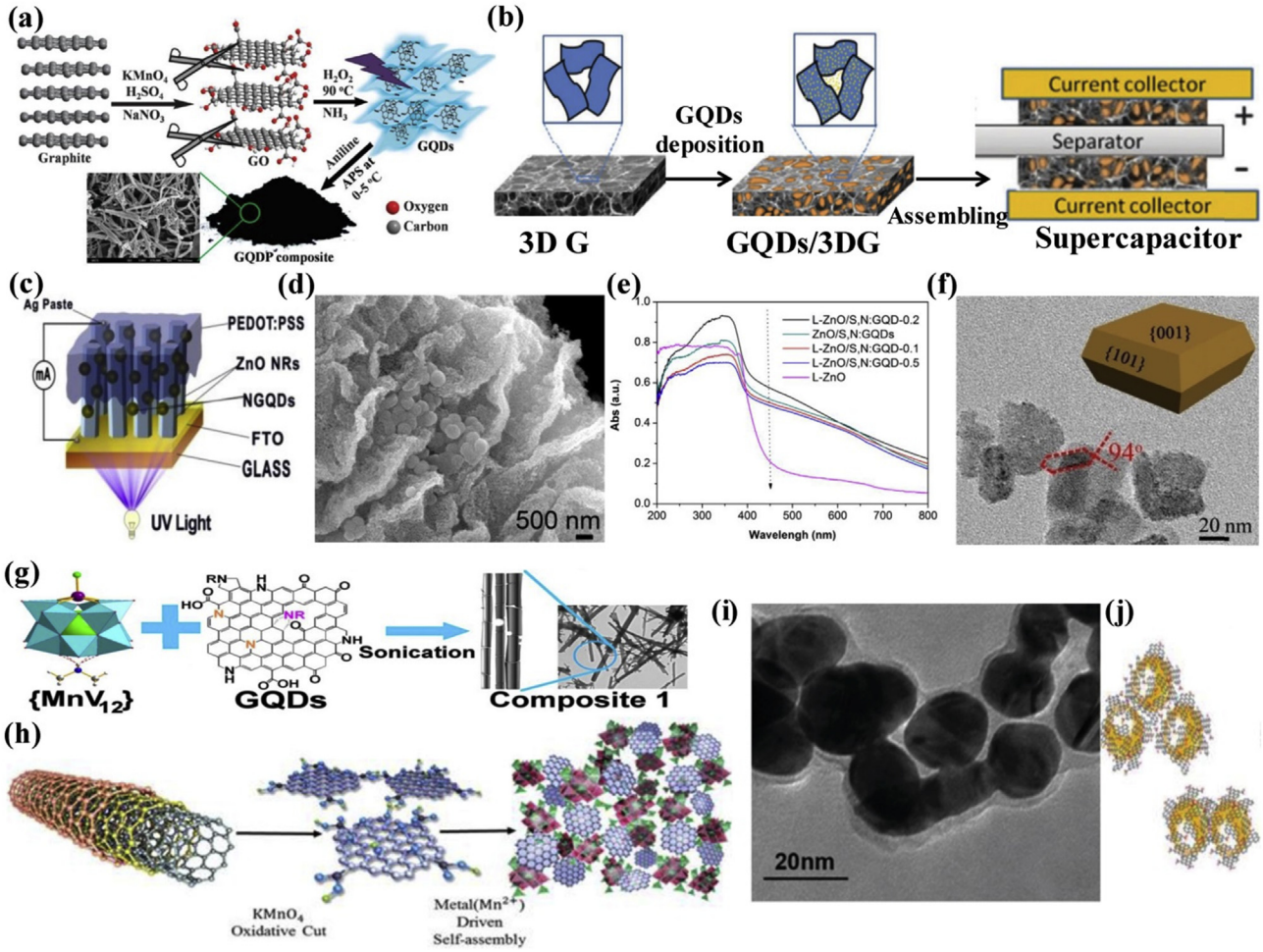

Fig. 21. Illustration and corresponding images of the GQDs composites with organic and inorganic materials. (a) Schematic diagram of the fabrication process of GQDs composites with polyaniline (PANI) [199]; (b) Cartoon representation of fabricating a symmetrical supercapacitor based on the GQDs–3DG composite material [200]; (c) Schematic diagram on the structure of UV photodetector using composites of ZnO and GQDs as active layer [201]; (d) and (e) show SEM image and UV–vis absorption of composites of leaf-templated ZnO and GQDs, respectively [202]; (f) TEM image of black TiO2 [203]; (g) Schematic illustration of the fabrication of composite of a manganese vanadium oxide and (GQDs) using a molecular manganese vanadate precursor [204]; (h) The synthesis route for the GQD–Mn3O4 nanocomposite using MWCNTs as the precursor of GQDs [205]; (i) and (j) represent TEM image and the structure of composites of Au nanoparticles and GQDs [206].

shown in Fig. 21d. UV–vis absorption of the composite showed an increase in the absorbance intensity as well as extended spectrum (refer to Fig. 21e). In the same manner, TiO_2 and GQDs nanocomposites were fabricated by Bu [203]. TEM image of the nanocomposites is shown in Fig. 21f. The nanocomposites were used as photocatalysts, which exhibited extremely high photocatalytic activity due to the larger energy barrier between NGQDs and B–TiO_2, resulting in enhanced light absorption and higher electron density. Ji et al. [204] assembled lithium ion battery using composite of MnV_{12} and GQDs. The fabrication process is shown in Fig. 21g. The bar shaped composites can maximize the interfacial contact area and improve charging/discharging behavior, thus optimizing the performances of the lithium ion battery. Another interesting experiment [205] was performed by assembling Mn_3O_4 and GQDs into nanocomposites, which can change the energy level of the materials instead of doping with heteroatoms or controlling the size and shape of GQDs. As shown in Fig. 21h, the multi-walled carbon nanotubes (MWCNTs), acted as the GQDs' precursor, were mixed with the Mn_3O_4 to form the composites which exhibited intensive Raman scattering. This could be used in bioimaging to discriminate cancer cells and normal cells. Due to the large surface area to volume ratio of the GQDs, the composite materials are frequently used as catalysts. Wu et al. [206] fabricated the composites of GQDs and Au nanoparticles as catalysts. TEM image and structure of the composites are displayed in Fig. 21i and j, respectively.

Many inorganic materials have been used in forming composites with GQDs, such as SnO_2 [207], ZnS [208], MoS_2 [209], ferroelectric liquid crystal [210], ceria [211], Zn [212] and Fe_2O_3 [213] etc.

In brief, GQD composites have shown to improve and optimize the performances of devices. Novel functionalities of GQDs can be developed using techniques, such as doping, controlling size/shape and composites, which would open up new applications for GQDs.

4. The applications of graphene quantum dots

The extensive properties of GQDs (and functionalized GQDs) would benefit many applications in a variety of fields. As shown in Fig. 22, GQDs have found many potiential applications in fields, such as medical [214–219], optical [85,220–224] and energy [139,225–229], which will impact our quality of life and attract significant commercial interests. Much research has been carried out to understand the unique properties of GQDs and tailoring its

Fig. 22. The extensive applications of the GQDs on medicine, optics and energy. The red-carp represent the vitality of the GQDs.

properties using different techniques, such as doping, controlling of size/shape and developing composite material and so forth.

In the next decade, GQDs may become a popular material for advanced technology. They have already been exploited in a number of applications, such as biological imaging [230,231], drug delivery [232,233], photodetector [234,235], LEDs [236–238] and battery [239] etc. In this section, we will present the current applications of GQDs in medical, optical and energy-related fields. Each of these fields will be subdivided into detailed applications.

4.1. Medical applications

Due to the biocompatibility and nontoxicity of the GQDs, the nanomaterials have been exploited for medical applications and demonstrated some excellent performances, which could potentially replace some traditional materials in this field. There have been continuous efforts in exploiting GQDs for other novel medical applications due to the recent promising outcomes in the field.

4.1.1. Biological imaging

GQDs have been used in biological imaging for medical diagnostic as they can assist in locating cancerous cells and determining if drugs have been delivered to targeted cells as well as locating the drugs within cells [242]. The strong and tunable PL of GQDs allow the materials to be used in biological imaging. Pu and co-workers [240] used the modified GQDs as efficient fluorescent probes for highly selective detection. The entire fabrication process is shown in Fig. 23a. Firstly, the GQDs were stripped from graphene oxide sheets and amine-modified. Anti-human IgG antibodies were conjugated with Fe_3O_4 nanoparticles to detect casts in urine. The modified GQDs were then linked on to the surface of anti-IgG functionalized Fe_3O_4 nanoparticles. Finally, the Fe_3O_4/GQDs fluorescent probes were added into the sample to detect casts through fluorescent imaging. For comparing the efficiency of fluorescent probe using GQDs and Fe_3O_4/GQDs, a series of pre-quantitative casts (2, 4, 8, and 10 casts/ml) were analyzed by microscopy and fluorescent imaging assay, and the results are shown in Fig. 23b–d. At the same concentration of casts, the counts of fluorescent imaging assay from Fe_3O_4/GQDs (Fig. 23d) were approximately 10 times higher than that of microscopy (Fig. 23b) and GQDs only (Fig. 23c). Their results indicated the detection efficiency of this fluorescent imaging assay was higher than microscopy mainly due to the magnetic enrichment of Fe_3O_4/GQDs nanocomposites. Such magnetic enrichment was efficient and simple.

Yang and co-workers [241] demonstrated that GQDs can be widely utilized for biological imaging in different kinds of cells. They prepared GQDs with uniform size and strong yellow emission by using top-down method. Three different kinds of stem cells, namely neurospheres cells (NSCs), pancreas progenitor cells (PPCs) and cardiac progenitor cells (CPCs), were used in the studied and cultured in different mediums. On the day of treatment, the cells were incubated with GQDs at a final concentration of 25 mg mL^{-1}

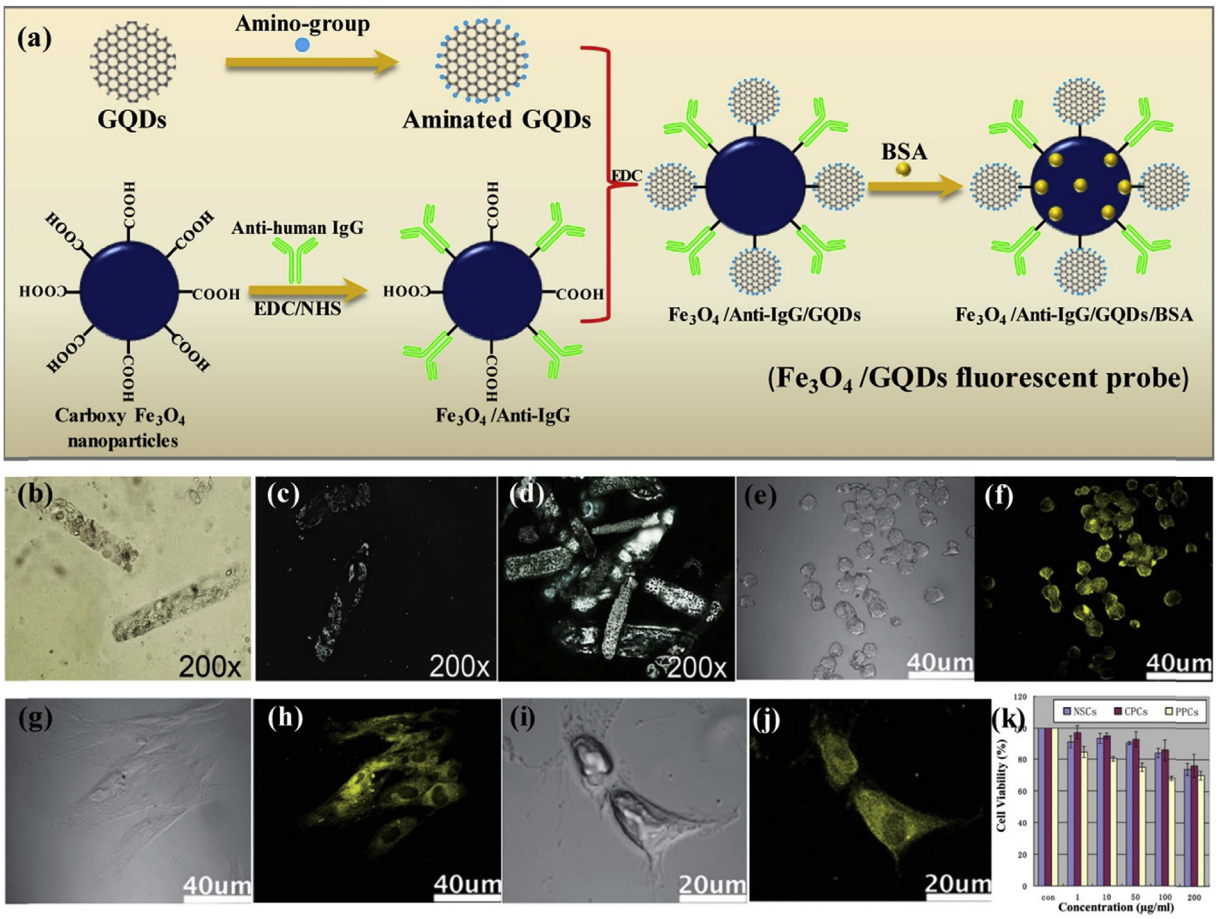

Fig. 23. Preparation process of the fluorescent probe and biological imaging of the GQDs. (a) Preparation of Fe_3O_4/GQDs fluorescent probe [240]; (b) is microscopy of cast (control method), (c) and (d) are detection efficiency of fluorescent imaging assay by using GQDs and Fe_3O_4/GQDs probes, respectively [240]; (e), (g) and (i) are micrographs of stem cells under bright field, (f), (h) and (j) show the fluorescent image of stem cells via using fluorescent agents with NSCs, PPCs and CPCs incorporated with GQDs at 405 nm excitation, respectively [241]; (k) Cell viability for the stem cells of NSCs, CPCs and PPCs as a function of the added GQDs concentration [241].

for 24 h at 37 °C. Subsequently, the cells were washed three times with PBS and then fixed with 4% paraformaldehyde for 20 min at room temperature. Fig. 23f, h and j show the confocal fluorescent images of NSCs, PPCs and CPCs with an excitation wavelength of 405 nm, respectively. As shown in Fig. 23e, g and i, the morphology of the cells can be discerned from the internalized GQDs. These results demonstrated that the GQDs can be used in different cells for biological imaging. However, there was slight cytotoxicity of GQDs in these cells as observed in Fig. 23k. The average cell viability of NSCs and CPCs was above 80% after 3 days culturing with GQDs at a concentration of 100 mg mL^{-1}, and was about 65% for PPCs.

In summary, the biocompatibility, strong fluorescence and nontoxicity of the GQDs have been investigated and they are an excellent choice for biological imaging in medical applications.

4.1.2. Drug delivery

Compact drug delivery nanosystems with multifunctional features are currently of considerable interest for cancer therapy owing to their improved dose tolerance and therapeutic efficacy [243]. GQDs have many attractive properties, such as sp^2 carbons, rich in π electrons and having a variety of functional groups (e.g. carboxyl, hydroxyl, carbonyl and epoxy).

This is in addition to the reduced size of GQDs and different chemical reactivity as compared to other graphene based materials, such as GO or CNTs [245]. These characteristics would make GQDs an ideal candidate for drug delivery platform through π-π interactions and easy functionalization via the oxygen functional groups [243].

Hu and co-workers [243] fabricated SCNAs by employing GQDs as the substrate of the vehicles, as shown in Fig. 24a. Both GQDs and SCNAs were incubated with RG2 cells (a rat glioma cell line) at various concentrations for 24 h in order to evaluate the effects of the particles on cell viability. As shown in Fig. 24b–e, CLSM images of RG2 cells incubated for 0.5 h showed the presence of SCNAs in the cytoplasm, and with increasing incubation time to 4 h, most of the particles were surrounding the cell nuclei. In addition to the fluorescence signal from DOX, the fluorescence of the GQDs could also be observed in RG2. When comparing the fluorescence signals between DOX and GQDs, most of them actually overlapped, which indicated good affinity in the cell. A detailed schematic illustration of the drug delivery is represented in Fig. 24f. The effectiveness of GQDs as drug delivery was studied by Some [244] et al. They used graphene-derivatives (such as DGO and GQD) as nanovectors for the delivery of the hydrophobic anticancer drug Cur and performed clinical studies using the technique. As shown in Fig. 24g, while tumor growth was initially inhibited to some extent (blue line) in the control group treated with free Cur, the tumor size did eventually increase. In stark contrast, the DGO-Cur and GQD-Cur groups exhibited a remarkable inhibition of tumor growth. Both GQD-Cur and DGO-Cur treated mice survived more than 14 days with almost no observable increase in tumor size (yellow and green lines). The photographic images showing the size of the tumor in response to

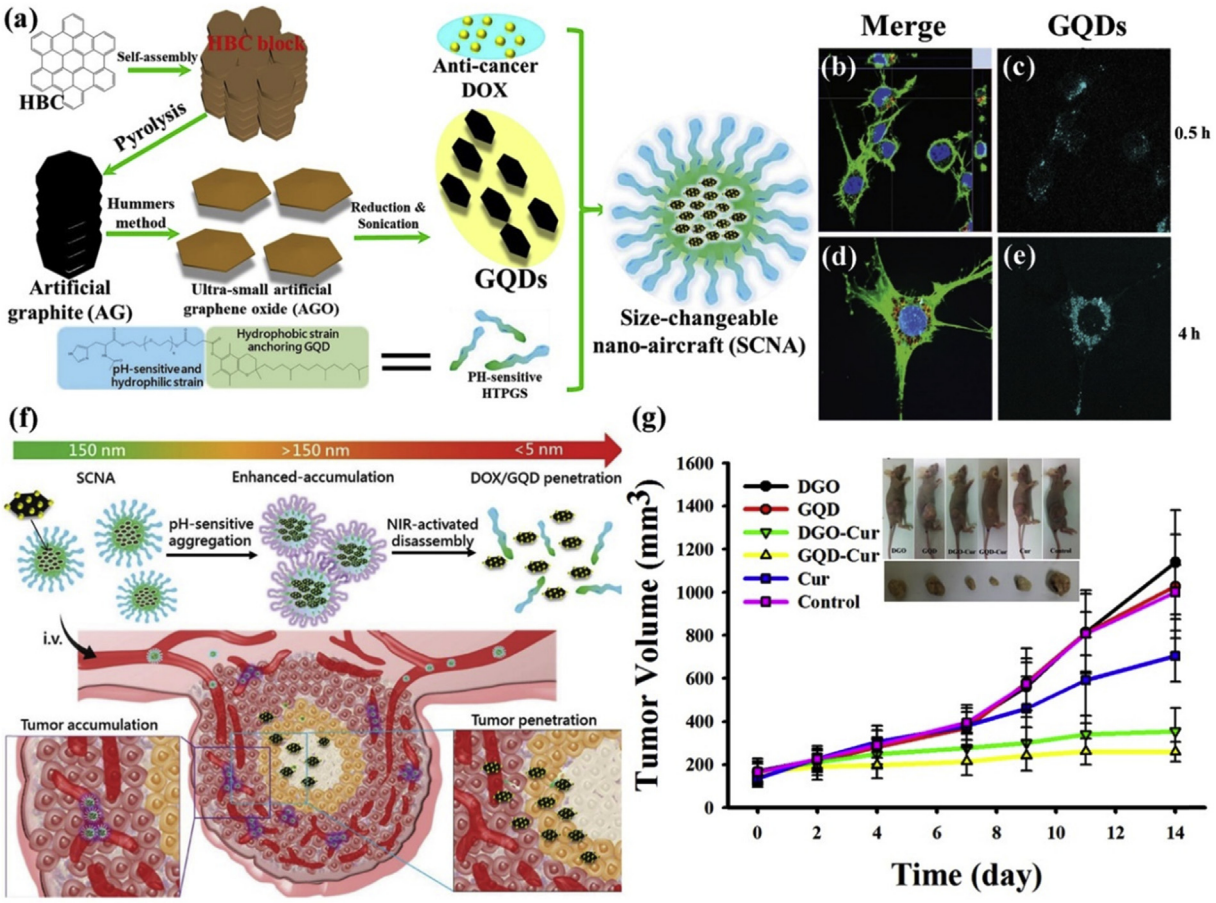

Fig. 24. Schematic and some clinical results on the application of GQDs on drug delivery. (a) Schematic illustration on the key steps in the size-changeable nanoaircraft (SCNA) synthesis process [243]; (b–e) Confocal laser scanning microscope (CLSM) image of cellular uptake after 24 h, doxorubicin (DOX) appears in red, and GQDs appears in cyan [243]; (f) Size-changeable nanoaircrafts (SCNAs) for hierarchical tumor targeting through an aggregation transition in the weak acidity of the tumor environment and photopenetrating drug/GQD delivery. i) The SCNAs delivered DOX/GQD to the tumor through intravenous injection. ii) The aggregation transition of the SCNAs in the weak acidity of the tumor environment enhanced tumor accumulation. iii) NIR-activated disassembly of SCNAs into DOX/GQDs facilitated penetration deep into tumors [243]; (g) Relative tumor volumes of mice (n = 6) treated with PBS (control sample), double-oxidize graphene oxide (DGO), GQD, DGO-Cur, GQD-Cur, and curcumin (Cur), top planar and bottom section of inset show photographs of mice and tumors treated with PBS, DGO, GQD, DGO-Cur, GQD-Cur, and Cur after 14 days, respectively [244].

the treatments can be seen in the inset. Besides, GQDs can also be used in gene delivery due to its favorable properties. For instance, Zhang's [248] and Guo's [249] team demonstrated such delivery by using GQDs.

In brief, the preliminary work on using GQDs as drug delivery system demonstrated the superior stability, good biocompatibility and excellent therapeutic performance of the material, which is a promising candidate for in-vivo therapeutic agent.

4.1.3. Photodynamic therapy

Photodynamic therapy (PDT), also known as photochemotherapy, is a form of phototherapy involving the use of light and a photosensitizing chemical substance that applied in conjunction to elicit cell death by molecular oxygen (phototoxicity). An interesting phenomenon that GQDs can generate the reactive oxygen species (ROS) in tumor cells was observed [250]. In addition, the upconversion characteristic of GQDs can convert low energy NIR light to UV–visible light, which has been widely examined for biological applications. Therefore, GQDs can be considered excellent materials for photodynamic therapy. Xing and co-workers [246] explained the mechanism of PDT (refer to Fig. 25a). The effectiveness of PDT using GQDs was investigated through clinical evaluation as shown in Fig. 25g. Furthermore, photoinduced cytotoxicity and oxidative stress of GQDs were also studied by Yin et al. [247] as shown in Fig. 25b–e. Their findings suggested GQDs as anti-oxidants and pro-oxidants upon irradiation because they have the potential to become potent anti-oxidants for controlling ROS-induced cell damage.

4.1.4. Photothermal therapy

Apart from the above-mentioned PDT, another therapeutic technique has been performed using GQDs. Photothermal therapy (PTT) refers to the use of electromagnetic radiation (e.g. often in infrared wavelengths) for the treatment of various medical conditions, such as cancer. This approach is an extension of photodynamic therapy, in which a photosensitizer is excited with a specific band of light. This activation brings the sensitizer to an excited state where it then releases vibrational energy in the form of heat that kills the targeted cells.

Unlike photodynamic therapy, PTT does not require oxygen to interact with the target cells or tissues. Current studies on PTT are investigating the use of longer wavelength light, which is less energetic, and therefore less harmful to surrounding cells and tissues. For instance, Zhu and co-workers [58] fabricated DOX-MMSN/GQDs which were used as multifunctional platform for controlled drug delivery, magnetic hyperthermia and photothermal therapy, as shown in Fig. 25f. Many more studies have recently been carried out, such as from Lee's [253] and Yang's [254] research group. In

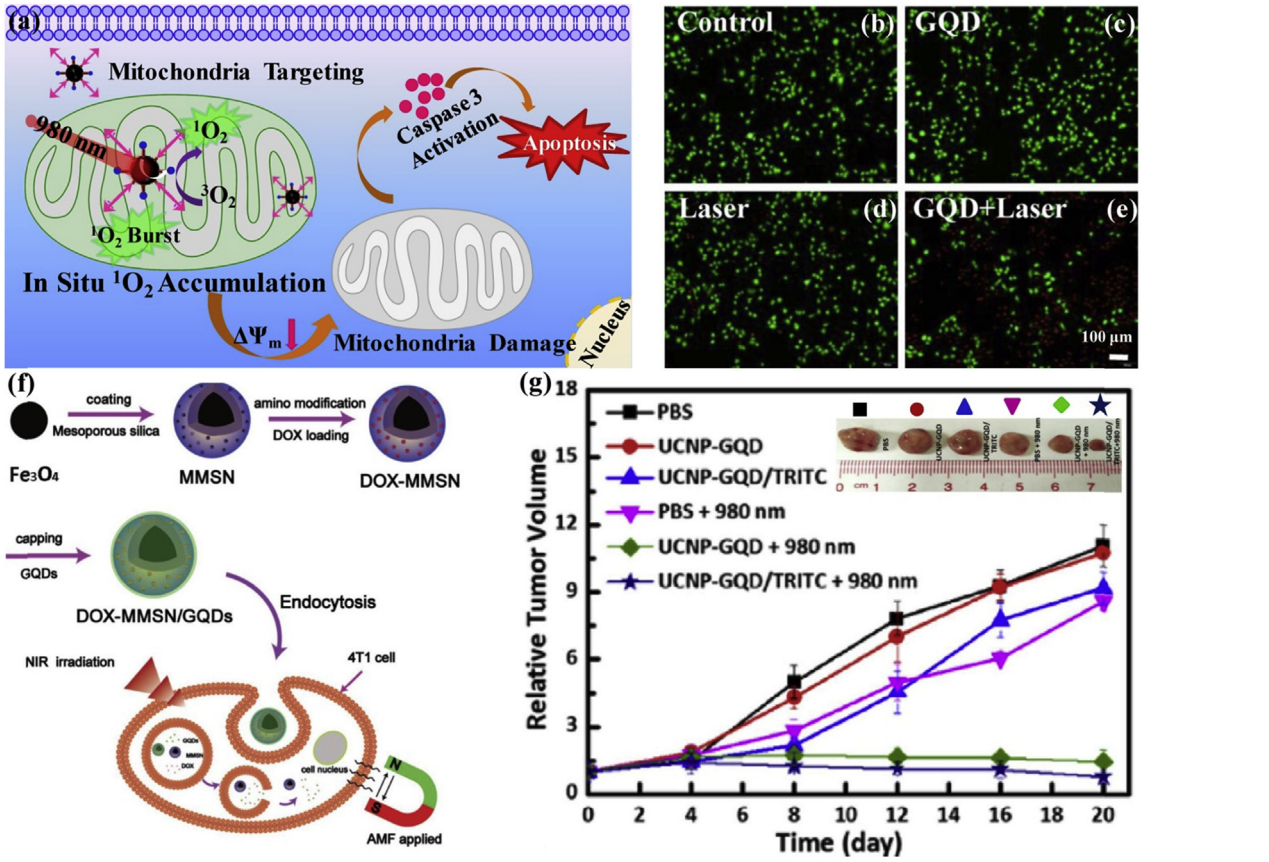

Fig. 25. Representation and clinical results on the photodynamic therapy application of GQDs. (a) Schematic illustration on the fabrication of upconversion nanoparticles-GQDs/Tetramethylrhodamine-5-isothiocyanate (UCNP-GQDs/TRITC) with mitochondria-targeting potency [246]. (b–e) A549 cells fluorescence-based LIVE/DEAD assays (b) after 24 h under irradiation at 405 nm excited [247]. (f) Schematic illustration of the preparation process of the doxorubicin loading GQDs-capped magnetic mesoporous silica (DOX-MMSN/GQDs) nanoparticles and synergistic therapy combined with controlled drug release, magnetic hyperthermia, and photothermal therapy [58]; (g) Growth curves of mouse mammary tumor cell (4T1 tumors) in each group, inset is typical photographs of tumor tissue after each treatment [246].

short, GQDs has enormous prospect in medicine therapy and researchers are working tirelessly to develop advanced and novel therapeutic technologies based on the materials.

4.1.5. Antimicrobial materials

Infectious diseases caused by bacteria continue to be one of the greatest health problems worldwide, afflicting millions of people annually. Antibacterial materials are widely used in daily life and can effectively protect the public health [255]. GQDs have some remarkable behavior, which has been exploited as antimicrobial materials. For example, GQDs can produce toxicity under special wavelength irradiation.

This was demonstrated by Wang et al. [251] as they fabricated antimicrobial materials using GQDs. The clinical results of N-GQDs (5.1%)-AbLPS-treated-bacteria in *E. coli* under 670 nm laser photoexcitation are shown in Fig. 26a–c, which indicated the GQDs played an important role in killing the bacteria. Qu and co-workers [252] designed an antibacterial system based on GQDs and low dose of H_2O_2. The system, represented in Fig. 26d, benefitted from the peroxidase-like activity and excellent biocompatibility of GQDs. Clinical studies were performed to assess the efficacy of the designed antibacterial system (shown in Fig. 26e–i) in wound disinfection. GQDs band-aids were prepared and showed excellent antibacterial property in-vivo with the assistance of low concentration of H_2O_2, which indicated that GQDs band-aids have potential use for wound disinfection.

As shown, GQDs have been studied for use in the medical applications due to the many unique properties of the materials. There remain much potential of GQDs in this field that has yet to be fully explored, which could lead to many more exciting applications. Many of the above-mentioned applications are still at its early stage of development however they have given us some ideas on the future of nanomedicine based on GQDs.

4.2. Optical applications

Due to the unique optical properties of the GQDs, different optodevices have been developed, such as photodetector [265,266], light emitting diodes [267–270] and photocatalysis [271–274] etc. This is based on some special characteristics of GQDs, for example, upconversion, strong photoluminescence and tuning of energy gap by controlling size/shape, which are different from traditional quantum dots, such as ZnO QDs and TiO_2 QDs etc. Different functionalization techniques of the GQDs were studied and achieved excellent performances in related applications. There are many potiential applications of GQDs in the optical field, which will be the topic for the following sections. Following the main lines of optoelectrical detector, LEDs and photocatalysis, many interesting researches related to these applications will be described.

4.2.1. Optoelectrical detector

Photodetectors or photosensors are sensors of light or electromagnetic energy [275], and they play an important role in national defense, real-time monitoring and space exploration and so on. Due to the ease of functionalization and uncommon optical properties of GQDs, many research groups have worked on the nanomaterials

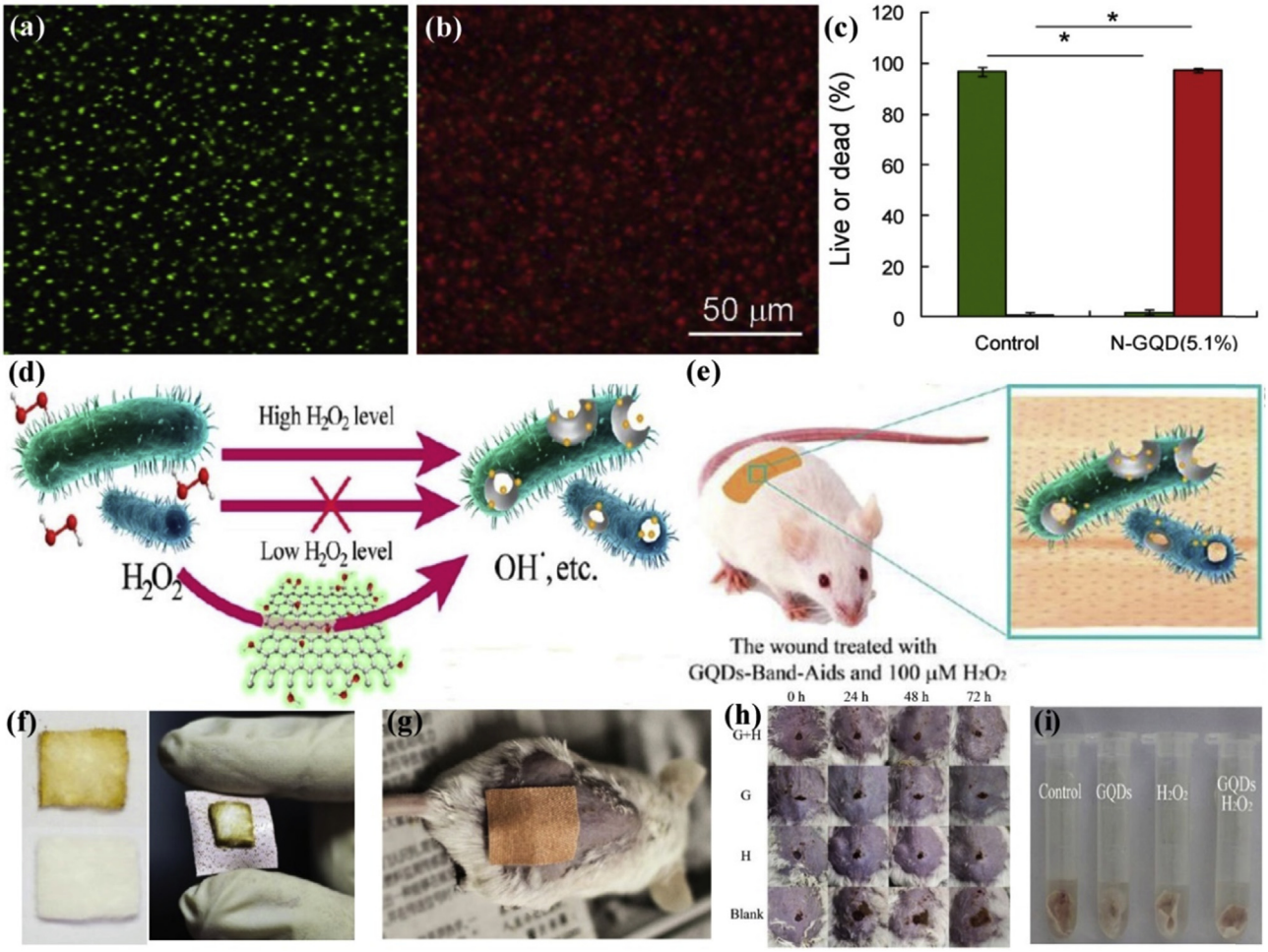

Fig. 26. Mechanism and clinical photos of antimicrobial materials using GQDs. (a–c) Images and viability of *E. coli* [251]; (d–i) The designed system is based on GQDs and low level of H_2O_2 for the antibacterial application, the photography of wound disinfection [252].

and developed various methods to enhance the performance of photodetectors by utilizing GQDs. Among these methods, GQDs composited with traditional materials, such as silicon, ZnO or P3HT, with different dimensions, for example, Si nanowire [256] (Fig. 27a), Si nanoparticles [257] (Fig. 27b), Si pyramid [258] (Fig. 27d–e), ZnO nanorods [259,260] (Fig. 27c and f) and P3HT [261] (Fig. 27g), have been investigated for use in photodetectors. In addition, GQDs have also been used to form hybrid composites with other 2D materials, such as graphene [35,38,263,264] (Fig. 27i, j, m and n), MoS_2 [262] (Fig. 27h) and WSe_2 [133] (Fig. 27l) etc. It is rare to use pure GQDs as an active layer, even though they have been attempted by some groups, due to the absorption peak position of GQDs is mainly located at the ultraviolet range, hence the photodetector would generally respond to short wavelength range, as shown in Fig. 27k, which led to deep ultraviolet photodetector [39] using pure GQDs. Interestingly, Tang and co-workers [27] developed a photodetector that exhibited photoresponse over UV to NIR range by doping pure GQDs with nitrogen. Such novel technique is generally known as Tang-Lau method.

Table 2 provides a detailed list of merits of the different GQDs based photodetectors. According to the listed merits, it is apparent that there is a great prospect in using GQDs based photodetector in the near future. It has indeed inspired researchers to perform further research and development work in using GQDs as an active layer in the photodetector.

4.2.2. Light emitting diodes

Luminescence is a phenomenon where light is emitted from a material excited by an external energy. Such phenomenon has major scientific and technological roles in a variety of applications [275–277]. With a significant portion of global energy consumption going towards lighting, it is important to develop efficient illumination-grade lighting technologies [278]. The excellent optical properties of GQDs have been exploited in LEDs. There are two main approaches in the application of GQDs in LEDs. The first approach is to coat LEDs with GQDs to modify its lighting intensity and emitting wavelength (Fig. 28a) [279–282]. Second approach is to develop emitting layer using GQDs within the structure of LEDs (Fig. 28b) [283,284].

GQDs have been frequently used as phosphors coated on to the surface of LEDs, which led to the modification of color [285] (refer to Fig. 28c) as well as enhancement in intensity of emitting lights [286,287] (refer to Fig. 28f–h). Besides, the GQDs can also be used as the active layer by forming composite with other emitting materials to improve the performance of LEDs. The intensity of LEDs irradiation can be controlled by changing the content of GQDs in the composites [49] (refer to Fig. 28d and e). Furthermore, the color of GQDs based LEDs can be tuned by functionalizing the GQDs with different functional group agents [288–290] (refer to Fig. 28i–m).

The recent research has demonstrated that GQDs can be applied in LEDs using different approaches, namely as phosphors or active

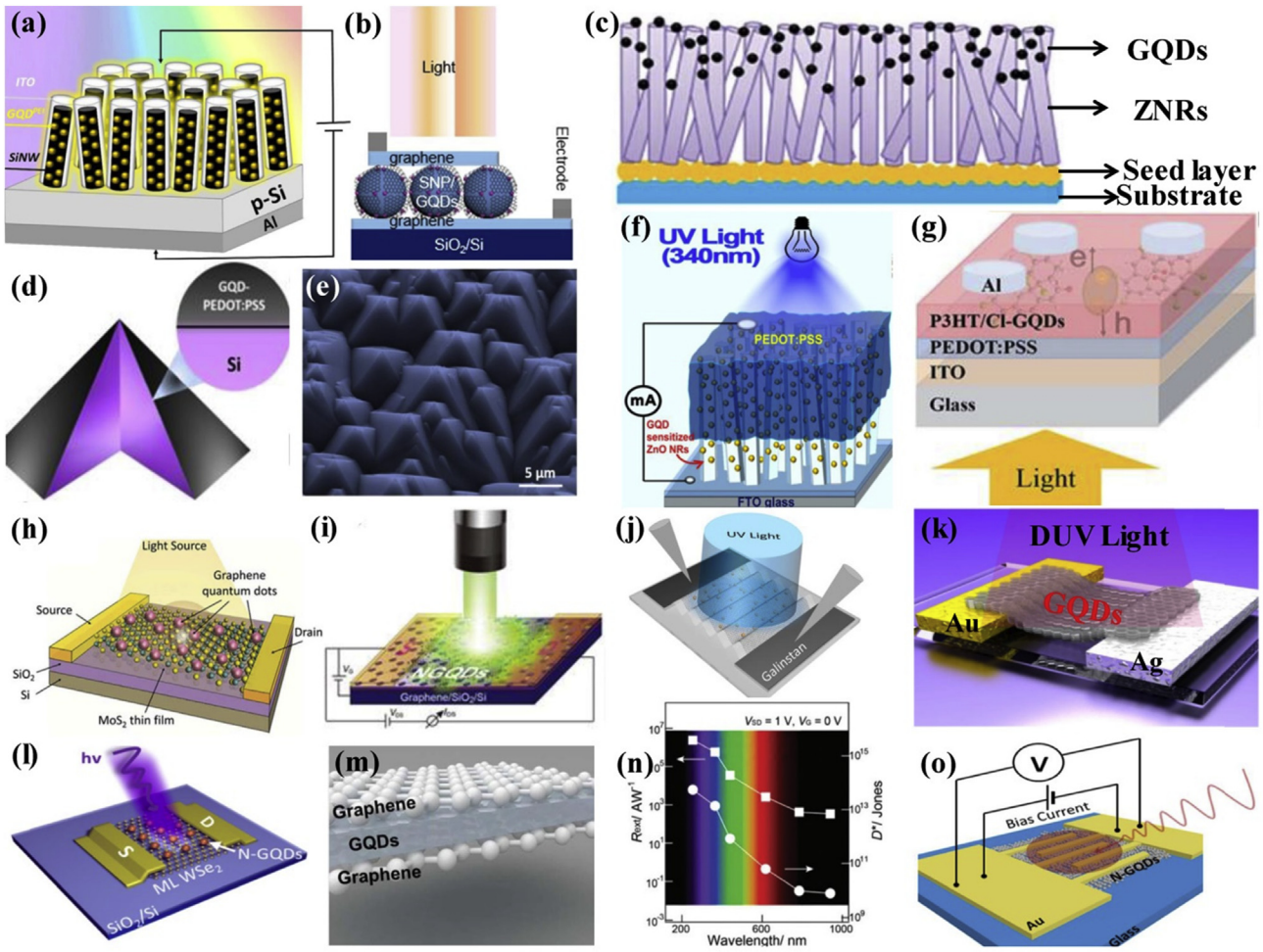

Fig. 27. Schematic and performance of various photodetectors based on GQDs. (a) Photodetector based the shell structure of GQDs sensitive Si nanowires (SiNWs) [256]; (b) Schematic of photodetector composed of the GQDs/Si nanoparticle (GQDs/SiNPs) [257]; (c) Illustration of photodetector based on ZnO nanorod array sensitized with GQDs [258]; (d–e) Schematic and SEM image of the photodetector by hybridization with GQDs and Si [259]; (f) Representation of photodetector consisting of ZnO nanorods and GQDs [260]; (g) Diagram of photovoltaic detector based P3HT/GQDs [261]; (h) Schematic of a MoS_2-GQDs heterostructure phototransistor [262]; (i) Schematic representation of a graphene/NGQDs hybrid phototransistor [263]; (j) Diagram of photodetector hybridization with GQDs and graphene [38]; (k) Schematic illustration of the pure GQDs photodetector with asymmetric Ag–Au electrodes [39]; (l) Schematic illustration of an ML WSe_2/N-GQDs photodetector [133]; (m) Schematics of a typical GQDs photodetector device [264]; (n) Photoresponsivity and specific detectivity versus laser wavelengths of 254–940 nm for the GQDs/Graphene hybrid photodetector [35]; (o) Schematic diagram of the N-GQDs photodetector [27].

Table 2
The related merits of photodetectors based on active layer with GQDs.

Active materials	Performance						Structure	Ref.
	Detectivity ($cmHz^{1/2}W^{-1}$)	Responsivity (AW^{-1})	Response time	*EQE* (%)	Tested temperature	Cover spectral range		
GQDs/SiNW	11.9×10^{12}	40.6	—	8150	RT	UV-NIR	Vertical	[256]
GQDs/SiNP	—	0.31	—	—	—	UV-NIR	Vertical	[257]
GQDs/Si	8.0×10^{11}	1.02	80 μs	—	—	Visible	Vertical	[259]
GQDs/ZnOND	—	—	150–200 s	—	—	UV	Vertical	[258]
GQDs/ZnOND	1.3×10^{12}	36	—	13161	—	UV	Vertical	[260]
GQDs/ZnOND	2.4×10^{11}	247	0.94 s	90063	—`	UV	Vertical	[265]
GQDs/MoS2	—	1.6×10^{4}	1.23 s	—	RT	Visible	Planar	[262]
GQDs/Graphene	1.2×10^{12}	3.5×10^{4}	0.61 s	—	—	UV-NIR	Planar	[263]
GQDs/Graphene	5.5×10^{13}	2.3×10^{6}	0.69 s	—	RT	UV-NIR	Planar	[35]
GQDs/WSe2	—	2578	—	—	RT	Visible	Planar	[133]
GQDs	9.6×10^{11}	2.1×10^{-3}	64 ms	—	RT	UV	Planar	[39]
GQDs	—	14.1 (VW^{-1})	50 s	—	RT	UV-NIR	Planar	[27]
GQDs	$>10^{11}$	0.2–0.5	2μs	—	RT	UV-NIR	Vertical	[264]

(Notes: SiNW, SiNP, ZnOND and RT represents Si nanowire, Si nanoparticle, ZnO nanorod and room temperature, respectively.).

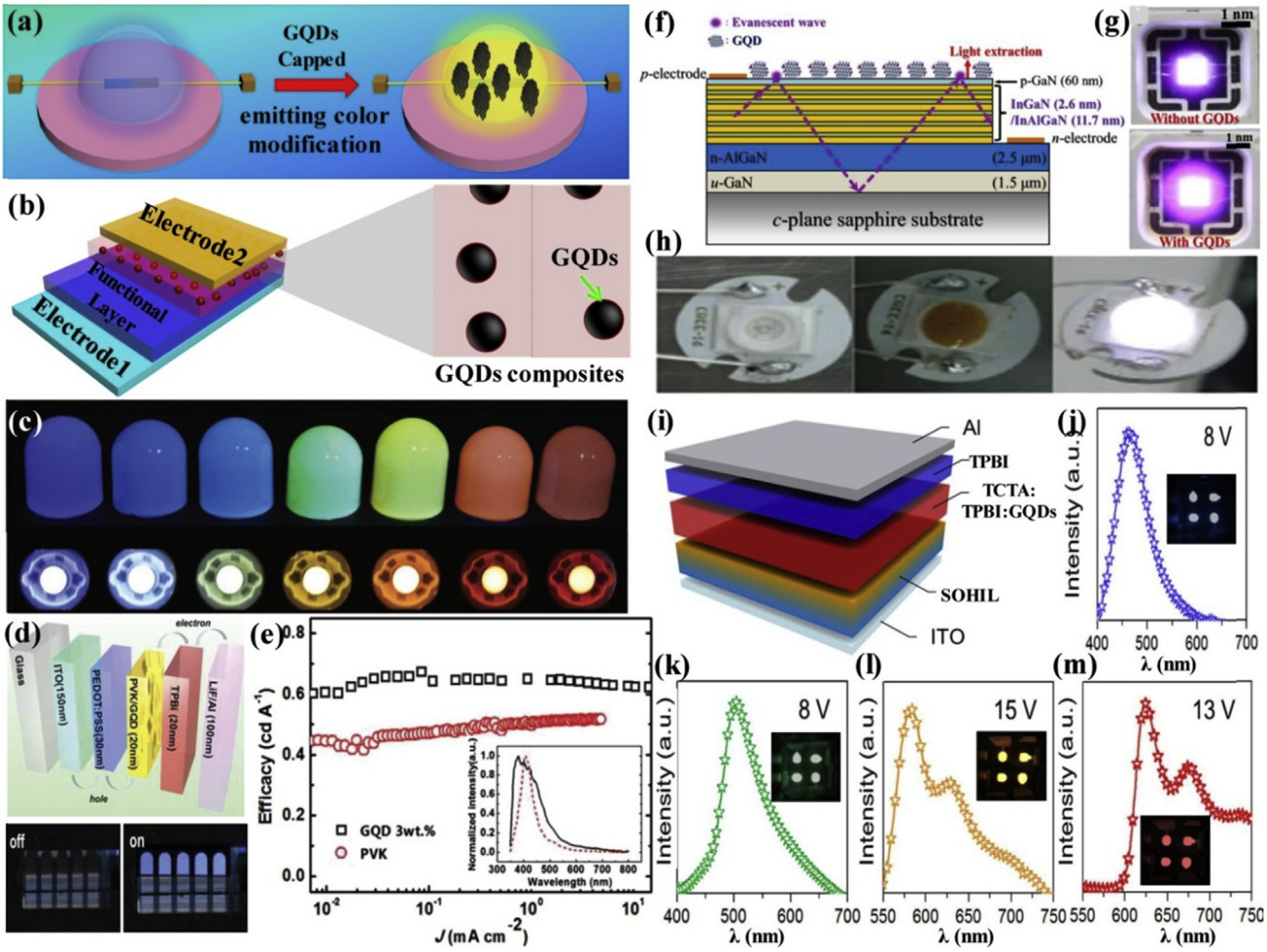

Fig. 28. Illustrative diagrams and results on the application of GQDs in LEDs. (a) Schematic of covering on LEDs route with GQDs; (b) Diagram of using the GQDs as emitting layer; (c) Top and bottom plane show fluorescence image of the GQDs phosphors/PDMS composites under 365 nm irradiation and photos of single color GQDs-covering LEDs operating under the voltage of 3.0 V, respectively [285]; (d) Schematic illustration of the GQD-LEDs structure and the corresponding band diagram (top plane), electroluminescent image of GQDs-LEDs, consisting of five emitting areas (bottom plane) [49]; (e) Luminous efficiencies and emission spectra of the devices, inset shows the emission spectra of LEDs composed of pure PVK (red dot line) and with 3 wt % (dark dot line) [49]; (f) and (g) show schematic cross section of the InGaN/InAlGaN UV LEDs coated with the GQDs and optical micrographs of the InGaN/InAlGaN LEDs without (top) and with (bottom) deposition of GQDs under an injection current of 100 mA, respectively [286]; (h) Photographs of the fabricated white LED lamp with no coating (left) and coated (middle) with GQDs as well as LEDs coated with GQDs ON states (right) [287]; (i) Structure of LEDs with GQDs as active layer [288]; (j–m) Electroluminescence spectra of the LEDs with different functionalized GQDs, each inset show the photos of LEDs [288].

layers. Another important aspect of GQDs based LEDs is that the color and intensity of the emitting light can be tuned by modifying the GQDs and its composite materials. In brief, the application of the GQDs on LEDs is fast becoming a reality in the near future.

4.2.3. Photocatalysis

Photocatalysis, which is the acceleration of a chemical reaction by light in the presence of a catalyst, has attracted considerable attention due to its application in renewable energy source. For example, clean energy can be generated by water-splitting into H_2 and O_2 using sunlight [291–295]. A visible light sensitive material capable of splitting water into H_2 and O_2 is critical in photocatalytic water-splitting [296], as shown in Fig. 29a. Another important criterion for such application is the use of low-cost, scalable and sustainable materials as photocatalysts. Carbon materials, which are low-cost, abundant and environmentally friendly, have been investigated as photocatalysts for cost-effective hydrogen production. Among the carbon materials, GQDs stand out as the best candidate for photocatalysis applications due to its many outstanding properties. For example, GQDs are 0D semiconductors with a bandgap that can be tailored by varying its size/shape and edge chemistry. Moreover, they exhibit large surface area, high electron mobility and can provide a direct path for the transport of photo- generated charge carriers, which will increase the lifetime of electron–hole pairs and upconversion behavior. Different methods to enhance photocatalysis performances have been investigated recently [77,297–302]. Photocatalysts comprising of GQDs composites with other inorganic materials in different shapes, such as nanoparticle [308–310], nanobelt [307] and nanowire [310,311] have been synthesized and studied. As shown in Fig. 29b, the composites of GQDs and CdS were fabricated, where the GQDs were attached on to the surface of CdS nanoparticles. This resulted in enhancing the intensity of absorption for visible light and the mechanism was explained in detail by Lei and co-workers [303]. Titanium dioxide (TiO_2), which has been frequently used as catalyst, was hybridized with GQDs and the hybridization mechanism was proposed by Yang and co-workers [304], as shown in Fig. 29c. Li [172] et al. explained the possible mechanism for the photocatalytic H_2 evolution of S,N-GQD/TiO_2 composites under UV–vis light irradiation using the band gap diagram shown in Fig. 29d. Composites of GQDs and ZnO NWs were also prepared for used as photocatalysts under solar irradiation [311], as illustrated in

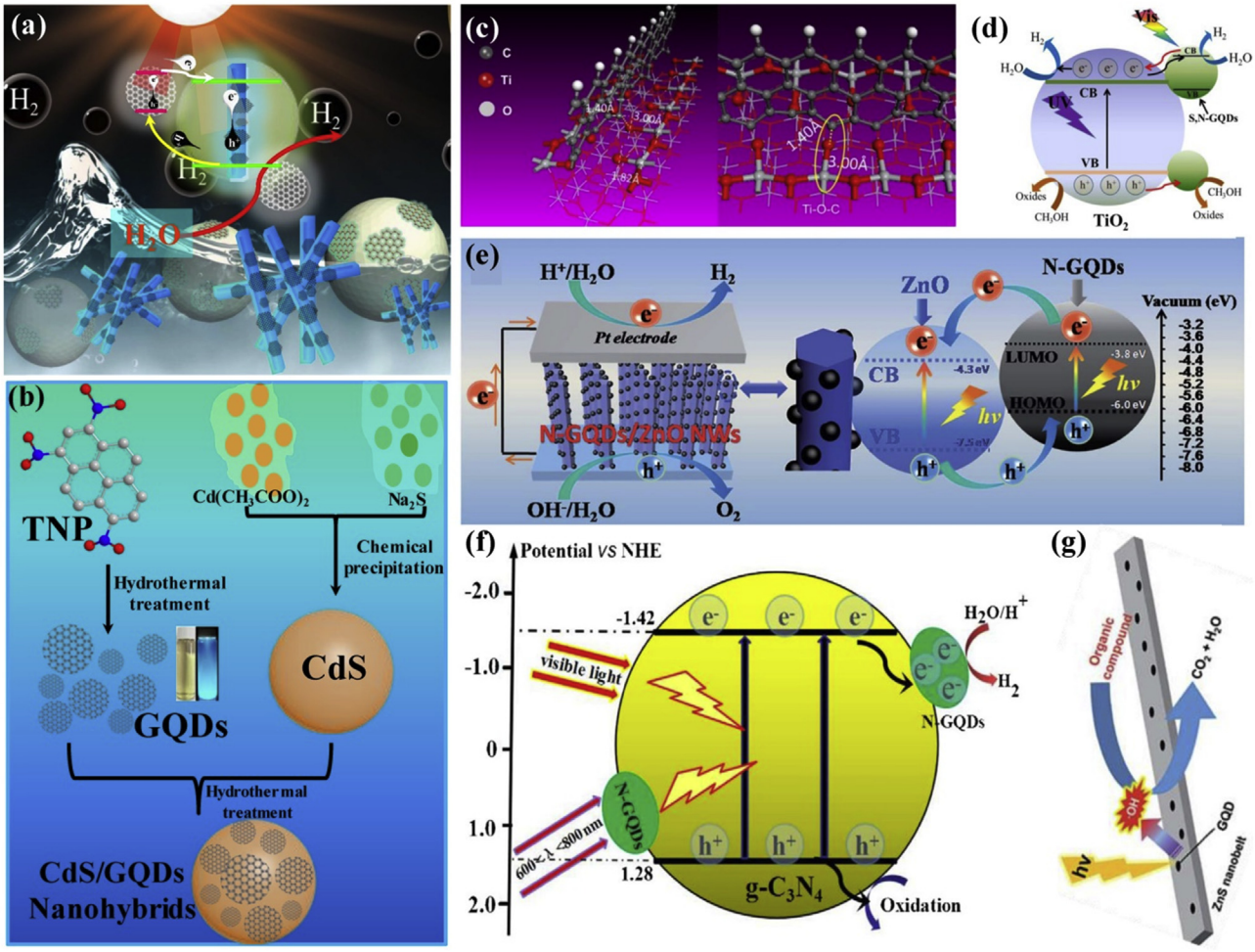

Fig. 29. Schematic illustration and mechanism of photocatalysis composed of GQDs. (a) Illustration of photocatalysts consisting of GQDs with different catalysts shapes; (b) Representation of preparation process of CdS/GQDs nanohybrids, inset shows the photography of GQDs and solution of GQDs under irradiation of 365 nm lamp [303]; (c) Simulation model of the cross-interaction in TiO_2 between carbon atoms and lattice oxygen (Ti–O) [304]; (d) Proposed mechanism for the photocatalytic H_2 evolution of S,N-GQD/TiO_2 composites under UV–vis light irradiation [172]; (e) Schematic illustration of splitting mechanism over the N-GQDs/ZnO NW heterostructure under simulated solar light irradiation [305]; (f) Photocatalytic mechanism for hydrogen evolution over NGQDs/g-C_3N_4 under visible light irradiation [306]; (g) Schematic for a plausible decomposition mechanism of GQDs/ZnS nanocomposite under light irradiation [307].

Fig. 29e. Moreover, the upconversion behavior of GQDs can also be observed in the composites of GQDs and g-C_3N_4 [306]. It can enhance the intensity of visible light by converting the NIR spectra to visible range, as shown in Fig. 29f. Nanobelts possess greater surface areas, as compared to nanowire, hence increasing the loading of GQDs to enhance photocatalytic performances. Jang et al. [307] prepared ZnS nanobelts decorated with GQDs for photodegradation reaction of rhodamine B, as shown in Fig. 29g.

The unique properties of GQDs have been exploited in the above-mentioned optical applications. With the continuous efforts in understanding the properties of GQDs and developing new functionalities of the nanomaterials, it is anticipated that new and novel optical applications will continue to be developed in the near future.

4.3. Energy-related applications

As the growth of population and the reduction of resources continue, it becomes an urgent quest to explore new and sustainable energy for the future. As carbon is one of the most abundant materials in the world, it can be considered as an excellent candidate for energy-related applications. Solar energy is clean and renewable energy that can be converted in to electrical energy to support our daily life. However, solar energy is only available in the day but not at night. Therefore, energy storage is an important topic in energy applications and it remains one of the major challenges in renewable energy. In the following sections, the use of GQDs in solar cells and energy storage battery are presented.

4.3.1. Solar cells

Solar cells, which can covert sunlight to electricity, provide clean and renewable energy source. It is also an essential energy source for society which has scarce resources to generate electricity using conventional methods. The characteristics of GQDs, such as the downconversion, strong fluorescence, intensive absorption at UV range and easily-functionalization etc., have led to development of different solar cells using GQDs to enhance the performances of the cells. Some of the solar cells were based on traditional silicon solar cells [322], polymer solar cells [31,323–332] and other novel solar cells [183,333–345] etc.

Hybrid of Si and GQDs remain the leader in all solar cells as its power conversion efficiency was significantly enhanced to 16.55% via utilizing the properties of GQDs, such as strong absorption at UV range [32,312] (Fig. 30a and e), down-shift energy [33,313] (Fig. 30b

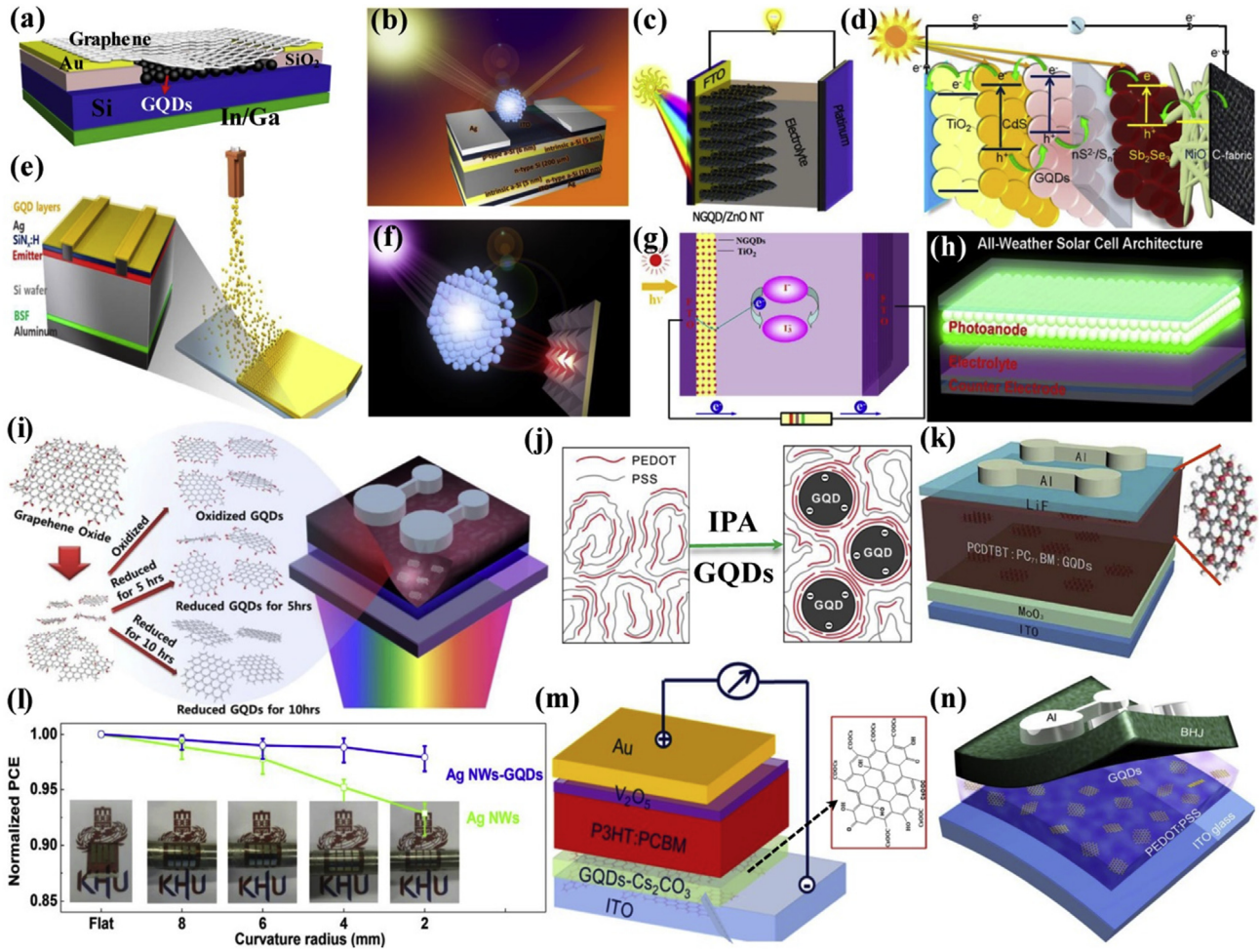

Fig. 30. Diagrams on the different structures of solar cells based on GQDs. (a) Schematic illustration of the GQDs/Si heterojunction solar cell with graphene film on top as the transparent electrode [312]; (b) [33], (e) [313] and (f) [32] show the GQDs/Si solar cells by taking advantage of downconversion of GQDs [32,33]; (c) Diagram of a typical quantum dot sensitized solar cells (QDSSC) based ZnO/GQDs device [314]; (d) Schematic structure of TiO_2/CdS/GQDs−nS^{2-}/$Sn^{2-}Sb_2Se_3$/NiO/C-fabric cell [315]; (g) The schematic device structure of NCQDs-sensitized TiO_2 solar cell [316]; (h) Diagram of all-weather GQDs solar cell [30]; (i) Schematic of a BHJ solar cell based on GQDs with different edge functional groups [317]; (j) Representation of the formation process of the GQDs@PEDOT core−shell nanostructure (CSNS) [203]; (k) Schematic structure of typical polymer solar cells based on GQDs [318]; (l) Normalized PCEs of the Ag NWs mixed with GQDs/graphene transparent conductive electrodes/flexible organic solar cells (TCE/FOSCs) as functions of bending radius. The inset shows real images of the FOSCs at different radium [319]; (m) Schematic structure of an inverted polymer solar cell with GQDs−Cs2CO3 buffer layer, inset shows the molecular structure of Cs_2CO_3 [320]; (n) Schematic of organic photovoltaic (OPV) device with a GQDs-incorporated PEDOT:PSS layer [321].

and f) and so on. Besides, the GQDs composites with other inorganic materials, such as ZnO [137,171,314,346–348], TiO_2 [315,316,349] and some classical solar materials [350–356], have also been reported, the power conversion efficiency of optimized devices were enhanced to 1.26%, 7.19% and 35% respectively. The structures of these solar cells are shown in Fig. 30c, d and g. Apart from using GQDs as active materials, they have been exploited for other functional layers, such as fluorescent layer of all-weather solar cells [30,357,358] (Fig. 30h), transporting layer [203] (Fig. 30j) and buffer layer [320] (Fig. 30m) etc. Organic materials were also used to form composites with GQDs [318] [359,360] (Fig. 30k) due to the ease of functionalization of the GQDs. Different functionalized types of the GQDs were investigated by Kim and co-workers [317] (refer to Fig. 30i). Their findings showed that enhanced optical absorptivity by rich functional groups in GQDs increased short-circuit current, while the improved conductivity of reduced GQDs led to an increase of fill factors and power conversion efficiency of up to 7.6%. The merit of organic solar cells is its flexibility, thus related research were studied by Shin and co-workers [319]. They have found that the GQDs enhanced the bending flexibility of the organic solar cells, as shown in Fig. 30l. Generally, the GQDs and organic materials were utilized to form the bulk heterojunction (BHJ) in organic solar cells [319,321], as shown in Fig. 30k and n.

In summary, GQDs have been applied as hybrid materials in both inorganic and organic solar cells. Besides, the performance of solar cells was enhanced by the special properties of the GQDs. Thus, the exploration of novel characteristics of GQDs will continue to make contribution towards the solar cells technology.

4.3.2. Energy storage battery

Most renewable energy sources, especially those harvested from nature, require storage via battery, thus it is important to develop supercapacitor battery technology that exhibit high efficiency, long-term cycling life, low weight, high energy density, and long-term stability to deal with the energy demand. The excellent properties of GQDs, such as large surface area and ease of functionalization, provide many advantages for energy storage applications. As shown in Fig. 31a, the environmentally friendly and high performance battery is composed of GQDs and the GQDs play vital role in the enhancement of battery performances.

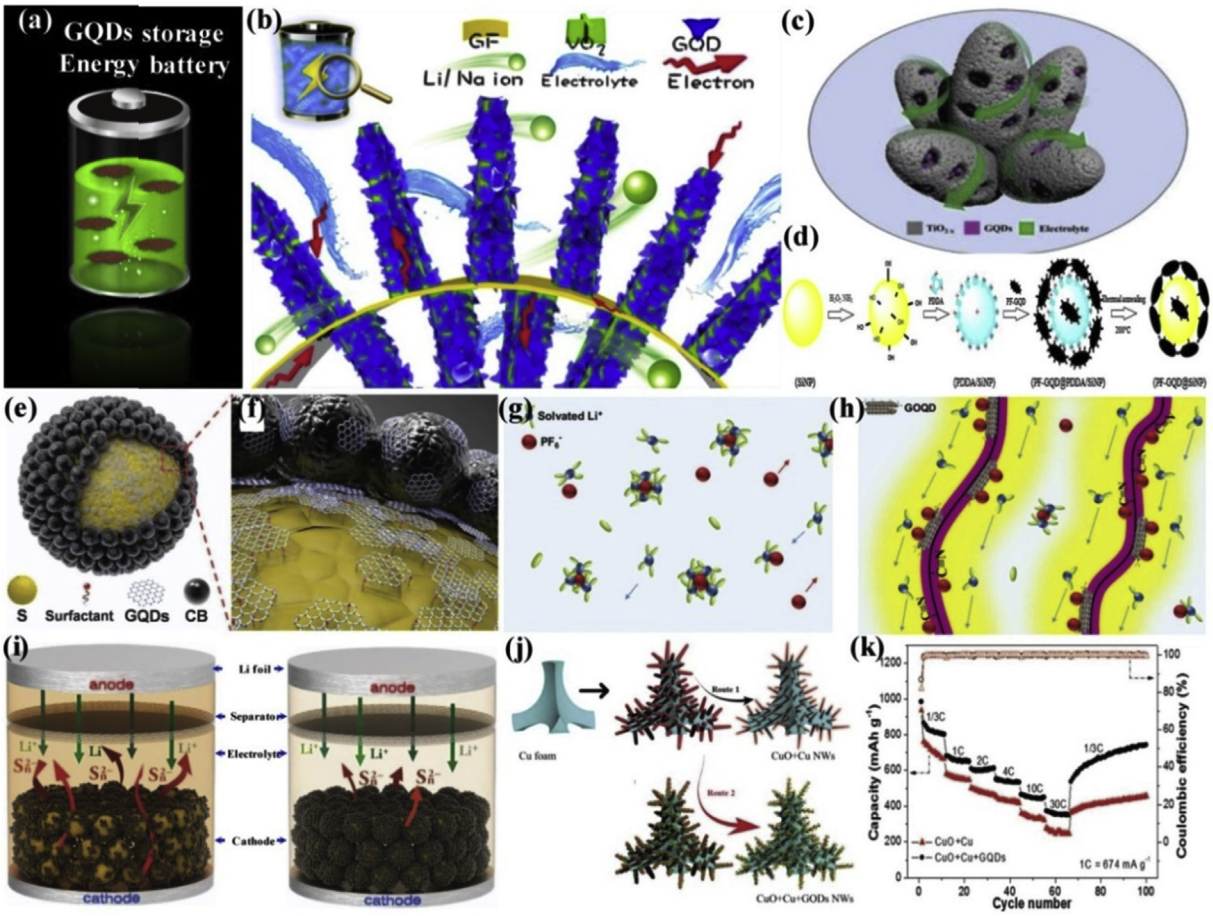

Fig. 31. Diagrams and performances of the different batteries with GQDs. (a) Schematic of battery based on GQDs; (b) Diagram of the GF supported GQD-anchored VO_2 arrays electrode.

Li ion and Na ion batteries have been widely investigated due to their high capacity, long cycle life and low cost. However, GQDs can be used as transporting materials to enhance the electrical properties of the battery [361] by introducing them into the electrolytes, as shown in Fig. 31b. In Li ion battery, TiO_2 has frequently been used as anodes. Wei and co-workers [362] fabricated hierarchical TiO_2 imbedded with GQDs (Fig. 31c), which were then applied to Li ion battery, and they reported a high specific capacity and excellent rate capability (160.1 $mAhg^{-1}$ at 10 C after 500 cycles). In addition, Li [363] *at el* synthesized GQDs composites with Si nanoparticles, as shown in Fig. 31d. They reported that the GQDs coated surface resulted in an improved with bicontinuous electron and Li/Na ion transfer channels [361]; (c) Schematic illustration of the electrochemical reaction process of TiO2/GQDs [362]; (d) The process for synthesis of GQDs/Si nanoparticles [363]; (e) and (f) show the structure and magnified structure of GQDs-sodium thiosulfate/carbon black (GQDs-S/CB), respectively [50]; (g) and (h) Conceptual illustrations of liquid electrolyte and Gel polymer electrolytes- a polymer framework comprising PAV and incorporated PMMA: Quantum Dots (GPE-PAVM:QD), respectively [364]; (i) Schematic configuration of S/CB (left) and GQDs-S/CB (right) employed as a cathode in a Li–S battery [50]; (j) Schematics of the fabrication process of CuO-based nanowire electrodes [365]; (k) Rate performance with coulombic efficiency of CuO, Cu, and GQDs (CCG) and CuO, Cu nanowires (CC) anodes [365]. electrical conductivity as well as effectively prevented (the capacity remained at 3068 $mAhg^{-1}$ after 100 cycles at 100 mAg^{-1}) the direct contact of silicon surface with the electrolyte molecules. Interestingly, Park and co-workers [50] coated both carbon black and GQDs on sodium thiosulfate (Fig. 31e and f) and investigated their characteristics, as well as demonstrated an excellent performance on discharge capacity of ~1000 $mAhg^{-1}$ even after 100 cycles. They discussed the structure of the cathode has a significant impact on the irreversible loss of high-order polysul-fides (HOPSs) during repeated battery operations, as shown in Fig. 31i. Furthermore, Teng et al. [364] demonstrated that GQDs can enhance the Li ion mobility in a gel polymer electrolyte (GPE) for Li ion batteries (LIBs) (delivering discharge capacity of 155 $mAhg^{-1}$) and the proposed mechanism of the enhancement is represented in Fig. 31g and h. Another experiment that can clearly account for the important role of GQDs in enhancing the performance of Li ion battery (having specific capacity of 780 $mAhg^{-1}$) was performed by Fan and co-workers [365]. The preparation process of their electrodes is shown in Fig. 31j. The plot, shown in Fig. 31k, reveals the different battery performances due to the different electrode structures.

As reported, the use of GQDs in batteries has led to improved performances in the battery. Importantly, such improvement in performances using GQDs is very cost-effective. Therefore the application of GQDs in battery to provide better energy storage is practical and commercially viable.

4.3.3. Fuel cell

Fuel cell can generate electricity through an electrochemical reaction of hydrogen fuel with oxygen. Unlike battery, fuel cell can provide a continuous supply of electricity as long as there is a constant source of fuel and oxygen (usually from air) to sustain the

chemical reaction. Such energy technology is sustainable and environmentally friendly. There are different types of fuel cell [366–368] but they all consist of an anode and a cathode, which are essential components of the fuel cell. In the past, the electrode materials were mainly made of precious metals, such as Pd, Pt, Ag and Au etc, hence leading to expensive fuel cell. Recent studies have demonstrated the use of functionalized GQDs as fuel cell electrodes [369,370]. Inner charge transfer of the functionalized GQDs has resulted in the enhancement of the catalytic activity and stability. Since then, there has been an increase in research activities to exploit functionalized GQDs as cathode materials for fuel cell.

5. Conclusions

In this review, the history of the GQDs is introduced. Most of the work performed so far indicates that the applications of GQDs are still at the early stage of development and have been progressing rapidly. Numerous methods in fabricating the GQDs have been reviewed. The different unique properties of the GQDs have been discussed. This included various functionalization routes of the GQDs to optimize or enhance its properties, such as water solubility, optical absorption and conductivity etc. Since the discovery of graphene, limited progress on the application of graphene has been achieved. It was understood that this is due to some practical problems of graphene, such as zero band gap and low absorptivity and so forth. The development of GQDs has therefore become an important catalyst for the application of graphene. Undoubtedly, this has led to significant research efforts in GQDs. As demonstrated by previous work, GQDs are becoming imperative functional materials that can find applications in medical, optical and energy-related fields. However, understanding of the mechanism in some of the GQDs applications remains unclear and requires further investigations. Nevertheless, this area of research has received much attention by researchers due to the enormous benefits of the GQDs can bring in the different applications.

In conclusion, this review has provided the developments, fabrication methods, different functionalization routes and applications of the GQDs with detailed discussions in those contexts. It also suggested the future direction for the development of GQDs.

Acknowledgements

This work was supported by National Natural Science Foundation of China (Grant Nos. 61106098, 51201150, and 11374250), the Key Project of Applied Basic Research of Yunnan Province, China (Grant No. 2012FA003), PolyU grant (1-ZVGH) and the Research Grants Council (RGC) of Hong Kong (Project Nos. PolyU 153030/15P and PolyU 153271/16P).

Appendix A. Supplementary data

Supplementary data to this article can be found online at https://doi.org/10.1016/j.mtchem.2018.09.007.

References

[1] B.C. Brodie, On the atomic weight of graphite, Phil. Trans. Roy. Soc. Lond. 149 (1859) 249–259.
[2] V. Kohlschütter, P. Haenni, Zur Kenntnis des Graphitischen Kohlenstoffs und der Graphitsäure, Z. Anorg. Allg. Chem. 105 (1919) 121–144.
[3] J.D. Bernal, The structure of graphite, Proc. R. Soc. Lond. Ser. A Contain. Pap. Math. Phys. Character 106 (1924) 749–773.
[4] P.R. Wallace, The band theory of graphite, Phys. Rev. 71 (1947) 622–634.
[5] G. Ruess, F. Vogt, Höchstlamellarer Kohlenstoff aus Graphitoxyhydroxyd, Monatsh. Chem. 78 (1948) 222–242.
[6] W.S. Hummers, R.E. Offeman, Preparation of graphitic oxide, J. Am. Chem. Soc. 80 (1958) 1339.
[7] H.P. Boehm, A. Clauss, G.O. Fischer, U. Hofmann, Das adsorptionsverhalten sehr dünner Kohlenstoff-Folien, Z. Anorg. Allg. Chem. 316 (1962) 119–127.
[8] D. DiVincenzo, E. Mele, Self-consistent effective-mass theory for intralayer screening in graphite intercalation compounds, Phys. Rev. B 29 (1984) 1685–1694.
[9] H.W. Kroto, J.R. Heath, S.C. O'Brien, R.F. Curl, R.E. Smalley, C60: buckminsterfullerene, Nature 318 (1985) 162–163.
[10] S. Mouras, A. Hamm, D. Djurado, J.-C. Cousseins, Synthesis of first stage graphite intercalation compounds with fluorides, Rev. Chim. Miner. 24 (1987) 151.
[11] S. Lijima, Helical microtubules of graphitic carbon, Nature 354 (1991) 56–58.
[12] K.S. Novoselov, A.K. Geim, S.V. Morozov, D. Jiang, Y. Zhang, S.V. Dubonos, I.V. Grigorieva, A.A. Firsov, Electric field effect in atomically thin carbon films, Science 306 (2004) 666–669.
[13] L.A. Ponomarenko, F. Schedin, M.I. Katsnelson, R. Yang, E.W. Hill, K.S. Novoselov, A.K. Geim, Chaotic dirac billiard in graphene quantum dots, Science 320 (2008) 356–358.
[14] X.Y. Xu, R. Ray, Y.L. Gu, H.J. Ploehn, L. Gearheart, K. Raker, W.A. Scrivens, Electrophoretic analysis and purification of fluorescent single-walled carbon nanotube fragments, J. Am. Chem. Soc. 126 (2004) 12736–12737.
[15] D. Wang, J.-F. Chen, L. Dai, Recent Advances in graphene quantum dots for fluorescence bioimaging from cells through tissues to animals, Part. Part. Syst. Char 5 (2015) 515–523.
[16] D. Pan, J. Zhang, Z. Li, M. Wu, Hydrothermal route for cutting graphene sheets into blue-Luminescent graphene quantum dots, Adv. Mater. 6 (2010) 734–738.
[17] Y. Zhao, C.G. Hu, Y. Hu, H.H. Cheng, G.Q. Shi, L.T. Qu, A versatile, ultralight, nitrogen-doped graphene framework, Angew. Chem. Int. Ed. 51 (2012) 11371–11375.
[18] X. Yan, X. Cui, L.-S. Li, Synthesis of large, stable colloidal graphene quantum dots with tunable Size, J. Am. Chem. Soc. 17 (2010) 5944–5945.
[19] S. Kim, S.W. Hwang, M.-K. Kim, D.Y. Shin, D.H. Shin, C.O. Kim, S.B. Yang, J.H. Park, E. Hwang, S.-H. Choi, G. Ko, S. Sim, C. Sone, H.J. Choi, S. Bae, B.H. Hong, Anomalous behaviors of visible luminescence from graphene quantum dots: interplay between size and shape, ACS Nano 9 (2012) 8203–8208.
[20] Y. Dong, H. Pang, S. Ren, C. Chen, Y. Chi, T. Yu, Etching single-wall carbon nanotubes into green and yellow single-layer graphene quantum dots, Carbon 64 (2013) 245–251.
[21] J. Peng, W. Gao, B.K. Gupta, Z. Liu, R. Romero-Aburto, L. Ge, L. Song, L.B. Alemany, X. Zhan, G. Gao, S.A. Vithayathil, B.A. Kaipparettu, A.A. Marti, T. Hayashi, J.-J. Zhu, P.M. Ajayan, Graphene quantum dots derived from carbon fibers, Nano Lett. 2 (2012) 844–849.
[22] Y. Dong, C. Chen, X. Zheng, L. Gao, Z. Cui, H. Yang, C. Guo, Y. Chi, C.M. Li, One-step and high yield simultaneous preparation of single- and multi-layer graphene quantum dots from CX-72 carbon black, J. Mater. Chem. 18 (2012) 8764.
[23] Y. Sun, S. Wang, C. Li, P. Luo, L. Tao, Y. Wei, G. Shi, Large scale preparation of graphene quantum dots from graphite with tunable fluorescence properties, Phys. Chem. Chem. Phys. 24 (2013) 9907.
[24] R.Q. Ye, C.S. Xiang, J. Lin, Z.W. Peng, K.W. Huang, Z. Yan, N.P. Cook, E.L.G. Samuel, C.C. Hwang, G.D. Ruan, G. Ceriotti, A.R.O. Raji, A.A. Marti, J.M. Tour, Coal as an abundant source of graphene quantum dots, Nat. Commun. 4 (2013) 2943.
[25] K. Habiba, V.I. Makarov, J. Avalos, M.J.F. Guinel, B.R. Weiner, G. Morell, Luminescent graphene quantum dots fabricated by pulsed laser synthesis, Carbon 64 (2013) 341–350.
[26] R. Liu, D. Wu, X. Feng, K. Müllen, Bottom-up fabrication of photoluminescent graphene quantum dots with uniform morphology, J. Am. Chem. Soc. 39 (2011) 15221–15223.
[27] L. Tang, R. Ji, X. Li, G. Bai, C.P. Liu, J. Hao, J. Lin, H. Jiang, K.S. Teng, Z. Yang, S.P. Lau, Deep ultraviolet to near-infrared emission and photoresponse in layered N-doped graphene quantum dots, ACS Nano 6 (2014) 6312–6320.
[28] J. Lu, P.S.E. Yeo, C.K. Gan, P. Wu, K.P. Loh, Transforming C-60 molecules into graphene quantum dots, Nat. Nanotechnol. 4 (2011) 247–252.
[29] S.Y. Lim, W. Shen, Z. Gao, Carbon quantum dots and their applications, Chem. Soc. Rev. 44 (2015) 362–381.
[30] Q. Tang, W. Zhu, B. He, P. Yang, Rapid conversion from carbohydrates to large-scale carbon quantum dots for all-weather solar cells, ACS Nano 11 (2017) 1540–1547.
[31] Y. Li, Y. Hu, Y. Zhao, G. Shi, L. Deng, Y. Hou, L. Qu, An Electrochemical avenue to green-luminescent graphene quantum dots as potential electron-acceptors for photovoltaics, Adv. Mater. 6 (2011) 776–780.
[32] M.-L. Tsai, W.-R. Wei, L. Tang, H.-C. Chang, S.-H. Tai, P.-K. Yang, S.P. Lau, L.-J. Chen, J.-H. He, Si Hybrid solar cells with 13% efficiency via concurrent improvement in optical and electrical properties by employing graphene quantum dots, ACS Nano 1 (2015) 815–821.
[33] M.-L. Tsai, W.-C. Tu, L. Tang, T.-C. Wei, W.-R. Wei, S.P. Lau, L.-J. Chen, J.-H. He, Efficiency enhancement of silicon heterojunction solar cells via photon management using graphene quantum dot as downconverters, Nano Lett. 1 (2015) 309–313.

[34] J. Ryu, J.W. Lee, H. Yu, J. Yun, K. Lee, J. Lee, D. Hwang, J. Kang, S.K. Kim, J. Jang, Correction: size effects of a graphene quantum dot modified-blocking TiO2 layer for efficient planar perovskite solar cells, J. Mater. Chem. A 34 (2017) 18276.

[35] H. Tetsuka, A. Nagoya, S.-I. Tamura, Graphene/nitrogen-functionalized graphene quantum dot hybrid broadband photodetectors with a buffer layer of boron nitride nanosheets, Nanoscale 47 (2016) 19677–19683.

[36] G. Haider, P. Roy, C.-W. Chiang, W.-C. Tan, Y.-R. Liou, H.-T. Chang, C.-T. Liang, W.-H. Shih, Y.-F. Chen, Electrical-polarization-induced ultrahigh responsivity photodetectors based on graphene and graphene quantum dots, Adv. Funct. Mater. 4 (2016) 620–628.

[37] T. Yu, F. Wang, Y. Xu, L. Ma, X. Pi, D. Yang, Graphene coupled with silicon quantum dots for high-performance bulk-silicon-based Schottky-junction photodetectors, Adv. Mater. 24 (2016) 4912–4919.

[38] C.-W. Chiang, G. Haider, W.-C. Tan, Y.-R. Liou, Y.-C. Lai, R. Ravindranath, H.-T. Chang, Y.-F. Chen, Highly stretchable and sensitive photodetectors based on hybrid graphene and graphene quantum dots, ACS Appl. Mater. Interfaces 1 (2016) 466–471.

[39] Q. Zhang, J. Jie, S. Diao, Z. Shao, Q. Zhang, L. Wang, W. Deng, W. Hu, H. Xia, X. Yuan, S.-T. Lee, Solution-processed graphene quantum dot deep-UV photodetectors, ACS Nano 2 (2015) 1561–1570.

[40] G. Konstantatos, M. Badioli, L. Gaudreau, J. Osmond, M. Bernechea, F.P.G. Arquer, F. Gatti, F.H.L. Koppens, Hybrid graphene-quantum dot phototransistors with ultrahigh gain, Nat. Nanotechnol. 6 (2012) 363–368.

[41] S. Zhu, J. Zhang, C. Qiao, S. Tang, Y. Li, W. Yuan, B. Li, L. Tian, F. Liu, R. Hu, H. Gao, H. Wei, H. Zhang, H. Sun, B. Yang, Strongly green-photoluminescent graphene quantum dots for bioimaging applications, Chem. Commun. 24 (2011) 6858.

[42] H. Shen, L. Zhang, M. Liu, Z. Zhang, Biomedical applications of graphene, Theranostics 3 (2012) 283–294.

[43] P.-C. Wu, J.-Y. Wang, W.-L. Wang, C.-Y. Chang, C.-H. Huang, K.-L. Yang, J.-C. Chang, C.-L.L. Hsu, S.-Y. Chen, T.-M. Chou, W.-S. Kuo, Efficient two-photon luminescence for cellular imaging using biocompatible nitrogen-doped graphene quantum dots conjugated with polymers, Nanoscale 1 (2018) 109–117.

[44] K. Li, W. Liu, Y. Ni, D. Li, D. Lin, Z. Su, G. Wei, Technical synthesis and biomedical applications of graphene quantum dots, J. Mater. Chem. B 5 (2017) 4811–4826.

[45] Q. Xu, Q. Zhou, Z. Hua, Q. Xue, C. Zhang, X. Wang, D. Pan, M. Xiao, Single-particle spectroscopic measurements of fluorescent graphene quantum dots, ACS Nano 12 (2013) 10654–10661.

[46] P. Nuengmatcha, P. Sricharoen, N. Limchoowong, R. Mahachai, S. Chanthai, The use of $S_2O_8^{2-}$ and H_2O_2 as novel specific masking agents for highly selective "turn-on" fluorescent switching recognition of CN^- and I^- based on $Hg2^+$–graphene quantum dots, RSC Adv. 8 (2018) 1407–1417.

[47] M. Mehrzad-Samarin, F. Faridbod, A.S. Dezfuli, M.R. Ganjali, A novel metronidazole fluorescent nanosensor based on graphene quantum dots embedded silica molecularly imprinted polymer, Biosens. Bioelectron. 92 (2017) 618–623.

[48] L. Zhou, F. Wu, J. Yu, Q. Deng, F. Zhang, G. Wang, Titanium carbide ($Ti_3C_2T_x$) MXene: a novel precursor to amphiphilic carbide-derived graphene quantum dots for fluorescent ink, light-emitting composite and bioimaging, Carbon 118 (2017) 50–57.

[49] S.H. Song, M.-H. Jang, J. Chung, S.H. Jin, B.H. Kim, S.-H. Hur, S. Yoo, Y.-H. Cho, S. Jeon, Highly efficient light-emitting diode of graphene quantum dots fabricated from graphite intercalation compounds, Adv. Opt. Mater. 11 (2014) 1016–1023.

[50] J. Park, J. Moon, C. Kim, J.H. Kang, E. Lim, J. Park, K.J. Lee, S.-H. Yu, J.-H. Seo, J. Lee, J. Heo, N. Tanaka, S.-P. Cho, J. Pyun, J. Cabana, B.H. Hong, Y.-E. Sung, Graphene quantum dots: structural integrity and oxygen functional groups for high sulfur/sulfide utilization in lithium sulfur batteries, NPG Asia Mater. 5 (2016) 272.

[51] D. Raeyani, S. Shojaei, S. Ahmadi-Kandjani, Optical graphene quantum dots gas sensors: theoretical study, Superlattice. Microst. 114 (2018) 321–330.

[52] S. Benitez-Martinez, M. Valcarcel, Graphene quantum dots as sensor for phenols in olive oil, Sensor. Actuator. B Chem. 197 (2014) 350–357.

[53] J. Qiu, R. Zhang, J. Li, Y. Sang, W. Tang, P.R. Gil, H. Liu, Fluorescent graphene quantum dots as traceable, pH-sensitive drug delivery systems, Int. J. Nanomed. 10 (2015) 6709–6724.

[54] H. Chen, Z. Wang, S. Zong, P. Chen, D. Zhu, L. Wu, Y. Cui, A graphene quantum dot-based FRET system for nuclear-targeted and real-time monitoring of drug delivery, Nanoscale 7 (2015) 15477–15486.

[55] Z. Wang, J. Xia, C. Zhou, B. Via, Y. Xia, F. Zhang, Y. Li, L. Xia, J. Tang, Synthesis of strongly green-photoluminescent graphene quantum dots for drug Carrier, Colloids Surfaces B Biointerfaces 112 (2013) 192–196.

[56] J. Dong, K. Wang, L. Sun, B. Sun, M. Yang, H. Chen, Y. Wang, J. Sun, L. Dong, Application of graphene quantum dots for simultaneous fluorescence imaging and tumor-targeted drug delivery, Sensor. Actuator. B 256 (2017) 616–623.

[57] H. Ding, F. Zhang, C. Zhao, Y. Lv, G. Ma, W. Wei, Z. Tian, Beyond a Carrier: graphene quantum dots as a probe for programmatically monitoring anticancer drug delivery, release, and response, ACS Appl. Mater. Interfaces 33 (2017) 27396–27401.

[58] X. Yao, X. Niu, K. Ma, P. Huang, J. Grothe, S. Kaskel, Y. Zhu, Graphene quantum dots-capped magnetic mesoporous silica nanoparticles as a multifunctional platform for controlled drug delivery, magnetic hyperthermia, and photothermal yherapy, Small 2 (2017) 1602225.

[59] M. Arvand, S. Hemmati, Analytical methodology for the electro-catalytic determination of estradiol and progesterone based on graphene quantum dots and poly(sulfosalicylic acid) co-modified electrode, Talanta 174 (2017) 243–255.

[60] L. Li, G. Wu, G. Yang, J. Peng, J. Zhao, J.-J. Zhu, Focusing on luminescent graphene quantum dots: current status and future perspectives, Nanoscale 5 (2013) 4015–4039.

[61] L. Tian, D. Ghosh, W. Chen, S. Pradhan, X. Chang, S. Chen, Nanosized carbon particles from natural gas soot, Chem. Mater. 13 (2009) 2803–2809.

[62] G. Eda, Y.-Y. Lin, C. Mattevi, H. Yamaguchi, H.-A. Chen, I.-S. Chen, C.-W. Chen, M. Chhowalla, Blue photoluminescence from chemically derived graphene oxide, Adv. Mater. 4 (2010) 505–509.

[63] L. Tang, R. Ji, X. Li, K.S. Teng, S.P. Lau, Size-dependent structural and optical characteristics of glucose-derived graphene quantum dots, Part. Part. Syst. Char. 6 (2013) 523–531.

[64] S.K. Das, C.M. Luk, W.E. Martin, L. Tang, D.Y. Kim, S.P. Lau, C.I. Richards, Size and dopant dependent single particle fluorescence properties of graphene quantum dots, J. Phys. Chem. C 31 (2015) 17988–17994.

[65] S. Zhu, J. Zhang, X. Liu, B. Li, X. Wang, S. Tang, Q. Meng, Y. Li, C. Shi, R. Hu, B. Yang, Graphene quantum dots with controllable surface oxidation, tunable fluorescence and up-conversion emission, RSC Adv. 2 (2012) 2717–2720.

[66] S. Zhu, J. Zhang, S. Tang, C. Qiao, L. Wang, H. Wang, X. Liu, B. Li, Y. Li, W. Yu, X. Wang, H. Sun, B. Yang, Surface chemistry routes to modulate the photoluminescence of graphene quantum dots: from fluorescence mechanism to up-conversion bioimaging applications, Adv. Funct. Mater. 22 (2012) 4732–4740.

[67] L.-L. Feng, Y.-X. Wu, D.-L. Zhang, X.-X. Hu, J. Zhang, P. Wang, Z.-L. Song, X.-B. Zhang, W. Tan, Near infrared graphene quantum dots-based two-photon nanoprobe for direct bioimaging of endogenous ascorbic acid in living cells, Anal. Chem. 7 (2017) 4077–4084.

[68] T. Gao, X. Wang, L.-Y. Yang, H. He, X.-X. Ba, J. Zhao, F.-L. Jiang, Y. Liu, Red, yellow, and blue luminescence by graphene quantum dots: syntheses, mechanism, and cellular imaging, ACS Appl. Mater. Interfaces 29 (2017) 24846–24856.

[69] Y. Dong, J. Shao, C. Chen, H. Li, R. Wang, Y. Chi, X. Lin, G. Chen, Blue luminescent graphene quantum dots and graphene oxide prepared by tuning the carbonization degree of citric acid, Carbon 12 (2012) 4738–4743.

[70] J. Gu, X. Zhang, A. Pang, J. Yang, Facile synthesis and photoluminescence characteristics of blue-emitting nitrogen-doped graphene quantum dots, Nanotechnology 27 (16) (2016) 165704.

[71] A.B. Ganganboina, A.D. Chowdhury, R.-A. Doong, N-Doped graphene quantum dots-decorated V_2O_5 nanosheet for fluorescence turn off–on detection of cysteine, ACS Appl. Mater. Interfaces 1 (2017) 614–624.

[72] L. Wang, Y. Wang, T. Xu, H. Liao, C. Yao, Y. Liu, Z. Li, Z. Chen, D. Pan, L. Sun, M. Wu, Gram-scale synthesis of single-crystalline graphene quantum dots with superior optical properties, Nat. Commun. 5 (2014) 5357.

[73] Z. Guo, B. Cai, Q. Cao, Y. Su, M. Li, J. Hu, Z. Yang, Y. Zhang, Facile synthesis of amine-functionalized graphene quantum dots with highly pH-sensitive photoluminescence, Fullerenes, Nanotub. Carbon Nanostruct. 25 (2017) 704–709.

[74] X. Wu, F. Tian, W. Wang, J. Chen, M. Wu, J.X. Zhao, Fabrication of highly fluorescent graphene quantum dots using L-glutamic acid for in vitro/in vivo imaging and sensing, J. Mater. Chem. C 31 (2013) 4676–4684.

[75] J. Gu, M.J. Hu, Q.Q. Guo, Z.F. Ding, X.L. Sun, J. Yang, High-yield synthesis of graphene quantum dots with strong green photoluminescence, RSC Adv. 4 (2014) 50141–50144.

[76] S. Zhuo, M. Shao, S.-T. Lee, Upconversion and downconversion fluorescent graphene quantum dots: ultrasonic preparation and photocatalysis, ACS Nano 6 (2012) 1059–1064.

[77] L. Lin, M. Rong, S. Lu, X. Song, Y. Zhong, J. Yan, Y. Wang, X. Chen, Facile synthesis of highly luminescent nitrogen-doped graphene quantum dots for the detection of 2,4,6-trinitrophenol in aqueous solution, Nanoscale 7 (2015) 1872–1878.

[78] Y. Yin, Q. Liu, D. Jiang, X. Du, J. Qian, H. Mao, K. Wang, Atmospheric pressure synthesis of nitrogen doped graphene quantum dots for fabrication of BiOBr nanohybrids with enhanced visible-light photoactivity and photostability, Carbon 96 (2016) 1157–1165.

[79] Y.-F. Chen, C.-L. Kao, P.-C. Huang, C.-Y. Hsu, C.-H. Kuei, Facile synthesis of multi-responsive functional graphene quantum dots for sensing metal cations, RSC Adv. 6 (2016) 103006–103011.

[80] M. Yousaf, H. Huang, P. Li, C. Wang, Y. Yang, Fluorine functionalized graphene quantum dots as inhibitor against hlAPP amyloid aggregation, ACS Chem. Neurosci. 8 (2017) 1368–1377.

[81] L. Tang, R. Ji, X. Cao, J. Lin, H. Jiang, X. Li, K.S. Teng, C.M. Luk, S. Zeng, J. Hao, S.P. Lau, Deep ultraviolet photoluminescence of water-soluble self-passivated graphene quantum dots, ACS Nano 6 (2012) 5102–5110.

[82] Z. Huang, Y. Shen, Y. Li, W. Zheng, Y. Xue, C. Qin, B. Zhang, J. Hao, W. Feng, Facile synthesis of analogous graphene quantum dots with sp2 hybridized carbon atom dominant structures and their photovoltaic application, Nanoscale 6 (2014) 13043–13052.

[83] X. Hou, Y. Li, C. Zhao, Microwave-assisted synthesis of nitrogen-doped multilayer graphene quantum dots with oxygen-rich functional groups, Aust. J. Chem. 3 (2016) 357.

[84] R. Li, Y. Liu, Z. Li, J. Shen, Y. Yang, X. Cui, G. Yang, Bottom-up fabrication of single-layered nitrogen-doped graphene quantum dots through intermolecular carbonization arrayed in a 2D plane, Chem. Eur. J. 1 (2016) 272–278.

[85] S. Gao, L. Tang, J. Xiang, R. Ji, S.K. Lai, S. Yuan, S.P. Lau, Facile preparation of sulphur-doped graphene quantum dots for ultra-high performance ultraviolet photodetectors, New J. Chem. 18 (2017) 10447–10451.

[86] S. Do, W. K, S.-W. Rhee, Soft-template synthesis of nitrogen-doped carbon nanodots: tunable visible-light photoluminescence and phosphor-based light-emitting diodes, J. Mater. Chem. C 2 (2014) 4221–4226.

[87] A. Ciesielski, S. Haar, A. Aliprandi, M.E. Garah, G. Tregnago, G.F. Cotella, M.E. Gemayel, F. Richard, H. Sun, F. Cacialli, F. Bonaccorso, P. Samori, Modifying thesSize of ultrasound-induced liquid-phase exfoliated graphene: from nanosheets to nanodots, ACS Nano 10 (2016) 10768–10777.

[88] E. Blanco, G. Blanco, J.M. Gonzalez-Leal, M.C. Barrera, M. Dominguez, M. Ramirez-del-Solar, Green and fast synthesis of amino-functionalized graphene quantum dots with deep blue photoluminescence, J. Nanopart. Res. 17 (2015) 214.

[89] J.P. Guin, S.K. Guin, T. Debnath, H.N. Ghosh, Chemically clean single-step oxido-reductive synthesis of green luminescent graphene quantum dots as impending electrocatalyst, Carbon 109 (2016) 517–528.

[90] D.K. Nguyen, T.Y. Kim, Graphene quantum dots produced by exfoliation of intercalated graphite nanoparticles and their application for temperature sensors, Appl. Surf. Sci. 427 (2018) 1152–1557.

[91] S. Maiti, S. Kundu, C.N. Roy, T.K. Das, A. Saha, Synthesis of excitation independent highly luminescent graphene quantum dots through perchloric acid oxidation, Langmuir 33 (2017) 14634–14642.

[92] M. Li, C. Yu, C. Hu, W. Yang, C. Zhao, S. Wang, M. Zhang, J. Zhao, X. Wang, J. Qiu, Solvothermal conversion of coal into nitrogen-doped carbon dots with singlet oxygen generation and high quantum yield, Chem. Eng. J. 320 (2017) 570–575.

[93] Z. Luo, G. Qi, K. Chen, M. Zou, L. Yuwen, X. Zhang, W. Huang, L. Wang, Microwave-assisted preparation of white fluorescent graphene quantum dots as a novel phosphor for enhanced white-light-emitting diodes, Adv. Funct. Mater. 26 (2016) 2739–2744.

[94] W. Zuo, L. Tang, J. Xiang, R. Ji, L. Luo, L. Rogee, S.P. Lau, Functionalization of graphene quantum dots by fluorine: preparation, properties, application, and their mechanisms, Appl. Phys. Lett. 110 (2017) 221901.

[95] Y.-W. Shih, G.-W. Tseng, C.-Y. Hsieh, Y.-Y. Li, A. Sakoda, Graphene quantum dots derived from platelet graphite nanofibers by liquid-phase exfoliation, Acta Mater. 78 (2014) 314–319.

[96] L. Lu, Y. Zhu, C. Shi, Y.T. Pei, Large-scale synthesis of defects-selective graphene quantum dots by ultrasonic assisted liquid-phase exfoliation, Carbon 109 (2016) 373–383.

[97] S. Sarkar, D. Gandla, Y. Venkatesh, P.R. Bangal, S. Ghosh, Y. Yang, S. Misra, Graphene quantum dots from graphite by liquid exfoliation showing excitation-independent emission, fluorescence upconversion and delayed fluorescence, Phys. Chem. Chem. Phys. 18 (2016) 21278–21287.

[98] M. Xu, W. Zhang, Z. Yang, F. Yu, Y. Ma, N. Hu, D. He, Q. Liang, Y. Su, Y. Zhang, One-pot liquid-phase exfoliation from graphite to graphene with carbon quantum dots, Nanoscale 7 (2015) 10527–10534.

[99] J. Zhao, L. Tang, J. Xiang, R. Ji, J. Yuan, J. Zhao, R. Yu, Y. Tai, L. Song, Chlorine doped graphene quantum dots: preparation, properties, and photovoltaic detectors, Appl. Phys. Lett. 105 (2014) 111116.

[100] H. Huang, S. Yang, Q. Li, Y. Yang, G. Wang, X. You, B. Mao, H. Wang, Y. Ma, P. He, Z. Liu, G. Ding, X. Xie, Electrochemical cutting in weak aqueous electrolytes: the strategy for efficient and controllable preparation of graphene quantum dots, Langmuir 34 (2018) 250–258.

[101] Y. Yan, H. Li, Q. Wang, H. Mao, W. Kun, Controllable ionic liquid-assisted electrochemical exfoliation of carbon fibers for the green and large-scale preparation of functionalized graphene quantum dots endowed with multicolor emission and size tenability, J. Mater. Chem. C 5 (2017) 6092–6100.

[102] T.-F. Yeh, S.-J. Chen, H. Teng, Synergistic effect of oxygen and nitrogen functionalities for graphene-based quantum dots used in photocatalytic H2 production from water decomposition, Nano Energy 12 (2015) 476–485.

[103] H. Zhu, A. Liu, Y. Xu, F. Shan, A. Li, J. Wang, W. Yang, C. Barrow, J. Liu, Graphene quantum dots directly generated from graphite via magnetron sputtering and the application in thin-film transistors, Carbon 88 (2015) 225–232.

[104] X. Hai, Q.-X. Mao, W.-J. Wang, X.-F. Wang, X.-W. Chen, J.-H. Wang, An acid-free microwave approach to prepare highly luminescent boron-doped graphene quantum dots for cell imaging, J. Mater. Chem. B 3 (2015) 9109–9114.

[105] Z. Fan, Y. Li, X. Li, L. Fan, S. Zhou, D. Fang, S. Yang, Surrounding media sensitive photoluminescence of boron-doped graphene quantum dots for highly fluorescent dyed crystals, chemical sensing and bioimaging, Carbon 70 (2014) 149–156.

[106] T.V. Tam, S.G. Kang, K.F. Babu, E.-S. Oh, S.G. Lee, W.M. Choi, Synthesis of B-doped graphene quantum dots as a metal-free electrocatalyst for the oxygen reduction reaction, J. Mater. Chem. A 5 (2017) 10537–10543.

[107] F. Qian, X. Li, L. Tang, S.K. Lai, C. Lu, S.P. Lau, Potassium doping: tuning the optical properties of graphene quantum dots, AIP Adv. 6 (2016) 075116.

[108] N.-U. Ain, M.O. Eriksson, S. Schmidt, M. Asghar, P.-C. Lin, P.O. Holtz, M. Syväjärvi, G.R. Yazdi, Tuning the emission energy of chemically doped graphene quantum dots, Nanomaterials (Basel) 6 (2016) 198.

[109] Q. Li, S. Zhang, L. Dai, L.-S. Li, Nitrogen-doped colloidal graphene quantum dots and their size-dependent electrocatalytic activity for the oxygen reduction reaction, J. Am. Chem. Soc. 134 (2012) 18932–18935.

[110] B. Zheng, Y. Chen, P. Li, Z. Wang, B. Cao, F. Qi, J. Liu, Z. Qiu, W. Zhang, Ultrafast ammonia-driven, microwave-assisted synthesis of nitrogen-doped graphene quantum dots and their optical properties, Nnaophotics 6 (2017) 259–267.

[111] X. Deng, J. Sun, S. Yang, H. Shen, W. Zhou, J. Lu, G. Ding, Z. Wang, The emission wavelength dependent photoluminescence lifetime of the N-doped graphene quantum dots, Appl. Phys. Lett. 107 (2015) 241905.

[112] M. Fan, C. Zhu, J. Yang, D. Sun, Facile self-assembly N-doped graphene quantum dots/graphene for oxygen reduction reaction, Electrochim. Acta 216 (2016) 102–109.

[113] Y. Bian, B. He, J. Li, A One-step hydrothermal method of nitrogen-doped graphene quantum dots decorated graphene for fabrication of paper-based fluorescent composite, BioResources 11 (2016) 6299–6308.

[114] S.B. Aoun, Nanostructured carbon electrode modified with N-doped graphene quantum dots-chitosan nanocomposite: a sensitive electrochemical dopamine sensor, Roy. Soc. Open Sci. 4 (2017) 171199.

[115] S. Kumar, S.K.T. Aziz, O. Girshevitz, G.D. Nessim, One-step synthesis of N-doped graphene quantum dots from chitosan as a sole precursor using chemical vapor deposition, J. Phys. Chem. C 122 (2018) 2343–2349.

[116] Y. Deng, L. Tang, C. Feng, G. Zeng, J. Wang, Y. Lu, Y. Liu, J. Yu, S. Chen, Y. Zhou, Construction of plasmonic Ag and nitrogen-doped graphene quantum dots codecorated ultrathin graphitic carbon nitride nanosheet composites with enhanced photocatalytic activity: full-spectrum response ability and mechanism insight, ACS Appl. Mater. Interfaces 9 (2017) 42816–42828.

[117] J. Ju, R. Zhang, S. He, W. Chen, Nitrogen-doped graphene quantum dots-based fluorescent probe for the sensitive turn-on detection of glutathione and its cellular imaging, RSC Adv. 4 (2014) 52583–52589.

[118] Y. Li, Y. Zhao, H. Cheng, Y. Hu, G. Shi, L. Dai, L. Qu, Nitrogen-doped graphene quantum dots with oxygen-rich functional groups, J. Am. Chem. Soc. 134 (2012) 15–18.

[119] S. Kundu, B. Malik, D.K. Pattanayak, P. Ragupathy, V.K. Pillai, Role of specific N-containing active sites in interconnected graphene quantum dots for the enhanced electrocatalytic activity towards oxygen evolution reaction, Chemisteryselect 2 (2017) 9943–9946.

[120] T.V. Tam, N.B. Trung, H.R. Kim, J.S. Chung, W.M. Choi, One-pot synthesis of N-doped graphene quantum dots as a fluorescent sensing platform for Fe^{3+} ions detection, Sensor. Actuator. B 202 (2014) 568–573.

[121] U. Saleem, F.A. Permatasari, F. Iskandar, T. Ogi, K. Okuyama, Y. Darma, M. Zhao, K.P. Loh, A. Rusydi, P. Coquet, M.D. Birowosuto, H. Wang, Surface plasmon enhanced nitrogen-doped graphene quantum dot emission by single bismuth telluride nanoplates, Adv. Opt. Mater. 5 (2017) 1700176.

[122] T. Pillar-Little, D.Y. Kim, Differentiating the impact of nitrogen chemical states on optical properties of nitrogen-doped graphene quantum dots, RSC Adv. 7 (2017) 48263–48267.

[123] Y. Dai, H. Long, X. Wang, Y. Wang, Q. Gu, W. Jiang, Y. Wang, C. Li, T.H. Zeng, Y. Sun, J. Zeng, Versatile graphene quantum dots with tunable nitrogen doping, Part. Part. Syst. Char. 31 (2014) 597–604.

[124] W.A. Saidi, Oxygen reduction electrocatalysis using N-doped graphene quantum-dots, J. Phys. Chem. Lett. 23 (2013) 4160–4165.

[125] S.R.M. Santiago, Y.A. Wong, T.-N. Lin, C.-H. Chang, C.-T. Yuan, J.-L. Shen, Effect of nitrogen doping on the photoluminescence intensity of graphene quantum dots, Opt. Lett. 42 (2017) 3642–3645.

[126] N.D. Anh, M.O. Hye, T.D. Ngoc, S. Bang, S.J. Yoon, M.S. Jeong, Highly enhanced photoresponsivity of a monolayer WSe2 photodetector with nitrogen-doped graphene quantum dots, ACS Appl. Mater. Interfaces 10 (2018) 10322–10329.

[127] X. Xu, F. Gao, X. Bai, F. Liu, W. Kong, M. Li, Tuning the photoluminescence of graphene quantum dots by photochemical doping with nitrogen, Materials 10 (2017) 1328.

[128] L. Lin, X. Song, Y. Chen, M. Rong, T. Zhao, Y. Jiang, Y. Wang, X. Chen, One-pot synthesis of highly greenish-yellow fluorescent nitrogen-doped graphene quantum dots for pyrophosphate sensing via competitive coordination with Eu3+ ions, Nanoscale 7 (2015) 15427–15433.

[129] Q. Liu, B. Guo, Z. Rao, B. Zhang, J.R. Gong, Strong two-photon-induced fluorescence from photostable, biocompatible nitrogen-doped graphene quantum dots for cellular and deep-tissue imaging, Nano Lett. 13 (2013) 2436–2441.

[130] T. Majumder, K. Debnath, S. Dhar, J.J.L. Hmar, S.P. Mondal, Nitrogen-doped graphene quantum dot-decorated ZnO nanorods for improved electrochemical solar energy conversion, Energy Technol. 4 (2016) 1–10.

[131] B. Zhang, C. Xiao, Y. Xiang, B. Dong, S. Ding, Y. Tang, Nitrogen-doped graphene quantum dots anchored on thermally reduced graphene oxide as an electrocatalyst for the oxygen reduction reaction, ChemElectroChem 3 (2016) 864–870.

[132] B.J. Moon, D. Jang, Y. Yi, H. Lee, S.J. Kim, Y. Oh, S.H. Lee, M. Park, S. Lee, S. Bae, Multi-functional nitrogen self-doped graphene quantum dots for boosting the photovoltaic performance of BHJ solar cells, Nano Energy 34 (2017) 36–46.

[133] L. Sun, Y. Luo, M. Li, G. Hu, Y. Xu, T. Tang, J. Wen, X. Li, L. Wang, Role of pyridinic-N for nitrogen-doped graphene quantum dots in oxygen reaction reduction, J. Colloid Interface Sci. 508 (2017) 154–158.

[134] L. Li, L. Li, C. Wang, K. Liu, R. Zhu, H. Qiang, Y. Lin, Synthesis of nitrogen-doped and amino acid-functionalized graphene quantum dots from glycine, and their application to the fluorometric determination of ferric ion, Microchim. Acta 182 (2015) 763–770.
[135] C. Zhu, S. Yang, G. Wang, R. Mo, P. He, J. Sun, Z. Di, N. Yuan, J. Ding, G. Ding, X. Xie, Negative induction effect of graphite N on graphene quantum dots: tunable band gap photoluminescence, J. Mater. Chem. C 3 (2015) 8810–8816.
[136] J. Sun, S. Yang, Z. Wang, H. Shen, T. Xu, L. Sun, H. Li, W. Chen, X. Jiang, G. Ding, Z. Kang, X. Xie, M. Jiang, Ultra-high quantum yield of graphene quantum dots: aromatic-nitrogen doping and photoluminescence mechanism, Part. Part. Syst. Char. 32 (2015) 434–440.
[137] W. Zhu, H. Song, L. Zhang, Y. Weng, Y. Su, Y. Lv, Fabrication of fluorescent nitrogen-rich graphene quantum dots by tin (IV) catalytic carbonization of ethanolamine, RSC Adv. 5 (2015) 60085–60089.
[138] Z.L. Wu, M.X. Gao, T.T. Wang, X.Y. Wan, L.L. Zheng, C.Z. Huang, A general quantitative pH sensor developed with dicyandiamide N-doped high quantum yield graphene quantum dots, Nanoscale 6 (2014) 3868–3874.
[139] M. Li, W. Wu, W. Ren, H.-M. Cheng, N. Tang, W. Zhong, Y. Du, Synthesis and upconversion luminescence of N-doped graphene quantum dots, Appl. Phys. Lett. 101 (2012) 103107.
[140] J. Qian, C. Shen, J. Yan, F. Xi, X. Dong, J. Liu, Tailoring the electronic properties of graphene quantum dots by P doping and their enhanced performance in metal-free composite photocatalyst, J. Phys. Chem. C 122 (2018) 349–358.
[141] Y. Li, S. Li, Y. Wang, J. Wang, H. Liu, X. Liu, L. Wang, X. Liu, W. Xue, N. Ma, Electrochemical synthesis of phosphorus-doped graphene quantum dots for free radical scavenging, Phys. Chem. Chem. Phys. 19 (2017) 11631–11638.
[142] D. Qu, M. Zheng, J. Li, Z. Xie, Z. Sun, Tailoring color emissions from N-doped graphene quantum dots for bioimaging applications, Light Sci. Appl. 4 (2015) 364.
[143] Z. Liu, Y. Gong, Z. Fan, Cysteine detection using a high-fluorescence sensor based on a nitrogen-doped graphene quantum dot–mercury (II) system, J. Lumin. 175 (2016) 129–134.
[144] Y. Zhang, X. Su, Q. Ma, Novel formaldehyde sensor based on hydrogen peroxide/melamine modulated photoluminescence of nitrogen-doped graphene quantum dots, J. Wuhan Univ. Technol. 32 (2017) 1481–1486.
[145] S. Kim, D.H. Shin, C.O. Kim, S.S. Kang, K.W. Lee, J. Kim, S.-H. Choi, S.W. Hwang, Effect of nitrogen doping on the structural and the optical variations of graphene quantum dots by using hydrazine treatment, J. Kor. Phys. Soc. 67 (2015) 746–751.
[146] D. Qu, M. Zheng, L. Zhang, H. Zhao, Z. Xie, X. Jing, R.E. Haddad, H. F, Z. Sun, Formation mechanism and optimization of highly luminescent N-doped graphene quantum dots, Sci. Rep. 4 (2014) 5294.
[147] X. Li, S.P. Lau, L. Tang, R. Ji, P. Yang, Sulphur doping: a facile approach to tune the electronic structure and optical properties of graphene quantum dots, Nanoscale 6 (2014) 5323–5328.
[148] K. Jin, H. Gao, L. Lai, Y. Pang, S. Zheng, Y. Niu, X. Li, Preparation of highly fluorescent sulfur doped graphene quantum dots for live cell imaging, J. Lumin. 197 (2018) 147–152.
[149] G. Wang, G. Guo, D. Chen, Z. Liu, X. Zheng, A. Xu, S. Yang, G. Ding, Facile and highly effective synthesis of controllable lattice sulfur-doped graphene quantum dots via hydrothermal treatment of durian, ACS Appl. Mater. Interfaces 10 (2018) 5750–5759.
[150] S. Yang, J. Sun, P. He, X. Deng, Z. Wang, C. Hu, G. Ding, X. Xie, Selenium doped graphene quantum dots as an ultrasensitive redox fluorescent switch, Chem. Mater. 27 (2015) 2004–2011.
[151] X. Li, S.P. Lau, L. Tang, R. Ji, P. Yang, Multicolour light emission from chlorine-doped graphene quantum dots, J. Mater. Chem. C 1 (2013) 7308–7313.
[152] D. Qu, Z. Sun, M. Zheng, J. Li, Y. Zhang, G. Zhang, H. Zhao, X. Liu, Z. Xie, Three colors emission from S,N co-doped graphene quantum dots for visible light H2 production and bioimaging, Adv. Opt. Mater. 3 (2015) 360–367.
[153] C. Shen, S. Ge, Y. Pang, F. Xi, J. Liu, X. Dong, P. Chen, Facile and scalable preparation of highly luminescent N,S co-doped graphene quantum dots and their application for parallel detection of multiple metal ions, J. Mater. Chem. B 5 (2017) 6593–6600.
[154] S.-J. Jeon, T.-W. Kang, J.-M. Ju, M.-J. Kim, J.H. Park, F. Raza, J. Han, H.-R. Lee, J.-H. Kim, Modulating the photocatalytic activity of graphene quantum dots via atomic tailoring for highly enhanced photocatalysis under visible light, Adv. Funct. Mater. 26 (2016) 8211–8219.
[155] Y. Luo, M. Li, L. Sun, Y. Xu, G. Hu, T. Tang, J. Wen, X. Li, Tuning the photoluminescence of graphene quantum dots by co-doping of nitrogen and sulfur, J. Nanopart. Res. 19 (2017) 363.
[156] H. Xu, S. Zhou, L. Xiao, Q. Yuan, W. Gan, Time-efficient syntheses of nitrogen and sulfur co-doped graphene quantum dots with tunable luminescence and their sensing applications, RSC Adv. 6 (2016) 36554–36560.
[157] A. Ananthanarayanan, Y. Wang, P. Routh, M.A. Sk, A. Than, M. Lin, J. Zhang, J. Chen, H. Sun, P. Chen, Nitrogen and phosphorus co-doped graphene quantum dots: synthesis from adenosine triphosphate, optical properties, and cellular imaging, Nanoscale 7 (2015) 8159–8165.
[158] D. Qu, M. Zheng, P. Du, Y. Zhou, L. Zhang, D. Li, H. Tan, Z. Zhao, Z. Xie, Z. Sun, Highly luminescent S, N co-doped graphene quantum dots with broad visible absorption bands for visible light photocatalysts, Nanoscale 5 (2013) 12272–12277.
[159] M. Favaro, L. Ferrighi, G. Fazio, L. Colazzo, C.D. Vaentin, C. Durante, F. Sedona, A. Gennaro, S. Agnoli, G. Granozzi, Single and multiple doping in graphene quantum dots: unraveling the origin of selectivity in the oxygen reduction reaction, ACS Catal. 5 (2015) 129–144.
[160] R.S. Li, B. Yuan, J.H. Liu, M.L. Liu, P.F. Gao, Y.F. Li, M. Li, C.Z. Huan, Boron and nitrogen co-doped single-layered graphene quantum dots: a high-affinity platform for visualizing the dynamic invasion of HIV DNA into living cells through fluorescence resonance energy transfer, J. Mater. Chem. B 5 (2017) 8719–8724.
[161] R. Liu, J. Zhao, Z. Huang, L. Zhang, M. Zou, B. Shi, S. Zhao, Nitrogen and phosphorus co-doped graphene quantum dots as a nano-sensor for highly sensitive and selective imaging detection of nitrite in live cell, Sensor. Actuator. B Chem. 240 (2017) 604–612.
[162] J.J.L. Hmar, T. Majumder, S. Dhar, S.P. Mondal, Sulfur and Nitrogen Co-doped graphene quantum dot decorated ZnO nanorod/polymer hybrid flexible device for photosensing applications, Thin Solid Films 612 (2016) 274–283.
[163] H. Xie, C. Hou, H. Wang, Q. Zhang, Y. Li, S, N co-doped graphene quantum dot/TiO_2 composites for efficient photocatalytic hydrogen generation, Nanoscale Res. Lett. 12 (2017) 400.
[164] H. Tian, K. Shen, X. Hu, L. Qiao, W. Zheng, N, S co-doped graphene quantum dots-graphene-TiO2 nanotubes composite with enhanced photocatalytic activity, J. Alloy. Comp. 691 (2017) 369–377.
[165] M. Mahyari, Y. Bide, J.N. Gavgani, Iron(III) porphyrin supported on S and N co-doped graphene quantum dot as an efficient photocatalyst for aerobic oxidation of alcohols under visible light irradiation, Appl. Catal. Gen. 517 (2016) 100–109.
[166] T.K. Mondal, D. Dinda, S.K. Saha, Nitrogen, sulphur co-doped graphene quantum dot: an excellent sensor for nitroexplosives, Sensor. Actuator. B 207 (2018) 586–593.
[167] Y. Dong, H. Pang, H.B. Yang, C. Guo, J. Shao, Y. Chi, C.M. Li, T. Yu, Carbon-based dots co-doped with nitrogen and sulfur for high quantum yield and excitation-independent emission, Angew. Chem. Int. Ed. 52 (2013) 7800–7804.
[168] Z. Luo, D. Yang, G. Qi, J. Shang, H. Yang, Y. Wang, L. Yuwen, T. Yu, W. Huang, L. Wang, Microwave-assisted solvothermal preparation of nitrogen and sulfur co-doped reduced graphene oxide and graphene quantum dots hybrids for highly efficient oxygen reduction, J. Mater. Chem. A 2 (2014) 20605–20611.
[169] N.T.N. Anh, A.D. Chowdhury, R.-A. Doong, Highly sensitive and selective detection of mercury ions using N, S-codoped graphene quantum dots and its paper strip based sensing application in wastewater, Sensor. Actuator. B 252 (2017) 1169–1178.
[170] M. Wang, Y. Sun, M. Yang, CdS QDs amplified electrochemiluminescence of N,S co-doped graphene quantum dots and its application for Pb(II) determination, Chem. Lett. 47 (2018) 44–47.
[171] O.J. Achadu, J. Britton, T. Nyokong, Graphene quantum dots functionalized with 4-amino-2, 2, 6, 6-tetramethylpiperidine-N-oxide as fluorescence “turn-on” nanosensors, J. Fluoresc. 26 (2016) 2199–2212.
[172] M. Dinari, M.M. Momeni, M. Goudarzirad, Nanocomposite films of polyaniline/graphene quantum dots and its supercapacitor properties, Surf. Eng. 32 (2016) 535–540.
[173] S. Kundu, R.M. Yadav, T.N. Narayanan, M.V. Shelke, R. Vajtai, P.M. Ajayan, V.K. Pillai, Synthesis of N, F and S co-doped graphene quantum dots, Nanoscale 7 (2015) 11515–11519.
[174] S. Kundu, P. Sarojinijeeva, R. Karthick, G. Anantharaj, G. Saritha, R. Bera, S. Anandan, A. Patra, P. Ragupathy, M. Selvaraj, D. Jeyakumar, K.V. Pillai, Enhancing the efficiency of DSSCs by the modification of TiO_2 photoanodes using N, F and S, co-doped graphene quantum dots, Electrochim. Acta 242 (2017) 337–343.
[175] M.A. Sk, A. Ananthanarayanan, L. Huang, K.H. Lim, P. Chen, Revealing the tunable photoluminescence properties of graphene quantum dots, J. Mater. Chem. C 2 (2014) 6954–6960.
[176] R. Ye, Z. Peng, A. Metzger, J. Lin, J.K. Mann, K. Huang, C. Xiang, X. Fan, E.L.G. Samuel, L.B. Alemany, A.A. Marti, J.M. Tour, Bandgap engineering of coal-derived graphene quantum dots, ACS Appl. Mater. Interfaces 7 (2015) 7041–7048.
[177] B. Mandal, S. Sarkar, P. Sarkar, Exploring the electronic structure of graphene quantum dots, J. Nanoparticle Res. 14 (2012) 1317.
[178] S. Kim, D.H. Shin, C.O. Kim, S.S. Kang, S.S. Joo, S.-H. Choi, S.W. Hwang, C. Sone, Size-dependence of Raman scattering from graphene quantum dots: interplay between shape and thickness, Appl. Phys. Lett. 102 (2013) 053108.
[179] T. Espiosa-Ortega, I.A. Luk'Yanchuk, Y.G. Rubo, Density of states in randomly shaped graphene quantum dots, Superlattice. Microst. 49 (2011) 283–287.
[180] J.S. Nascimento, D.R.D. Costa, M. Zarenia, A. Chaves, J.J.M. Pereira, Magnetic properties of bilayer graphene quantum dots in the presence of uniaxial strain, Phys. Rev. B 96 (2017) 115428.
[181] T. Espinosa-Ortega, I.A. Luk'yanchuk, Y.G. Rubo, Magnetic properties of graphene quantum dots, Phys. Rev. B 87 (2013) 205434.
[182] J. Vahakangas, P. Lantto, J. Vaara, Faraday rotation in graphene quantum dots: interplay of size, perimeter type, and functionalization, J. Phys. Chem. C 118 (2014) 23996–24005.
[183] R. Zhang, S. Qi, J. Jia, B. Torre, H. Zeng, H. Wu, X. Xu, Size and refinement edge-shape effects of graphene quantum dots on UV-visible absorption, J. Alloy. Comp. 623 (2015) 186–191.
[184] F. Liu, M.-H. Jang, H.D. Ha, J.-H. Kim, Y.-H. Cho, T.S. Seo, Facile synthetic method for pristine graphene quantum dots and graphene oxide quantum

dots: origin of blue and green luminescence, Adv. Mater. 25 (2013), 3657-3622.
[185] P. Zhang, Q. Hu, X. Yang, X. Hou, J. Mi, L. Liu, M. Dong, Size effect of oxygen reduction reaction on nitrogen-doped graphene quantum dots, RSC Adv. 8 (2018) 531–536.
[186] P. Elvati, E. Baumeister, A. Violi, Graphene quantum dots: effect of size, composition and curvature on their assembly, RSC Adv. 7 (2017) 17704–17710.
[187] H. Yang, K.H. Ku, J.M. Shin, J. Lee, C.H. Park, H.-H. Cho, S.G. Jang, B.J. Kim, Engineering the shape of block copolymer particles by surface-modulated graphene quantum dots, Chem. Mater. 28 (2016) 830–837.
[188] T. Wen, B. Yang, Y. Guo, J. Sun, C. Zhao, S. Zhang, M. Zhang, Y. Wang, Organosilane-functionalized graphene quantum dots and their encapsulation into bi-layer hollow silica spheres for bioimaging applications, Phys. Chem. Chem. Phys. 16 (2014) 23188–23195.
[189] L. Chen, C.X. Guo, Q. Zhang, Y. Lei, J. Xie, S. Ee, G. Guai, Q. Song, C.M. Li, Graphene quantum-dot-doped polypyrrole counter electrode for high-performance dye-sensitized solar cells, ACS Appl. Mater. Interfaces 5 (2013) 2047–2052.
[190] E. Zor, E. Morales-Narvaez, A. Zamora-Galvez, H. Bingol, M. Ersoz, A. Merkoci, Graphene quantum dots-based photoluminescent sensor: a multifunctional composite for pesticide detection, ACS Appl. Mater. Interfaces 7 (2015) 20272–20279.
[191] H.C. Lim, S.H. Min, E. Lee, J. Jang, S.H. Kim, J.-I. Hong, Self-assembled poly(3,4-ethylene dioxythiophene):poly(styrenesulfonate)/graphene quantum dot organogels for efficient charge transport in photovoltaic devices, ACS Appl. Mater. Interfaces 7 (2015) 11069–11073.
[192] C.M. Luk, L.B. Tang, W.F. Zhang, S.F. Yu, K.S. Teng, S.P. Lau, An efficient and stable fluorescent graphene quantum dot-agar composite as a converting material in white light emitting diodes, J. Mater. Chem. 22 (2012) 22378–22381.
[193] M.L. Lam, N.D. Nguyen, Q.T. Tran, Synthesis and characterization of polymeric graphene quantum dots based nanocomposites for humidity sensing, J. Nanomater. 2016 (2016) 5849018.
[194] X. Zhou, X. Gao, F. Song, C. Wang, F. Chu, S. Wu, A sensing approach for dopamine determination by boronic acid-functionalized molecularly imprinted graphene quantum dots composite, Appl. Suf. Sci. 423 (2017) 810–816.
[195] X. Chu, P. Dai, Y. Dong, W. Sun, L. Bai, W. Zhang, The acetic acid gas sensing properties of graphene quantum dots (GQDs)-ZnO nanocomposites prepared by hydrothermal method, J. Mater. Sci. Mater. Electron. 28 (2017) 19164–19173.
[196] X. Wu, Y. Zhang, T. Han, H. Wu, S. Guo, J. Zhang, Composite of graphene quantum dots and Fe_3O_4 nanoparticles: peroxidase activity and application in phenolic compound removal, RSC Adv. 4 (2014) 3299–3305.
[197] J. Liu, L. Qin, S.-Z. Kang, G. Li, X. Li, Gold nanoparticles/glycine derivatives/graphene quantum dots composite with tunable fluorescence and surface enhanced Raman scattering signals for cellular imaging, Mater. Des. 123 (2017) 32–38.
[198] D.K.L. Chan, P.L. Cheung, J.C. Yu, A visible-light-driven composite photocatalyst of TiO_2 nanotube arrays and graphene quantum dots, Beilstein J. Nanotechnol. 5 (2014) 689–695.
[199] S. Mondal, U. Rana, S. Malik, Graphene quantum dot-doped polyaniline nanofiber as high performance supercapacitor electrode materials, Chem. Commun. 51 (2015) 12365–12368.
[200] Q. Chen, Y. Hu, C. Hu, H. Cheng, Z. Zhang, H. Shao, L. Qu, Graphene quantum dots-three-dimensional graphene composites for high-performance supercapacitors, Phys. Chem. Chem. Phys. 16 (2014) 19307–19313.
[201] S. Dhar, T. Majumder, S.P. Mondal, Phenomenal improvement of external quantum efficiency, detectivity and responsivity of nitrogen doped graphene quantum dot decorated zinc oxide nanorod/polymer Schottky junction UV detector, Mater. Res. Bull. 95 (2017) 198–203.
[202] A. Cai, X. Wang, Y. Qi, Z. Ma, Hierarchical ZnO/S,N:GQD composites: biotemplated synthesis and enhanced visible-light-driven photocatalytic activity, Appl. Surf. Sci. 391 (2017) 484–490.
[203] X. Bu, S. Yang, Y. Bu, P. He, Y. Yang, G. Wang, H. Li, P. Wang, X. Wang, G. Ding, J. Yang, X. Xie, Highly active black TiO_2/N-doped graphene quantum dots nanocomposites for sunlight driven photocatalytic sewage treatment, ChemistrySelect 3 (2018) 12260–12265.
[204] Y. Ji, J. Hu, J. Biskupek, U. Kaiser, Y.-F. Song, C. Streb, Polyoxometalate-based bottom-up fabrication of graphene quantum dot/manganese vanadate composites as lithium ion battery anodes, Chem. Eur J. 23 (2017) 16637–16643.
[205] C. Lan, J. Zhao, L. Zhang, C. Wen, Y. Huang, S. Zhao, Self-assembled nanoporous graphene quantum dot-Mn3 O4 nanocomposites for surface-enhanced Raman scattering based identification of cancer cells, RSC Adv. 7 (2017) 18658–18667.
[206] X. Wu, S. Guo, J. Zhang, Selective oxidation of veratryl alcohol with composites of Au nanoparticles and graphene quantum dots as catalysts, Chem. Commun. 51 (2015) 6318–6321.
[207] X. Chu, J. Wang, J. Zhang, Y. Dong, W. Sun, W. Zhang, L. Bai, Preparation and gas-sensing properties of SnO_2/graphene quantum dots composites via solvothermal method, J. Mater. Sci. 52 (2017) 9441–9451.
[208] Z. Zhang, C. Fang, X. Bing, Y. Lei, Graphene quantum dots-ZnS nanocomposites with improved photoelectric performances, Materials 11 (2018) 512.
[209] J. Guo, H. Zhu, Y. Sun, L. Tang, X. Zhang, Doping MoS_2 with graphene quantum dots: structural and electrical engineering towards enhanced electrochemical hydrogen evolution, Electrochim. Acta 211 (2016) 603–610.
[210] V. Kumar, A. Kumar, A.M. Biradar, G.B. Reddy, D. Sachdev, R. Pasricha, Enhancement of electro-optical response of ferroelectric liquid crystal: the role of graphene quantum dots, Liq. Cryst. 41 (2014) 1719–1725.
[211] P.R. Kharangarh, S. Umapathy, G. Singh, Synthesis and luminescence of ceria decorated graphene quantum dots (GQDs): evolution of band gap, Integr. Ferroelectr. 184 (2017) 114–123.
[212] Z. Protich, P. Wong, K.S.V. Santhanam, Composite of zinc Using graphene quantum dot bath: a prospective material for energy storage, ACS Sustain. Chem. Eng. 4 (2016) 6177–6185.
[213] T. Hu, X. Chu, F. Gao, Y. Dong, W. Sun, L. Bai, Trimethylamine sensing properties of graphene quantum dots/α-Fe2O3 composites, J. Solid State Chem. 237 (2016) 284–291.
[214] H. Liu, W. Na, Z. Liu, X. Chen, X. Su, A novel turn-on fluorescent strategy for sensing ascorbic acid using graphene quantum dots as fluorescent probe, Biosens. Bioelectron. 92 (2017) 229–233.
[215] Z.S. Qian, X.Y. Shan, L.J. Chai, J.R. Chen, H. Feng, Dual-colored graphene quantum dots-labeled nanoprobes/graphene oxide: functional carbon materials for respective and simultaneous detection of DNA and thrombin, Nanotechnology 25 (2014) 415501.
[216] S. Xiao, D. Zhou, P. Luan, B. Gu, L. Feng, S. Fan, W. Liao, W. Fang, L. Yang, E. Tao, R. Guo, J. Liu, Graphene quantum dots conjugated neuroprotective peptide improve learning and memory capability, Biomaterials 106 (2016) 98–110.
[217] L. Chen, G. Yang, P. Wu, C. Cai, Real-time fluorescence assay of alkaline phosphatase in living cells using boron-doped graphene quantum dots as fluorophores, Biosens. Bioelectron. 96 (2017) 294–299.
[218] S. Radhakrishnan, A. Samanta, P.M. Sudeep, K.L. Maldonado, S.A. Mani, G. Acharya, C.S. Tiwary, A.K. Singh, P.M. Ajayan, Metal-free dual modal contrast agents based on fluorographene quantum dots, Part. Part. Syst. Char. 34 (2017) 1600221.
[219] Z.M. Markovic, B.Z. Ristic, K.M. Arsikin, D.G. Klisic, L.M. Harhaji-Trajkovic, B.M. Todorovic-Markovic, D.P. Kepic, T.K. Kravic-Stevovic, S.P. Jovanovic, M.M. Milenkovic, D.D. Milivojevic, V.Z. Bumbasirevic, M.D. Dramicanin, V.S. Trajkovic, Graphene quantum dots as autophagy-inducing photodynamic agents, Biomaterials 33 (2012) 7084–7092.
[220] M. Zubair, M. Mustafa, A. Ali, Y.H. Doh, K.H. Choi, Improvement of solution based conjugate polymer organic light emitting diode by ZnO-graphene quantum dots, J. Mater. Sci. Mater. Electron. 26 (2015) 3344–3351.
[221] D.H. Kim, T.W. Kim, Ultrahigh current efficiency of light-emitting devices based on octadecylamine-graphene quantum dots, Nano Energy 32 (2017) 441–447.
[222] W. Zhang, X. Zhang, X. Dong, H. Ma, G. Wang, Synthesis of N-doped graphene oxide quantum dots with the internal P-N heterojunction and its photocatalytic performance under visible light illumination, J. Adv. Oxid. Technol. 21 (2018) 201700331.
[223] Y. Yan, J. Chen, N. Li, J. Tian, K. Li, J. Jiang, J. Liu, Q. Tian, P. Chen, Systematic bandgap engineering of graphene quantum dots and applications for photocatalytic water splitting and CO_2 reduction, ACS Nano 12 (2018) 3523–3532.
[224] T.T. Do, K.B. Ko, Z. Khurelbaatar, C.-J. Choi, C.-H. Hong, V.C. Tran, Transparent and flexible ultraviolet photoconductors based on solution-processed graphene quantum dots on reduced graphene oxide films, Mater. Res. Bull. 91 (2017) 49–53.
[225] P. Sudhagar, I. Herraiz-Cardona, H. Park, T. Song, S.H. Noh, S. Gimenez, I.M. Sero, F. Fabregat-Santiago, J. Bisquert, C. Terashima, U. Paik, Y.S. Kang, A. Fujishima, T.H. Han, Exploring graphene quantum dots/TiO_2 interface in photoelectrochemical reactions: solar to fuel conversion, Electrochim. Acta 187 (2016) 249–255.
[226] Z. Zhu, J. Ma, Z. Wang, C. Mu, Z. Fan, L. Du, Y. Bai, L. Fan, H. Yan, D.L. Phillips, S. Yang, Efficiency enhancement of perovskite solar cells through fast electron extraction: the role of graphene quantum dots, J. Am. Chem. Soc. 136 (2014) 3760–3763.
[227] X. Yan, X. Cui, B. Li, L.-S. Li, Large, Solution-processable graphene quantum dots as light absorbers for photovoltaics, Nano Lett. 10 (2010) 1869–1873.
[228] H. Wang, Y. Yang, X. Zhou, R. Li, Z. Li, $NiCo_2S_4$/tryptophan-functionalized graphene quantum dot nanohybrids for high-performance supercapacitors, New J. Chem. 41 (2017) 1110–1118.
[229] M. Wang, Z. Fang, K. Zhang, J. Fang, F. Qin, Z. Zhang, J. Li, Y. Liu, Y. Lai, Synergistically enhanced activity of graphene quantum dots/graphene hydrogel composites: a novel all-carbon hybrid electrocatalyst for metal/air batteries, Nanoscale 8 (2016) 11398–11402.
[230] Z. Su, H. Shen, H. Wang, J. Wang, J. Li, G.U. Nienhaus, L. Shang, G. Wei, Motif-designed peptide nanofibers decorated with graphene quantum dots for simultaneous targeting and imaging of tumor cells, Adv. Funct. Mater. 25 (2015) 5472–5478.
[231] J. Zhang, Y.-Q. Ma, N. Li, J.-L. Zhu, T. Zhang, W. Zhang, B. Liu, Preparation of graphene quantum dots and their application in cell imaging, J. Nanomater. 2016 (2016) 9245865.
[232] D. Wu, Y. Liu, Y. Wang, L. Hu, H. Ma, G. Wang, Q. Wei, Label-free electrochemiluminescent immunosensor for detection of prostate specific antigen

based on aminated graphene quantum dots and carboxyl graphene quantum dots, Sci. Rep. 6 (2016) 20511.
[233] M. Thakur, A. Mewada, S. Pandey, M. Bhori, K. Singh, M. Sharon, M. Sharon, Milk-derived multi-fluorescent graphene quantum dot-based cancer theranostic system, Mat. Sci. Eng. C Mater. 67 (2016) 468–477.
[234] V.T. Tran, S.H. Hur, J.S. Chung, W.M. Choi, Ultraviolet light sensor based on graphene quantum dots/reduced graphene oxide hybrid film, Sensor. Actuat. A. Phys. 233 (2015) 368–373.
[235] S.D. Zhuang, Y. Chen, W.C. Zhang, Z. Chen, Z.L. Wang, Humidity sensor and ultraviolet photodetector based on Carrier trapping effect and negative photoconductivity in graphene quantum dots, Sci. Chin. Phys. Mech. 61 (2018) 0142111.
[236] C. Xu, S. Yang, L. Tian, T. Guo, G. Ding, J. Zhao, J. Sun, J. Lu, Z. Wang, Fabrication of centimeter-scale light-emitting diode with improved performance based on graphene quantum dots, Appl. Phys. Express 10 (2017) 032102.
[237] J. Zhu, X. Bai, J. Bai, G. Pan, Y. Zhu, Y. Zhai, H. Shao, X. Chen, B. Dong, H. Zhang, H. Song, Emitting color tunable carbon dots by adjusting solvent towards light-emitting devices, Nanotechnology 29 (2018) 085705.
[238] J. Joseph, A.A. Anappara, White-light emitting carbon dots prepared by the electrochemical exfoliation of graphite, ChemPhysChem 18 (2017) 292–298.
[239] J. Guo, H. Zhu, Y. Sun, L. Tang, X. Zhang, Boosting the lithium storage performance of MoS2 with graphene quantum dots, J. Mater. Chem. A 4 (2016) 4783–4789.
[240] D. Jiang, D. Ni, F. Liu, L. Zhang, L. Liu, X. Pu, A fluorescent imaging assay of cast in renal disease based on graphene quantum dots and Fe3O4 nanoparticles, Clin. Chim. Acta 454 (2016) 94–101.
[241] M. Zhang, L. Bai, W. Shang, W. Xie, H. Ma, Y. Fu, D. Fang, H. Sun, L. Fan, M. Han, C. Liu, S. Yang, Facile synthesis of water-soluble, highly fluorescent graphene quantum dots as a robust biological label for stem cells, J. Mater. Chem. 22 (2012) 7461–7467.
[242] K.L. Schroeder, R.V. Goreham, T. Nann, Graphene quantum dots for theranostics and bioimaging, Pharm. Res. 33 (2016) 2337–2357.
[243] Y.-L. Su, T.-W. Yu, W.-H. Chiang, H.-C. Chiu, C.-H. Chang, C.-S. Chiang, S.-H. Hu, Hierarchically targeted and penetrated delivery of drugs to tumors by size-changeable graphene quantum dot nanoaircrafts for photolytic therapy, Adv. Funct. Mater. 27 (2017) 1700056.
[244] S. Some, A.-R. Gwon, E. Hwang, G.-H. Bahn, Y. Yoon, Y. Kim, S.-H. Kim, S. Bak, J. Yang, D.-G. Jo, H. Lee, Cancer therapy using ultrahigh hydrophobic drug-loaded graphene derivatives, Sci. Rep. 4 (2014) 6314.
[245] D. Iannazzo, I. Ziccarelli, A. Pistone, Graphene quantum dots: multifunctional nanoplatforms for anticancer therapy, J. Mater. Chem. B 5 (2017) 6471–6489.
[246] D. Zhang, L. Wen, R. Huang, H. Wang, X. Hu, D. Xing, Mitochondrial specific photodynamic therapy by rare-earth nanoparticles mediated near-infrared graphene quantum dots, Biomaterials 153 (2018) 14–26.
[247] M.J. Birnkrant, K. Bell, S. Coreth, P.R. Harris, A.M. Vincitore, J.M. Alexander, Detection system for measuring presence of multiple conditions in predetermined area of aircraft, has control system to analyze more than one signal and wavelength of scattered light associated with node to determine presence and magnitude, ACS Nano 10 (2016) 8690–8699.
[248] H. Dong, W. Dai, H. Ju, H. Lu, S. Wang, L. Xu, S.F. Zhou, Y. Zhang, X. Zhang, Multifunctional poly(L-lactide)–polyethylene glycol-grafted graphene quantum dots for intracellular microRNA imaging and combined specific-gene-targeting agents delivery for improved therapeutics, ACS Appl. Mater. Interfaces 7 (2015) 11015–11023.
[249] C. Luo, Y. Li, L. Guo, F. Zhang, H. Liu, J. Zhang, J. Zheng, J. Zhang, S. Guo, Graphene quantum dots downregulate multiple multidrug-resistant genes via interacting with their C-rich promoters, Adv. Healthcare Mater. (2017) 1700328.
[250] K. Hola, Y. Zhang, Y. Wang, E.P. Giannelis, R. Zboril, A.L. Rogach, Carbon dots-Emerging light emitters for bioimaging, cancer therapy and optoelectronics, Nano Today 9 (2014) 590–603.
[251] W.-S. Kuo, H.-H. Chen, S.-Y. Chen, C.-Y. Chang, P.-C. Chen, Y.-I. Hou, Y.-T. Shao, H.-F. Kao, C.-L.L. Hsu, Y.-C. Chen, S.-J. Chen, S.-R. Wu, J.-Y. Wang, Graphene quantum dots with nitrogen-doped content dependence for highly efficient dual-modality photodynamic antimicrobial therapy and bioimaging, Biomaterials 120 (2017) 185–194.
[252] H. Sun, N. Gao, K. Dong, J. Ren, X. Qu, Graphene quantum dots-band-aids used for wound disinfection, ACS Nano 8 (2014) 6202–6210.
[253] A. Tayyebi, O. Akhavan, B.-K. Lee, M. Outokesh, Supercritical water in top-down formation of tunable-sized graphene quantum dots applicable in effective photothermal treatments of tissues, Carbon 130 (2018) 267–272.
[254] S. Li, S. Zhou, Y. Li, X. Li, J. Zhu, L. Fan, S. Yang, Exceptionally high payload of the IR780 iodide on folic acid-functionalized graphene quantum dots for targeted photothermal therapy, ACS Appl. Mater. Interfaces 9 (2017) 22332–22341.
[255] L. Rizzello, P.P. Pompa, Nanosilver-based antibacterial drugs and devices: mechanisms, methodological drawbacks, and guidelines, Chem. Soc. Rev. 43 (2014) 1501–1518.
[256] I. Mihalache, A. Radoi, R. Pascu, C. Romanitan, E. Vasile, M. Kusko, Engineering graphene quantum dots for enhanced ultraviolet and visible light p-Si nanowire-based photodetector, ACS Appl. Mater. Interfaces 9 (2017) 29234–29247.
[257] S. Kim, D.H. Shin, J. Kim, C.W. Jang, S.S. Kang, J.M. Kim, J.H. Kim, D.H. Lee, J.H. Kim, S.-H. Choi, S.W. Hwang, Energy transfer from an individual silica nanoparticle to graphene quantum dots and resulting enhancement of photodetector responsivity, Sci. Rep. 6 (2016) 27145.
[258] B. Yang, J. Chen, L. Cui, W. Liu, Enhanced photocurrent of a ZnO nanorod array sensitized with graphene quantum dots, RSC Adv. 5 (2015) 59204–59207.
[259] M.-L. Tsai, D.-S. Tsai, L. Tang, L.-J. Chen, S.P. Lau, J.-H. He, Omnidirectional harvesting of weak light using a graphene quantum dot-modified organic/silicon hybrid device, ACS Nano 11 (2017) 4564–4570.
[260] S. Dhar, T. Majumder, S.P. Mondal, Graphene quantum dot-sensitized ZnO nanorod/polymer Schottky junction UV detector with superior external quantum efficiency, detectivity, and responsivity, ACS Appl. Mater. Interfaces 8 (2016) 31822–31831.
[261] J. Zhao, L. Tang, J. Xiang, R. Ji, Y. Hu, J. Yuan, J. Zhao, Y. Tai, Y. Cai, Fabrication and properties of a high-performance chlorine doped graphene quantum dot based photovoltaic detector, RSC Adv. 5 (2015) 29222–29229.
[262] C. Chen, H. Qiao, S. Lin, C.M. Luk, Y. Liu, Z. Xu, J. Song, Y. Xue, D. Li, J. Yuan, W. Yu, C. Pan, S.Pi Lau, Q. Bao, Highly responsive MoS2 photodetectors enhanced by graphene quantum dots, Sci. Rep. 5 (2015) 11830.
[263] H. Tetsuka, A. Nagoya, T. Fukusumi, T. Matsui, Molecularly designed, nitrogen-functionalized graphene quantum dots for optoelectronic devices, Adv. Mater. 28 (2016) 4632–4638.
[264] C.O. Kim, S.W. Hwang, S. Kim, D.H. Shin, S.S. Kang, J.M. Kim, C.W. Jang, J.H. Kim, K.W. Lee, S.-H. Choi, E. Hwang, High-performance graphene-quantum-dot photodetectors, Sci. Rep. 4 (2014) 5603.
[265] S. Dhar, T. Majumder, P. Chakraborty, S.P. Mondal, DMSO modified PEDOT: PSS polymer/ZnO nanorods Schottky junction ultraviolet photodetector: photoresponse, external quantum efficiency, detectivity, and responsivity augmentation using N doped graphene quantum dots, Org. Electron. 53 (2018) 101–110.
[266] K. Rahimi, A. Yazdani, M. Ahmadirad, Graphene quantum dots enhance UV photoresponsivity and surface-related sensing speed of zinc oxide nanorod thin films, Mater. Des. 140 (2018) 222–230.
[267] F. Zhang, X. Feng, Y. Zhang, L. Yan, Y. Yang, X. Liu, Photoluminescent carbon quantum dots as a directly film-forming phosphor towards white LEDs, Nanoscale 8 (2016) 8618–8632.
[268] G.S. Kumar, U. Thupakula, P.K. Sarkar, S. Acharya, Easy extraction of water-soluble graphene quantum dots for light emitting diodes, RSC Adv. 5 (2015) 27711–27716.
[269] J.K. Kim, S. Bae, Y. Yi, M.J. Park, S.J. Kim, N.S. Myoung, C.-L. Lee, B.H. Hong, J.H. Park, Origin of white electroluminescence in graphene quantum dots embedded host/guest polymer light emitting diodes, Sci. Rep. 5 (2015) 11032.
[270] D.H. Kim, T.W. Kim, Highly-efficient organic light-emitting devices based on poly(N,N '-bis-4-butylphenyl-N,N '-bisphenyl)benzidine: octadecylamine-graphene quantum dots, Org. Electron. 57 (2018) 305–310.
[271] H. Li, C. Sun, M. Ali, F. Zhou, X. Zhang, D.R. MacFarlane, Sulfated carbon quantum dots as efficient visible-light switchable acid catalysts for room-temperature ring-opening reactions, Angew. Chem. Int. Ed. 54 (2015) 8420–8424.
[272] S. Chinnusamy, R. Kaur, A. Bokare, F. Erogbogbo, Incorporation of graphene quantum dots to enhance photocatalytic properties of anatase TiO_2, MRS Commun. 8 (2018) 137–144.
[273] J. Xia, J. Di, H. Li, H. Xu, H. Li, S. Guo, Ionic liquid-induced strategy for carbon quantum dots/BiOX (X=Br, Cl) hybrid nanosheets with superior visible light-driven photocatalysis, Appl. Catal. B Environ. 181 (2016) 260–269.
[274] A. Cai, Q. Wang, Y. Chang, X. Wang, Graphitic carbon nitride decorated with S,N co-doped graphene quantum dots for enhanced visible-light-driven photocatalysis, J. Alloy. Comp. 692 (2017) 183–189.
[275] G. Bai, M.-K. Tsang, J. Hao, Luminescent ions in advanced composite materials for multifunctional applications, Adv. Funct. Mater. 26 (2016) 6330–6350.
[276] X. Qin, X. Liu, W. Huang, M. Bettinelli, X. Liu, Lanthanide-activated phosphors based on 4f-5d optical transitions: theoretical and experimental aspects, Chem. Rev. 117 (2017) 4488–4527.
[277] B. Wang, H. Lin, F. Huang, J. Xu, H. Chen, Z. Lin, Y. Wang, Non-rare-earth $BaMgAl_{10-2x}O_{17}$:xMn^{4+},xMg^{2+}: a narrow-band red phosphor for use as a high-power warm w-LED, Chem. Mater. 28 (2016) 3515–3524.
[278] W. Dai, Y. Lei, M. Xu, P. Zhao, Z. Zhang, J. Zhou, Rare-earth free self-activated graphene quantum dots and copper-cysteamine phosphors for enhanced white light-emitting-diodes under single excitation, Sci. Rep. 7 (2017) 12872.
[279] J. Zhu, X. Bai, X. Chen, Z. Xie, Y. Zhu, G. Pan, Y. Zhai, H. Zhang, B. Dong, H. Song, Carbon dots with efficient solid-state red-light emission through the step-by-step surface modification towards light-emitting diodes, Dalton T 47 (2018) 3811–3818.
[280] P. Dong, B.-P. Jiang, W.-Q. Liang, Y. Huang, Z. Shi, X.-C. Shen, Synthesis of white-light-emitting graphene quantum dots via a one-step reduction and their interfacial characteristics-dependent luminescence properties, Inorg. Chem. Front. 4 (2017) 712–718.
[281] Q. Liu, D. Li, Z. Zhu, S. Yu, Y. Zhang, D. Yu, Y. Jiang, N-doped carbon dots from phenol derivatives for excellent colour rendering WLEDs, RSC Adv. 8 (2018) 4850–4856.

[282] X.-F. Wang, G.-G. Wang, J.-B. Li, Z. Liu, W.-F. Zhao, J.-C. Han, Towards high-powered remote WLED based on flexible white-luminescent polymer composite films containing S, N co-doped graphene quantum dots, Chem. Eng. J. 336 (2018) 406–415.
[283] R. Sekiya, Y. Uemura, H. Murakami, T. Haino, White-light-emitting edge-functionalized graphene quantum dots, Angew. Chem. Int. Ed. 53 (2014) 5619–5623.
[284] X. Guo, C.-F. Wang, Z.-Y. Yu, L. Chen, S. Chen, Facile access to versatile fluorescent carbon dots toward light-emitting diodes, Chem. Commun. 48 (2012) 2692–2694.
[285] Z. Tian, X. Zhang, D. Li, D. Zhou, P. Jing, D. Shen, S. Qu, R. Zboril, A.L. Rogach, Full-color inorganic carbon dot phosphors for white-light-emitting diodes, Adv. Opt. Mater 5 (2017) 1700416.
[286] T.-N. Lin, S.R.M. Santiago, C.-T. Yuan, K.-P. Chiu, J.-L. Shen, T.-C. Wang, H.-C. Kuo, C.-H. Chiu, Y.-C. Yao, Y.-J. Lee, Enhanced performance of GaN-based ultraviolet light emitting diodes by photon recycling using graphene quantum dots, Sci. Rep. 7 (2017) 7108.
[287] D. Pan, L. Wang, Z. Li, B. Geng, C. Zhang, J. Zhan, L. Yin, L. Wang, Synthesis of graphene quantum dot/metal-organic framework nanocomposites as yellow phosphors for white light-emitting diodes, New J. Chem. 42 (2018) 5083–5089.
[288] W. Kwon, Y.-H. Kim, J.-H. Kim, T. Lee, S. Do, Y. Park, M.S. Jeong, T.-W. Lee, S.-W. Rhee, High color-purity green, orange, and red light-emitting didoes based on chemically functionalized graphene quantum dots, Sci. Rep. 6 (2016) 24205.
[289] T. Feng, Q. Zeng, S. Lu, X. Yan, J. Liu, S. Tao, M. Yang, B. Yang, Color-tunable carbon dots possessing solid-state emission for full color light-emitting diodes applications, ACS Photonics 5 (2018) 502–510.
[290] H. Tetsuka, A. Nagoya, R. Asahi, Highly luminescent flexible amino-functionalized graphene quantum dots@cellulose nanofiber–clay hybrids for white-light emitting diodes, J. Mater. Chem. C 3 (2015) 3536–3541.
[291] O. Khaselev, A Monolithic photovoltaic-photoelectrochemical device for hydrogen production via water splitting, Science 280 (1998) 425–427.
[292] M. Grätzel, Photoelectrochemical cells, Nature 414 (2001) 338–344.
[293] K. Maeda, K. Teramura, D.L. Lu, T. Takata, N. Saito, Y. Inoue, K. Domen, Photocatalyst releasing hydrogen from water - enhancing catalytic performance holds promise for hydrogen production by water splitting in sunlight, Nature 440 (2006) 7082.
[294] F.E. Osterloh, Inorganic materials as catalysts for photochemical splitting of water, Chem. Mater. 20 (2008) 35–54.
[295] Akihiko Kudo, Yugo Miseki, Heterogeneous photocatalyst materials for water splitting, Chem. Soc. Rev. 38 (2009) 253–278.
[296] T.-F. Yeh, C.-Y. Teng, S.-J. Chen, H. Teng, Nitrogen-doped graphene oxide quantum dots as photocatalysts for overall water-splitting under visible light illumination, Adv. Mater. 26 (2014) 3297–3303.
[297] B.K. Gupta, G. Kedawat, Y. Agrawal, P. Kumar, J. Dwivedi, S.K. Dhawan, A novel strategy to enhance ultraviolet light driven photocatalysis from graphene quantum dots infilled TiO_2 nanotube arrays, RSC Adv. 5 (2015) 10623–10631.
[298] D. Pan, C. Xi, Z. Li, L. Wang, Z. Chen, B. Luc, M. Wu, Electrophoretic fabrication of highly robust, efficient, and benign heterojunction photoelectrocatalysts based on graphene-quantum-dot sensitized TiO_2 nanotube arrays, J. Mater. Chem. A 1 (2013) 3551–3555.
[299] S. Bian, C. Zhou, P. Li, J. Liu, X. Dong, F. Xi, Graphene quantum dots decorated titania nanosheets heterojunction: efficient charge separation and enhanced visiblelight photocatalytic performance, ChemCatChem 9 (2016) 3349–3357.
[300] S. Wang, I.S. Cole, Q. Li, Quantum-confined bandgap narrowing of TiO2 nanoparticles by graphene quantum dots for visible-light-driven applications, Chem. Commun. 52 (2016) 9208–9211.
[301] S. Yu, Y.-Q. Zhong, B.-Q. Yu, S.-Y. Cai, L.-Z. Wu, Y. Zhou, Graphene quantum dots to enhance the photocatalytic hydrogen evolution efficiency of anatase TiO_2 with exposed {001} facet, Phys. Chem. Chem. Phys. 18 (2016) 20338–20344.
[302] K.-A. Tsai, Y.-J. Hsu, Graphene quantum dots mediated charge transfer of CdSe nanocrystals for enhancing photoelectrochemical hydrogen production, Appl. Catal. B Environ. 164 (2015) 271–278.
[303] Y. Lei, C. Yang, J. Hou, F. Wang, S. Min, X. Ma, Z. Jin, J. Xu, G. Lu, K.-W. Huang, Strongly coupled CdS/graphene quantum dots nanohybrids for highly efficient photocatalytic hydrogen evolution: unraveling the essential roles of graphene quantum dots, Appl. Catal. B Environ. 216 (2017) 59–69.
[304] J. Tang, Y. Liu, Y. Hu, G. Lv, C. Yang, G. Yang, Carbothermal reduction induced Ti3+ self-doped TiO2/GQD nanohybrids for high-performance visible light photocatalysis, Chem. Eur J. 24 (2018) 4390–4398.
[305] Z. Zeng, F.-X. Xiao, X. Gui, R. Wang, B. Liu, T.T. Yang Tan, Layer-by-layer assembly of nitrogen-doped graphene quantum dots monolayer decorated one dimensional semiconductor nanoarchitectures for solar-driven water splitting, J. Mater. Chem. A 4 (2016) 16383–16393.
[306] J.-P. Zou, L.-C. Wang, J. Luo, Y.-C. Nie, Q.-J. Xing, X.-B. Luo, H.-M. Du, S.-L. Luo, S.L. Suib, Synthesis and efficient visible light photocatalytic H2 evolution of a metal-free g-C3N4/graphene quantum dots hybrid photocatalyst, Appl. Catal. B Environ. 193 (2016) 103–109.
[307] S. Ham, Y. Kim, M.J. Park, B.H. Hong, D.-J. Jang, Graphene quantum dots-decorated ZnS nanobelts with highly efficient photocatalytic performances, RSC Adv. 6 (2016) 24115–24120.
[308] X. Hao, Z. Jin, J. Xu, S. Min, G. Lu, Functionalization of TiO2 with graphene quantum dots for efficient photocatalytic hydrogen evolution, Superlattice. Microst. 94 (2016) 237–244.
[309] D. Pan, J. Jiao, Z. Li, Y. Guo, C. Feng, Y. Liu, L. Wang, M. Wu, Efficient separation of electron-hole pairs in graphene quantum dots by TiO2 heterojunctions for dye degradation, ACS Sustain. Chem. Eng. 3 (2015) 2405–2413.
[310] B. De, J. Balamurugan, N.H. Kim, J.H. Lee, Enhanced electrochemical and photocatalytic performance of core–shell CuS@carbon quantum dots@carbon hollow nanospheres, ACS Appl. Mater. Interfaces 9 (2017) 2459–2468.
[311] M. Ebrahimi, M. Samadi, S. Yousefzadeh, M. Soltani, A. Rahimi, T.-C. Chou, L.-C. Chen, K.-H. Chen, A.Z. Moshfegh, Improved solar-driven photocatalytic activity of hybrid graphene quantum dots/ZnO nanowires: a direct Z-scheme mechanism, ACS Sustain. Chem. Eng. 5 (2017) 367–375.
[312] S. Diao, X. Zhang, Z. Shao, K. Ding, J. Jie, X. Zhang, 12.35% efficient graphene quantum dots/silicon heterojunction solar cells using graphene transparent electrode, Nano Energy 31 (2017) 359–366.
[313] K.D. Lee, M.J. Park, D.-Y. Kim, S.M. Kim, B. Kang, S. Kim, H. Kim, H.-S. Lee, Y. Kang, S.S. Yoon, B.H. Hong, D. Kim, Graphene quantum dot layers with energy-down-shift effect on crystalline-silicon solar cells, ACS Appl. Mater. Interfaces 7 (2015) 19043–19049.
[314] T. Majumder, S. Dhar, P. Chakraborty, K. Debnath, S.P. Mondal, Advantages of ZnO nanotaper photoanodes in photoelectrochemical cells and graphene quantum dot sensitized solar cell applications, J. Electroanal. Chem. 813 (2018) 92–101.
[315] A. Kolay, R.K. Kokal, A. Kalluri, I. Macwan, P.K. Patra, P. Ghosal, M. Deepa, New Antimony selenide/nickel oxide photocathode boosts the efficiency of graphene quantum-dot co-sensitized solar cells, ACS Appl. Mater. Interfaces 9 (2017) 34915–34926.
[316] Y.-Q. Zhang, D.-K. Ma, Y.-G. Zhang, W. Chen, S.-M. Huang, N-doped carbon quantum dots for TiO2-based photocatalysts and dye-sensitized solar cells, Nano Energy 2 (2013) 545–552.
[317] J.K. Kim, M.J. Park, S.J. Kim, D.H. Wang, S.P. Cho, S. Bae, J.H. Park, B.H. Hong, Balancing light absorptivity and Carrier conductivity of graphene quantum dots for high-efficiency bulk heterojunction solar cells, ACS Nano 7 (2013) 7207–7212.
[318] Y. Dang, X. Zhang, X. Chen, B. Kang, S.R.P. Silva, Heterojunction solar cells with improved power conversion efficiency using graphene quantum dots, RSC Adv. 6 (2016) 110493–110498.
[319] D.H. Shin, S.W. Seo, J.M. Kim, H.S. Lee, S.-H. Choi, Graphene transparent conductive electrodes doped with graphene quantum dots-mixed silver nanowires for highly-flexible organic solar cells, J. Alloy. Comp. 744 (2018) 1–6.
[320] H.B. Yang, Y.Q. Dong, X. Wang, S.Y. Khoo, B. Liu, Cesium carbonate functionalized graphene quantum dots as stable electron-selective layer for improvement of inverted polymer solar cells, ACS Appl. Mater. Interfaces 6 (2014) 1092–1099.
[321] J.K. Kim, S.J. Kim, M.J. Park, S. Bae, S.-P. Cho, Q.G. Du, D.H. Wang, J.H. Park, B.H. Hong, Surface-engineered graphene quantum dots incorporated into polymer layers for high performance organic photovoltaics, Sci. Rep. 5 (2015) 14276.
[322] P. Gao, K. Ding, Y. Wang, K. Ruan, S. Diao, Q. Zhang, B. Sun, J. Jie, Crystalline Si/graphene quantum dots heterojunction solar cells, J. Phys. Chem. C 118 (2014) 5164–5171.
[323] Z. Ding, Z. Hao, B. Meng, Z. Xie, J. Liua, L. Dai, Few-layered graphene quantum dots as efficient hole-extraction layer for high-performance polymer solar cells, Nano Energy 15 (2015) 186–192.
[324] H.B. Yang, Y.Q. Dong, X. Wang, S.Y. Khoo, B. Liu, C.M. Li, Graphene quantum dots-incorporated cathode buffer for improvement of inverted polymer solar cells, Sol. Energy Mater. Sol. Cell. 117 (2013) 214–218.
[325] Y. Yang, X. Lin, W. Li, J. Ou, Z. Yuan, F. Xie, W. Hong, D. Yu, Y. Ma, Z. Chi, X. Chen, One-pot large-scale synthesis of carbon quantum dots: efficient cathode interlayers for polymer solar cells, ACS Appl. Mater. Interfaces 9 (2017) 14953–14959.
[326] F. Li, L. Kou, W. Chen, C. Wu, T. Guo, Enhancing the short-circuit current and power conversion efficiency of polymer solar cells with graphene quantum dots derived from double-walled carbon nanotubes, NPG Asia Mater. 5 (2013) 60.
[327] M. Li, W. Ni, B. Kan, X. Wan, L. Zhang, Q. Zhang, G. Long, Y. Zuo, Y. Chen, Graphene quantum dots as the hole transport layer material for high-performance organic solar cells, Phys. Chem. Chem. Phys. 15 (2013) 18973–18978.
[328] V. Gupta, N. Chaudhary, R. Srivastava, G.D. Sharma, R. Bhardwaj, S. Chand, Luminescent graphene quantum dots for organic photovoltaic devices, J. Am. Chem. Soc. 133 (2011) 9960–9963.
[329] D.H. Wang, J.K. Kim, S.J. Kim, B.H. Hong, J.H. Park, Efficient solution-processed small-molecule solar cells by insertion of graphene quantum dots, Nanoscale 6 (2014) 15175–15180.
[330] T.H. Nhu, N.T. Huynh, S.-J. Jang, V. Senthilkumar, Y.C. Park, S. Cho, Y.S. Kim, Enhancement of recombination process using silver and graphene quantum dot embedded intermediate layer for efficient organic tandem cells, Sci. Rep. 6 (2016) 30327.
[331] Z. Yang, J. Xie, V. Arivazhagan, K. Xiao, Y. Qiang, K. Huang, M. Hu, C. Cui, X. Yu, D. Yang, Efficient and highly light stable planar perovskite solar cells with graphene quantum dots doped PCBM electron transport layer, Nano Energy 40 (2017) 345–351.

[332] T.G. Novak, J. Kim, S.H. Song, G.H. Jun, H. Kim, M.S. Jeong, S. Jeon, Fast P3HT exciton dissociation and absorption enhancement of organic solar cells by PEG-functionalized graphene quantum dots, Small 12 (2016) 994–999.
[333] Q. Chang, Z. Ma, J. Wang, P. Li, Y. Yan, W. Shi, Q. Chen, Y. Huang, L. Huang, Hybrid graphene quantum dots@graphene foam nanosheets for dye-sensitized solar cell electrodes, Energy Technol. 4 (2016) 256–262.
[334] X. Fang, J. Ding, N. Yuan, P. Sun, M. Lv, G. Ding, C. Zhu, Graphene quantum dot incorporated perovskite films: passivating grain boundaries and facilitating electron extraction, Phys. Chem. Chem. Phys. 19 (2017) 6057–6063.
[335] P. Wang, S. Lin, G. Ding, X. Li, Z. Wu, S. Zhang, Z. Xu, S. Xu, Y. Lu, W. Xu, Z. Zheng, Enhanced monolayer MoS2/InP heterostructure solar cells by graphene quantum dots, Appl. Phys. Lett. 108 (2016) 163901.
[336] B. Mandal, S. Sarkar, P. Sarkar, Theoretical studies on understanding the feasibility of porphyrin-sensitized graphene quantum dot solar cell, J. Phys. Chem. C 119 (2015) 3400–3407.
[337] X. Fang, M. Li, K. Guo, J. Li, M. Pan, L. Bai, M. Luoshan, X. Zhao, Graphene quantum dots optimization of dye-sensitized solar cells, Electrochim. Acta 137 (2014) 634–638.
[338] B. Cui, L. Yan, H. Gu, Y. Yang, X. Liu, C.-Q. Ma, Y. Chen, H. Jia, Fluorescent carbon quantum dots synthesized by chemical vapor deposition: an alternative candidate for electron acceptor in polymer solar cells, Opt. Mater. 75 (2018) 166–173.
[339] E. Lee, J. Ryu, J. Jang, Fabrication of graphene quantum dots via size-selective precipitation and their application in upconversion-based DSSCs, Chem. Commun. 49 (2013) 9995–9997.
[340] H. Teymourinia, M. Salavati-Niasari, O. Amiri, M. Farangi, Facile synthesis of graphene quantum dots from corn powder and their application as down conversion effect in quantum dot-dye-sensitized solar cell, J. Mol. Liq. 251 (2018) 267–272.
[341] Y. Zhang, Y. Zhao, J. Duan, Q. Tang, S-doped CQDs tailored transparent counter electrodes for high-efficiency bifacial dye-sensitized solar cells, Electrochim. Acta 261 (2018) 588–595.
[342] I. Mihalache, A. Radoi, M. Mihaila, C. Munteanu, A. Marin, M. Danila, M. Kusko, C. Kusko, Charge and energy transfer interplay in hybrid sensitized solar cells mediated by graphene quantum dots, Electrochim. Acta 153 (2015) 306–315.
[343] T. Majumder, S.P. Mondal, Advantages of nitrogen-doped graphene quantum dots as a green sensitizer with ZnO nanorod based photoanodes for solar energy conversion, J. Electroanal. Chem. 769 (2016) 48–52.
[344] F. Gao, C.-L. Yang, M.-S. Wang, X.-G. Ma, Computational studies on the absorption enhancement of nanocomposites of tetraphenylporphyrin and graphene quantum dot as sensitizers in solar cell, J. Mater. Sci. 53 (2018) 5140–5150.
[345] Wei, Q. Li, Top-down strategy toward versatile graphene quantum dots for organic/inorganic hybrid solar cells, ACS Sustain. Chem. Eng. 3 (2015) 637–644.
[346] M. Dutta, S. Sarkar, T. Ghosh, D. Basak, ZnO/graphene quantum dot solid-state solar cell, J. Phys. Chem. C 116 (2012) 20127–20131.
[347] S. Tamandani, G. Darvish, Charge transfer modeling in monolayer circular graphene quantum dots-ZnO nanowires system for application in photovoltaic devices, Int. J. Mod. Phys. B 31 (2017) 1650253.
[348] G. Zamiri, S. Bagheri, Fabrication of green dye-sensitized solar cell based on ZnO nanoparticles as a photoanode and graphene quantum dots as a photosensitizer, J. Colloid Interface Sci. 511 (2018) 318–324.
[349] Q. Zhang, G. Zhang, X. Sun, K. Yin, H. Li, Improving the power conversion efficiency of carbon quantum dot-sensitized solar cells by growing the dots on a TiO_2 photoanode in situ, Nanomaterials 130 (2017) 7060130.
[350] Q. Liu, Y. Yin, N. Hao, J. Qian, H. Mao, K. Wang, Self-templating synthesis of nitrogen doped graphene quantum dots/3D bismuth oxyiodine hybrid hollow microspheres with improved visible-light excited photocurrent generation: simultaneous electron transfer acceleration and bandgap narrowing, J. Alloy. Comp. 729 (2017) 27–37.
[351] X. Zhang, R. Ke, S. Zhang, H. Niu, J. Song, C. Mao, B. Jin, Y. Tian, One-step electrosynthesis and photoelectric conversion of selenium nanowires wrapped with graphene quantum dots, Electrochim. Acta 168 (2015) 116–124.
[352] Y. Zhong, H. Zhang, D. Pan, L. Wang, X. Zhong, Graphene quantum dots assisted photovoltage and efficiency enhancement in CdSe quantum dot sensitized solar cells, J. Energy Chem. 24 (2015) 722–728.
[353] J. Wang, X. Xin, Z. Lin, Cu_2ZnSnS_4 nanocrystals and graphene quantum dots for photovoltaics, Nanoscale 3 (2011) 3040–3048.
[354] C. Yu, Z. Liu, Y. Chen, X. Meng, M. Li, J. Qiu, CoS nanosheets-coupled graphene quantum dots architectures as a binder-free counter electrode for high-performance DSSCs, Sci. Chin. Mater. 59 (2016) 104–111.
[355] M. Dinari1, M.M. Momeni1, M. Goudarzirad, Dye-sensitized solar cells based on nanocomposite of polyaniline/graphene quantum dots, J. Mater. Sci. 51 (2016) 2964–2971.
[356] T.-N. Lin, S.R.M.S. Santiago, J.-A. Zheng, Y.-C. Chao, C.-T. Yuan, J.-L. Shen, C.-H. Wu, C.-A.J. Lin, W.-R. Liu, M.-C. Cheng, W.-C. Chou, Enhanced conversion efficiency of III-V triple-junction solar cells with graphene quantum dots, Sci. Rep. 6 (2016) 39163.
[357] Q. Tang, All-weather solar cells: a rising photovoltaic revolution, Chem. Eur J. 23 (2017) 8118–8127.
[358] Y. Meng, Y. Zhang, W. Sun, M. Wang, B. He, H. Chen, Q. Tang, Biomass converted carbon quantum dots for all-weather solar cells, Electrochim. Acta 257 (2017) 259–266.
[359] C.-P. Lee, K.-Y. Lai, C.-A. Lin, C.-T. Li, K.-C. Ho, C.-I. Wu, S.-P. Lau, J.-H. He, A paper-based electrode using a graphene dot/PEDOT:PSS composite for flexible solar cells, Nano Energy 36 (2017) 260–267.
[360] C.-P. Leea, C.-A. Lin, T.-C. Wei, M.-L. Tsai, Y. Meng, C.-T. Li, K.-C. Ho, C.-I. Wu, S.-P. Lau, J.-H. He, Economical low-light photovoltaics by using the Pt-free dye-sensitized solar cell with graphene dot/PEDOT:PSS counter electrodes, Nano Energy 18 (2015) 109–117.
[361] D. Chao, C. Zhu, X. Xia, J. Liu, X. Zhang, J. Wang, P. Liang, J. Lin, H. Zhang, Z.X. Shen, H.J. Fan, Graphene quantum dots coated VO_2 arrays for highly durable electrodes for Li and Na ion batteries, Nano Lett. 15 (2015) 565–573.
[362] W. Zhang, T. Xu, Z. Liu, N.-L. Wu, M. Wei, Hierarchical TiO2-x imbedded with graphene quantum dots for high-performance lithium storage, Chem. Commun. 54 (2018) 1413–1416.
[363] L. Kong, Y. Yang, R. Li, Z. Li, Phenylalanine-functionalized graphene quantum dot-silicon nanoparticle composite as an anode material for lithium ion batteries with largely enhanced electrochemical performance, Electrochim. Acta 198 (2016) 144–155.
[364] Y.-M. Chen, S.-T. Hsu, Y.-H. Tseng, T.-F. Yeh, S.-S. Hou, J.-S. Jan, Y.-L. Lee, H. Teng, Minimization of ion-solvent clusters in gel electrolytes containing graphene oxide quantum dots for lithium-ion batteries, Small 14 (2018) 1703571.
[365] C. Zhu, D. Chao, J. Sun, I.M. Bacho, Z. Fan, C.F. Ng, X. Xia, H. Huang, H. Zhang, Z.X. Shen, G. Ding, H.J. Fan, Enhanced lithium storage performance of CuO nanowires by coating of graphene quantum dots, Adv. Mater. Interface. 2 (2015) 1400499.
[366] S. Bose, T. Kuila, T.X.H. Nguyen, N.H. Kim, K.-T. Lau, J.H. Lee, Polymer membranes for high temperature proton exchange membrane fuel cell: recent advances and challenges, Prog. Polym. Sci. 36 (2011) 813–843.
[367] S.C. Singhal, Advances in solid oxide fuel cell technology, Solid State Ionics 135 (2000) 305–313.
[368] T. Burchardt, P. Gouérec, E. Sanchez-Cortezon, Z. Karichev, J.H. Miners, Alkaline fuel cells: contemporary advancement and limitations, Fuel 81 (2002) 2151–2155.
[369] H. Fei, R. Ye, G. Ye, Y. Gong, Z. Peng, X. Fan, E.L.G. Samuel, P.M. Ajayan, J.M. Tour, Boron- and nitrogen-doped graphene quantum dots/graphene hybrid nanoplatelets as efficient electrocatalysts for oxygen reduction, ACS Nano 8 (2014) 10837–10843.
[370] A. Dhand, S. Suresh, A. Jain, O.N. Varadan, M.A.K. Kerawalla, P. Goswami, Advances in materials for fuel cell technologies-a review, Int. J. Res. Appl. Sci. Eng. Technol. 5 (2017) 1672–1682.